PHOTONIC APPLICATIONS OF FUNCTIONALIZED GOLD NANORODS: PROGRESS TOWARDS NONLINEAR METAMATERIALS

by

Ryan Eric Michael Latterman

A dissertation submitted in partial fulfillment
of the requirements for the degree

of

Doctor of Philosophy

in

Chemistry

MONTANA STATE UNIVERSITY
Bozeman, Montana

March 2016

©COPYRIGHT

by

Ryan Eric Michael Latterman

2016

All Rights Reserved

DEDICATION

This thesis and academic endeavor is dedicated to my family. Along the way, my family has been the source of influence and motivation that pushed me to strive to be an effective and successful student over the years. My dad and stepmom both exposed me to science and technology throughout my childhood and constantly reminded me of my responsibility to use my time at school wisely. Without them, I'm not sure what kind of student I'd have been on my own. They were also responsible for keeping my church life a constant focus throughout my childhood which has influenced my character beyond words. My brother, who is pursuing a PhD in Statistics at the time of this writing, provided me the motivation to take A.P. Chemistry in high school which ultimately gave me the confidence to take General Chemistry during my first semester of college. I've always been stunned by the amount of time and energy he is able to dedicate to his coursework and I still strive to imitate him. My stepdad has been thoughtful, patient, and generous during all of our interactions and I endeavor to carry myself the way he does. And finally, my mom. She has provided for me at every stage of my life in every form one could imagine. Without her, I wouldn't have an artistic mind to complement my academic mind. I would honestly be half the person I am without her encouragement and influence. And, all of this, like everything, was possible only through Him.

ACKNOWLEDGEMENTS

Acknowledging such a diverse and far-reaching group of people is never an easy task. Academically, I owe much gratitude to every educator and academic role model extending from elementary school through my graduate education. As the most direct contributors to my success as a PhD student, I owe incalculable gratitude to Dr. Phil Sullivan and Dr. Rob Walker for their knowledge, support and encouragement as my graduate advisors. I also thank the past and current members of my committee, Dr. Paul Grieco, Dr. Trevor Rainey, Dr. Pat Callis, Dr. Mary Cloninger, Dr. Erik Grumstrup, and Dr. Florence Dunkel for their commitment to my education.

I also owe particular thanks to my undergraduate professors at Bethany Lutheran College. As my chemistry professors, Dr. Eric Woller and Dr. Matt Riehl deserve special thanks. Additionally, all of my religion, business, and science professors were highly influential in motivating me to pursue graduate studies with the goal of one day becoming professors like them.

I also thank my friends in Bozeman and fellow grad students at MSU that have helped make this experience more than just an education: Ky, Sarah, Jacob, Colin, Anna, Blondie, Brooks, Tyson, Christine, Eric, Joe, Paul, Courtney, Joel, and many others.

TABLE OF CONTENTS

1. INTRODUCTION – NONLINEAR METAMATERIALS 1

1.1 Metamaterials 1
1.2 Nonlinear Organic Materials 3
1.3 Nonlinear Metamaterials 8
1.4 Novel Achievements and Thesis Summary 11
1.5 References 14

2. LOWER POLING THRESHOLDS AND ENHANCED POCKELS COEFFICIENTS IN NANOPARTICLE-POLYMER COMPOSITES 16

2.1 Contribution of Authors and Co-Authors 16
2.2 Manuscript Information Page 17
2.3 Abstract 18
2.4 Introduction 18
2.5 Inhomogeneous Fields in Metamaterials 21
2.6 Pockels Coefficients of a Model Gold Nanorod Array 23
2.7 Conclusion 28
2.8 References 30

3. SYNTHESIS OF THIOL-FUNCTIONALIZED, RAFT POLYMERS WITH DIELS-ALDER ACTIVITY 33

3.1 Introduction 33
3.2 Synthesis of Thiol-Functionalized PMMA 38
3.3 Synthesis of Furan and Anthracene Polymer Derivatives: Scaffolds for Introduction of Nonlinear Organic Dyes 40
3.3.1 Furan Polymer Derivative 41
3.3.1a Thermogravimetric Analysis of Furan/Maleimide Diels-Alder Adducts 45
3.3.2 Anthracene Polymer Derivative 47
3.4 Synthesis of Gold-Reactive Polymer Derived From a Lipoic Acid Monomer 50
3.5 Conclusion 52
3.6 Experimental Section 52
3.6.1 Materials and General Procedures 52
3.6.2 Experimental Procedures and Spectra 54
3.7 References 85

TABLE OF CONTENTS – CONTINUED

4. SYNTHESIS AND FUNCTIONALIZATION OF GOLD NANORODS 88

4.1 Introduction 88
4.2 Synthesis of Gold Nanorods 91
4.2.1 Small Batch GNR Synthesis 91
4.2.2 GNR Synthesis Using Reductive Additives 94
4.3 Functionalization of GNRs with Thiol-Containing Polymers 98
4.3.1 Introduction 98
4.3.2 Functionalization of GNRs Using Thiol-Containing Poly(Methyl Methacrylate) 99
4.3.3 Functionalization of GNRs Using Thiol-Containing Polymers for Diels-Alder 104
4.3.4 Preparation of GNR-Doped Polymer Films 112
4.4 Conclusion 118
4.5 Experimental Section 119
4.5.1 Materials and Instrumentation 119
4.5.2 General Procedure for GNR Synthesis 120
4.5.3 General Procedure for GNR Functionalization 121
4.6 References 123

5. LINEAR AND NONLINEAR APPLICATIONS OF FUNCTIONALIZED GOLD NANORODS 126

5.1 Introduction 126
5.2 Introduction to Part 1 – Improved DPSSL Design Using Epoxy Films of Gold Nanorods 126
5.3 Epoxy-Soluble GNRs as Linear Absorbers 128
5.4 Synthesis of GNRs and Gold-Reactive Polymer 130
5.5 Fluorescence of GNR Coated Nd:YAG 135
5.6 Conclusion to Part 1 135
5.7 Introduction to Part 2 – SFG of Dye-Conjugated Gold Nanopillars 136
5.8 Modeling to Predict Ideal Metamaterial Structure 138
5.9 SFG of Flat and Nanopillar Gold Surfaces 139
5.10 Conclusion to Part 2 143
5.11 Experimental Section 144
5.11.1 Synthesis of Chromophore 3 144
5.11.2 Synthesis of Gold-Reactive Chromophore 5 145

TABLE OF CONTENTS – CONTINUED

5.11.3 Fabrication of Gold Nanopillar Samples 146
5.11.4 SFG Apparatus Description 147
5.12 References 151

6. CONCLUSION 156

6.1 Summary of Work 156
6.2 Future Work and Directions 158

REFERENCES CITED 161

LIST OF FIGURES

Figure Page

1.1 Poling of $\chi^{(2)}$ Chromophores 6

1.2 Nonlinear Organic Chromophores 7

1.3 Magnitude of the Pockels Coefficient Figures of Merit for the Gold Nanorod-ONLO Array 10

2.1 Sketch of a Pockels Cell Composed From a Nanoparticle-ONLO Composite 20

2.2 Illustration of a Nanorod-Polymer Array and the Plot of the Real and Imaginary Parts of Effective Indices 23

2.3 Schematic of the Local Fields and Estimate of the Local Field Enhancement in the Gaps Between Nanorods 25

2.4 Magnitude of the Pockels Coefficient Figures of Merit for the Gold Nanorod-ONLO Array, $(n_i n_j)^{3/2} r_{ijk}$ 27

3.1 Structures of Common RAFT Agents 35

3.2 Generally Accepted RAFT Mechanism 36

3.3 Summary of GNR Functionalization Process 38

3.4 Synthesis of Thiol-Containing Diblock Copolymer 39

3.5 Ideal GNR-Dye Hybrid 40

3.6 Synthesis of RL64 and RL65 41

3.7 Structure of Revised Version of Gold Reactive Furan-Containing Polymer 42

3.8 UvVis of Diels Alder Reaction Between RL121 and 3MPA 43

LIST OF FIGURES – CONTINUED

Figure Page

3.9 TGA of Diels-Alder Adduct RL115 44

3.10 Idealized Depiction of GNR-Polymer-Dye Hybrid 45

3.11 Co-Polymerization of MMA and
9-Anthracenylmethyl Methacrylate 46

3.12 Calibration Curve of 9-Anthracene Methanol 47

3.13 Absorption Spectrum of PMMA-co-PAnMMA 48

3.14 UvVis of Diels-Alder Reaction 49

3.15 Synthesis of Gold-Reactive Monomer, HEMA-LA 50

3.16 Synthesis of RL137 51

4.1 Small Batch Seed-Mediated GNR Synthesis 89

4.2 Absorption Spectra of GNR Growth Over Time 91

4.3 Absorption Spectra of Early Batches of GNRs
With Large Amounts of Spherical Impurities 92

4.4 TEM Images of Pure Batches of GNRs 94

4.5 Absorption Spectrum of Nearly Monodisperse GNRs 95

4.6 Absorption Spectra of GNRs Using
Ye and Vigderman Synthesis Methods 97

4.7 Structure of Gold Reactive Diblock Co-Polymer 99

4.8 Overview Of GNR Functionalization 100

4.9 Photo of GNRs in THF 101

4.10 TEM Images of Polymer-Coated GNRs 103

LIST OF FIGURES – CONTINUED

Figure Page

4.11 Absorption Spectrum of GNRs in Acetone Two Years After Synthesis 104

4.12 Absorption Spectra of GNRs With Four Different Coatings 105

4.13 Photos of GNR TGA Prep Process 106

4.14 TGA of CTAB and GNRs Coated with CTAB 107

4.15 TGA of CTAB, mPEG-SH and mPEG-SH Coated GNRs 108

4.16 Structures of Polymers Used in TGA Studies 109

4.17 TGA of GNRs Coated in RL91 Polymer 110

4.18 TGA of GNRs Coated in RL105 Polymer 111

4.19 TGA of GNRs Coated in RL137 Polymer 112

4.20 Absorption Spectra of GNRs Before Doping Into Polymer Films 113

4.21 Absorption Spectra of GNR-Doped Polymer Films 114

4.22 Absorption Spectrum of GNR-Doped Polymer Film Before and After Heating 116

4.23 Absorption Spectra of GNRs in Water, THF, and a Thin Polymer Film 117

4.24 Absorption Spectra of GNRs (With Lower Aspect Ratio) in a Thin Polymer Film 118

4.25 Absorption Spectrum of Typical Seed Solution 120

5.1 Synthesis of Gold-Reactive Polymer 130

LIST OF FIGURES – CONTINUED

Figure Page

5.2 Depiction of Gold Nanorod Functionalization 131

5.3 Absorption Spectra of GNRs in THF and Norland 65 Epoxy Film 132

5.4 Fluorescence Images at 1064 nm of Nd:YAG With and Without GNR Coating 133

5.5 Laser Efficiency of Production DPSSL With and Without GNR Coating 134

5.6 Depiction of Gold Nanopillar Sample Studied with SFG 139

5.7 SFG of Bare Flat Gold vs. Flat Gold with SAM of Dye 140

5.8 SFG of Bare Gold Nanopillars vs Bare Gold 141

5.9 SFG of Dye-Conjugated Gold Nanopillars 142

5.10 Absorption Spectrum of Chromophore 5 145

5.11 S-Polarized Absorption of Nanopillar Sample 1 147

5.12 S-Polarized Absorption of Nanopillar Sample 3 148

5.13 Diagram of SFG Setup 149

5.14 SFG of Bare Flat Gold Sample 150

ABSTRACT

Nonlinear processes are used to convert one color of laser light into another and are very useful to any research who needs multiple colors of light for basic research or commercial purposes. However, nonlinear processes are inherently very weak and require high input energy to utilize them. Using modeling, it was predicted that ordered arrays of gold nanorods (GNRs), acting as a metamaterial, could be used to fabricate a material that would exhibit field enhancement. Because nonlinear processes depend on the strength of the field in which they interact, enhancing the field strength while using the same amount of input power would make these processes much more efficient and useful. Progress towards these materials included the synthesis of GNRs and gold reactive polymers. These polymers were used to solubilize GNRs in organic solvents while also introducing attachment points for nonlinear chromophores.

To study a material which resembled the one in our modeling predictions, flat gold and two dimensional arrays of gold nanopillars were functionalized with gold-reactive nonlinear organic chromophores and studied using sum frequency generation. It was found that flat gold samples functionalized with a nonlinear chromophore exhibited a tremendous SFG signal, but only in one input polarization configuration. However, gold nanopillar samples exhibited a significant SFG signal in both PPP and SSP polarization configurations. These data agree with our modeling results and indicate that the materials produced here have the potential to be used as a mirror-less optical parametric oscillator.

Organic-soluble GNRs produced in this thesis were then used in an adjacent project to improve the efficiency of a diode-pumped solid state laser design. Nd:YAG lasers are routinely used to produced 1064 nm light by pumping at 808 nm with a semi-conductor diode laser. However, when 1064 nm light is reflected back into the laser cavity, a parasitic phenomenon called amplified spontaneous emission (ASE) occurs. ASE can be combatted by applying a material to the laser rod that absorbs at 1064 nm. GNRs were synthesized at a specific size to absorb at 1064 nm, solubilized in epoxy and applied to a Nd:YAG laser, increasing efficiency by almost two fold.

CHAPTER 1

INTRODUCTION – NONLINEAR METAMATERIALS

1.1 Metamaterials

Metamaterials (MMs) are artificial structures that exhibit properties not found in natural materials.[1-3] Review articles discussing the topic of MMs will almost invariably begin with Victor Veselago's 1968 paper which introduced the concept of a material with both negative permittivity and permeability.[4] Veselago's theory implied that a material could be produced that had a negative refractive index. The kinds of materials Veselago was proposing would need to be able to manipulate both the magnetic and electric fields of light, and would need to be 10 times smaller than the wavelength of light with which they were designed to interact. Because such materials did not occur naturally and there were no means to produce them, Veselago's theories were not considered seriously by scientists for many years. As fabrication and modeling techniques began to improve dramatically, the concept of metamaterials became more realistic. In 2000 Sir John Pendry's theoretical paper[5] proposing a new field of metamaterials sparked renewed interest in the topic. Although the concept of metamaterials was met with much criticism at the time, it stimulated more theory and modeling research to validate its claims. Pendry applied Veselago's theory of negative refraction

to the concept of a lens not limited by the laws of diffraction. This so-called "superlens", if constructed, could be a flat slab of material capable of producing images at much higher resolution than that of a conventional lens.

The next important leap in metamaterial research came in 2006 when David Smith and Sir John Pendry published an article in *Science*[6] which proposed a metamaterial that could cloak an object from incoming electromagnetic radiation. Optical MMs, like Smith's proposed cloak, attain their properties from a periodic arrangement of polarizable elements that are smaller than the wavelength of light with which the elements are designed to interact. These units, or "meta atoms", need to be small enough that the propagating field cannot resolve the spatial details of the material's overall structure. Later, Smith's research group was able to produce a device that had the ability to manipulate light around an object at microwave wavelengths.[7] Besides cloaking and superlensing, MMs have the potential to offer fascinating and useful properties such as sub wavelength imaging[8,9] and electromagnetic field enhancement.[10] A recent commercial application of MMs is a portable, reconfigurable, non-mechanical antenna being developed by Kymeta Corporation.[11] Rather than being mechanically steered, the metamaterial design allows electromagnetic signals to be redirected electronically, controlling the directionality of antenna gain without the use of costly phase-shifter technology. These types of devices will dramatically

reduce the size, power consumption, and ultimately the cost of access to high-speed telecommunication.

Because MMs must operate at a wavelength much larger than their constituent elements to avoid absorption and scattering losses, visible wavelength MMs require elements at the nanometer scale. Clearly, this requirement introduces many challenges in the case of the typical lithographic techniques used to produce most negative index MMs. The overall goal of the work described in this dissertation was to develop metallic nanomaterials and hybridize them with novel organic substrates. These hybrids have the potential to self-assemble into metamaterial structures or can be used in more traditional, bottom-up metamaterial constructs with the goal of enhancing nonlinear optical phenomena. Nonlinear organic materials will be discussed in the following section, and then strategies to hybridize these organic materials with metamaterials to produce nonlinear metamaterials will be discussed.

1.2 Nonlinear Organic Materials

Organic chromophores, commonly referred to as dyes, are molecules that contain extended π-electron conjugation, typically leading to intense visible colors. The associated delocalized electron density is easily polarized by an electric field. At the molecular level, the polarization, p, of a molecule

in response to an electric field of low intensity, E, is proportional to the strength of the field and is described by[12,13]

$$p = p_0 + \alpha E \qquad (1)$$

where p_0 is the ground state or equilibrium polarization and α is the linear polarizability. (Note that in reality, p and E are vector in nature but for simplicity will be described in scalar quantities.) In a bulk material, the equation becomes

$$P = P_0 + \chi^{(1)}E \qquad (2)$$

Where P and E are related by the linear susceptibility, $\chi^{(1)}$. When light of a certain frequency interacts with materials in a linear fashion, the material exhibits a time varying polarization response that is proportional to the strength of the incident field. A new field is produced at the same frequency but is phase shifted in time with respect to the incident field. This phase shift is proportional to the refractive index, n, of the material. A linear relationship holds true at low intensity light, but if a molecule is subjected to high intensity light, such as light from a laser, the polarization equation must be expanded to include higher order terms

$$p = p_0 + \alpha E + \beta EE + \gamma EEE \qquad (3)$$

where the first and second hyperpolarizabilities, β and γ, become significant and must be considered. Similarly, the bulk properties are described by

$$P = P_0 + \chi^{(1)}E + \chi^{(2)}EE + \chi^{(3)}EEE \qquad (4)$$

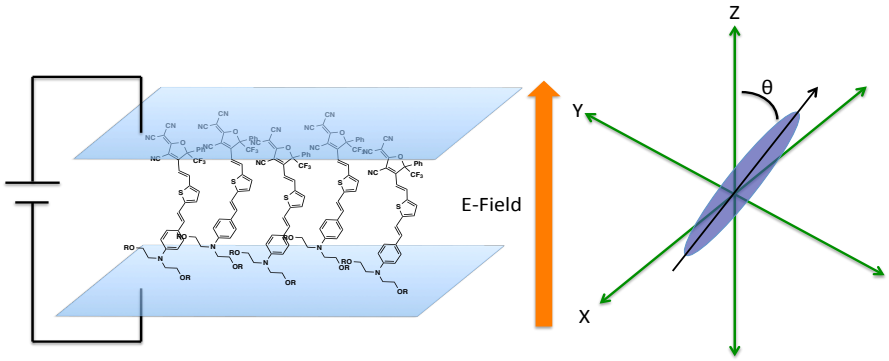
where $\chi^{(2)}$ and $\chi^{(3)}$ represent the first and second nonlinear susceptablities. In this case, the time varying polarization response produces a new optical field with a frequency that may deviate from that of the incident optical field. Very interesting and useful optical phenomena can occur such as second harmonic generation ($\chi^{(2)}$, second order effect) and third harmonic generation ($\chi^{(3)}$, third order effect). Additionally, $\chi^{(2)}$ materials exhibit the electro-optic, or Pockel's effect where the refractive index of the material changes linearly with an applied low frequency (compared to optical) electric field. $\chi^{(3)}$ materials also exhibit an interesting property called the optical Kerr effect where the refractive index change is proportional to the incident light field that interacts with the material. This can be thought of as light being controlled with light. Such a phenomenon could lead to the development of a computer that uses light (photons) instead of electrons as the fundamental carriers of information.

Some significant differences do exist between $\chi^{(2)}$ and $\chi^{(3)}$ effects. First, $\chi^{(3)}$ effects are significantly smaller in magnitude than $\chi^{(2)}$ effects – typically by 6 to 8 orders of magnitude[12]. $\chi^{(2)}$ effects, although potentially much stronger than $\chi^{(3)}$, are still very weak in comparison to linear $\chi^{(1)}$ effects – again, ~6 orders of magnitude less. One major challenge regarding development of $\chi^{(2)}$ materials is that a net assymtery in the bulk material is

required to realize any effect at all. This requirement can be better explained by the mathematical description:

$$\chi_{zzz}^{(2)}(\omega) = N\beta_{zzz}(\omega)\left\langle \cos^3\theta \right\rangle g(\omega) \qquad (5)$$

where N is the number density of molecules per cm^3, and β_{zzz} is the frequency (ω) and permittivity (ε) dependent hyperpolarizability tensor element. The overall value of $\chi^{(2)}$ also depends on the order parameter, $\left\langle \cos^3\theta \right\rangle$, which represents the acentric alignment of



$$\chi_{zzz}^{(2)}(\omega) = N\beta_{zzz}(\omega)\left\langle \cos^3\theta \right\rangle g(\omega)$$

Figure 1.1 Poling of $\chi^{(2)}$ chromophores. Magnitude of $\chi^{(2)}$ activity depends on $\left\langle \cos^3\theta \right\rangle$ order parameter

the molecules relative to the laboratory z axis. To achieve acentric alignment, chromophores are typically dissolved in a polymer host, spun on

conductive glass slides, then heated and poled using strong DC electric fields. A diagram of this kind of poling experiment is depicted in figure 1.1.

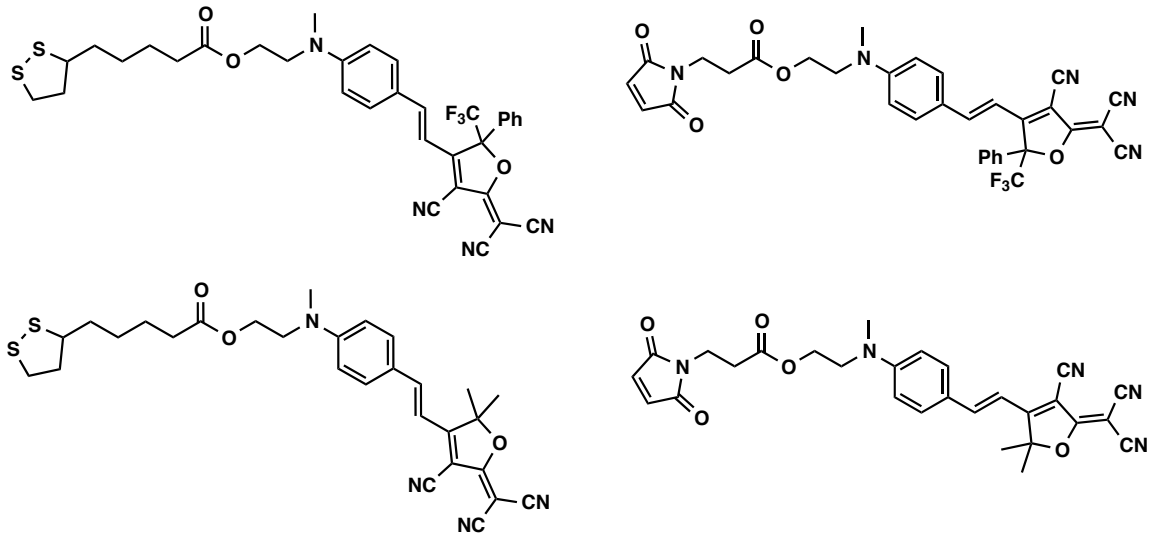


Figure 1.2 – Nonlinear organic chromophores. Disulfide functionalized (left) and maleimide functionalized (right)

Figure 1.2 shows representative examples of asymmetric $\chi^{(2)}$ chromophores that have been synthesized for use in this work**.** A strong electron donating group is attached to a conjugated bridge followed by a strong electron withdrawing group. The donor-acceptor structure increases the degree of ground-state polarization in the molecule and leads to strongly assymetric electron density distribution. This electron density assymetry also results in a strong dipole moment. This property makes $\chi^{(2)}$ chromophores align themselves with their dipoles alternating in an

antiparallel structure, thus negating any $\chi^{(2)}$ activity. Many efforts have been devoted to designing and optimizing organic chromophores and associated materials that have $\chi^{(2)}$ values much greater than typical inorganic crystals used in modern laser applications (e.g., lithium niobate, potassium titanyl phosphate).[13] The focus of this work is not to improve organic chromophore design, but rather use existing, highly active nonlinear chromophores in a novel metamaterial architecture. More background on the theory and progress of nonlinear organic materials can be found in the literature.[14-17] The next section will discuss a strategy to produce a nonlinear metamaterial able to overcome the obstacles of nonlinear organic material fabrication by selective enhancement of the metamaterial's nonlinear properties. 11

1.3 Nonlinear Metamaterials

Much progress has been made in the field of MMs in the past decade, but there are many advances that still need to be made. Nikolay Zheludev, the deputy director of the Optoelectronics Research Center at the University of Southhampton, wrote in a recent Science article[18],

> "The next stage of this technological revolution will be the development of active, controllable, and nonlinear

metamaterials surpassing natural media as platforms for optical data processing and quantum information applications."

Statements by Zheludev and others suggest an increasing belief that active, controllable nonlinear MMs will be responsible for the next optoelectronics technological revolution. Unfortunately, a practical obstacle of using current state-of-the-art nonlinear materials is that their effects are inherently weak and high intensity pulsed lasers and/or long interaction lengths coupled with high drive voltages, are required to take advantage of their ultrafast properties. Hybridizing metamaterials with nonlinear media has the potential to reduce the power needed to exploit their interesting properties through field enhancement. Reports[10,19] have shown that specially designed arrays of metal nanoparticles can localize and concentrate electromagnetic fields. Introducing nonlinear media into these fields would result in bulk materials with nonlinear properties that are enhanced proportionally to the square or cube of these concentrated fields. Such enhancements would lower the amount of power required to realize useful nonlinear effects. The overall magnitude of the effect depends on both the nonlinearity of the chosen media and the field enhancement produced by the metamaterial structure. As stated earlier, $\chi^{(2)}$ effects are only present when a net assymtry is achieved. Enhancing the electric field while achieving net assymetry is imperative for enhancing nonlinear $\chi^{(2)}$ effects.

Through collaborations with David Smith's research group at Duke University, nonlinear enhancements have been modeled and predicted using

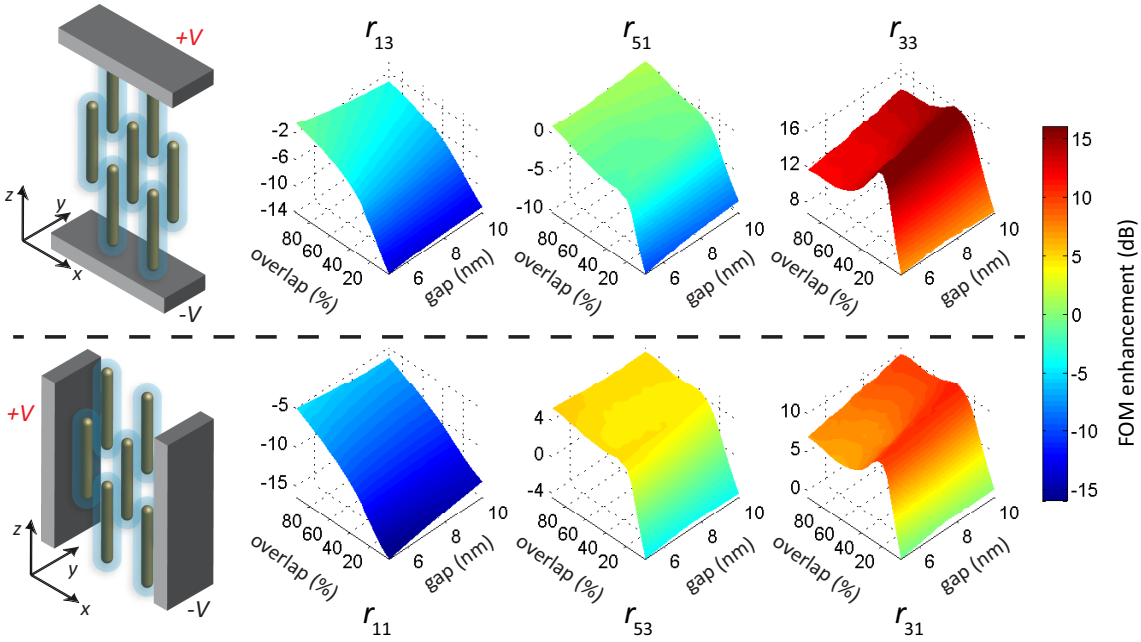


Figure 1.3. Magnitude of the Pockels coefficient figures of merit for the gold nanorod-ONLO array, $(n_i n_j)^{3/2} r_{ijk}$, normalized by the figure of merit for the ONLO itself, in dB. The plots are separated by row, corresponding to the two transverse poling configurations, shown schematically: poling field along $\hat{z}$ (top row) and poling field along $\hat{x}$ (bottom row).

full wave simulations (COMSOL Multiphysics software) coupled with a transfer-matrix-based nonlinear retrieval method that includes a nonlinear dielectric, having an arbitrary $\chi^{(2)}$ value, in the MM medium.[10] Results, discussed in detail in Chapter 2, are shown in figure 1.3. Included are figures of merit for second harmonic generation in the proposed nonlinear metamaterial. Input parameters such as rod length, rod diameter, and the

gap between rods can be modeled to design an ideal metamaterial structure. Efforts in this thesis used this novel modeling to aid in the design of optimized hybrid structures of gold nanorods, diblock copolymers and nonlinear organic chromophores that have the potential to create an ordered, self-assembled, three-dimensional metamaterial structure that operates at near-infrared (NIR) and/or infrared (IR) optical wavelengths where $\lambda \sim 1550 - 3000$ nm. Additionally, these modeling results show that potential field enhancements could be harnessed from two-dimensional gold nanorod arrays produced by more traditional bottom-up approaches rather than self-assembly. Collaborators from Dr. Anatoly Zayat's research group at King's College (UK) have synthesized horizontal arrays of vertically aligned gold nanorods which we have hybridized with nonlinear organic materials in order to study the potentially interesting field enhancement effects predicted by our modeling results. Results from this study are summarized in chapter 6.

1.4 Novel Achievements and Thesis Summary

The ultimate goal of this thesis was to hybridize nonlinear organic materials into a metamaterial architecture in order to enhance nonlinear effects through field enhancement. The following achievements were realized while pursuing these goals:

- A non-linear metamaterial was designed and modeling was used to predict its ability to enhance pockels effect.
- PMMA-furfuryl methacrylamide and PMMA-furfuryl methacrylate polymers, functionalized with cysteamine were synthesized.
- Lipoic acid-furan polymer was synthesized as an alternative to cysteamine polymer.
- Highly concentrated solutions of organic-soluble gold nanorods were synthesized.
- Organic-soluble gold nanorods were used to improve a diode-pumped solid-state laser design through a collaboration with a local technology company.
- Novel lipoic acid-functionalized nonlinear chromophores were synthesized, introduced to flat gold and gold nanopillar substrates and studied using SFG nonlinear techniques.

Chapter Two consists of modeling results showing how ordered arrays of gold nanorods hybridized with nonlinear organic chromophores have the potential to enhance nonlinear activity by more than an order of magnitude. Chapter Three describes the design, synthesis, and characterization of polymers with the ability to both attach to gold nanorods through sulfur functionality and covalently attach to nonlinear chromophores through Diels-Alder chemistry. Chapter Four discusses the synthesis and functionalization

of gold nanorods with novel thiol-containing polymers. Part one of Chapter Five shows how organic-soluble gold nanorods were used to improve the efficiency of a diode-pumped solid-state laser by coating the lasing medium with nanorods dissolved in UV-curable epoxy. Part 2 of Chapter 5 demonstrates how vertical arrays of gold nanorods were hybridized with nonlinear organic chromophores and studied using sum-frequency and sum-harmonic generation.

1.5 References

1. Smith, D., Pendry, J. & Wiltshire, M. Metamaterials and negative refractive index. *Science* **305**, 788–92 (2004).

2. Zheludev, N. & Kivshar, Y. From metamaterials to metadevices. *Nat Mater.* **11**, 917–24 (2012).

3. Liu, Y. & Zhang, X. Metamaterials: a new frontier of science and technology. *Chem. Soc. Rev.* **40**, 2494–507 (2011).

4. Veselago, V.G. The electrodynamics of substances with simultaneously negative values of ε and μ. *Sov. Phys. Usp.* **10**, 509-412 (1968)

5. Pendry, J. B. Negative refraction makes a perfect lens. *Phys. Rev. Lett.* **85,** 3966–9 (2000).

6. Pendry, J. B., Schurig, D. & Smith, D. R. Controlling electromagnetic fields. *Science* **312,** 1780–2 (2006).

7. Landy, N. & Smith, D. A full-parameter unidirectional metamaterial cloak for microwaves. *Nat. Mater.* **12**, 25–8 (2012).

8. Smith, D., Pendry, J. & Wiltshire, M. Metamaterials and negative refractive index. *Science* **305**, 788–92 (2004).

9. Zheludev, N. What diffraction limit? *Nat. Mater.* **7**, 420–2 (2008).

10. Rose, A., Larouche, S., Smith, D. R. Quantitative study of the enhancement of bulk nonlinearities in metamaterials. *Phys. Rev. Lett.* **84**, 053805 (2011).

11. http://www.kymetacorp.com/

12. Sullivan, P. & Dalton, L. Theory-inspired development of organic electro-optic materials. *Acc. Chem. Res.* **43**, 10–8 (2010).

13. Dalton, L., Sullivan, P. & Bale, D. Electric field poled organic electro-optic materials: state of the art and future prospects. *Chem. Rev.* **110**, 25–55 (2009)

14. Sullivan, P. A. & Dalton, L. R. Theory-inspired development of organic electro-optic materials. *Acc. Chem. Res.* **43,** 10–8 (2010).

15. Dalton. Rational design of organic electro-optic materials. *J. Phys. Condens. Matter.* **15,** R897 (2003).

16. Marder, S. Organic nonlinear optical materials: where we have been and where we are going. *Chemical Communications* **0,** 131–134 (2005).

17. Prasad, P. & Reinhardt, B. Is there a role for organic materials chemistry in nonlinear optics and photonics? *Chem. Mater.* (1990).

18. Zheludev, N. The road ahead for metamaterials. *Science* **328**, 582–3 (2010).

19. Pendry, J. B., Holden, A. J., Robbins, D. J. & Stewart, W. J. Magnetism from conductors and enhanced nonlinear phenomena. *IEEE Transactions on Microwave Theory and Techniques* **47,** (1999)

CHAPTER 2

LOWER POLING THRESHOLDS AND ENHANCED POCKELS COEFFICIENTS IN NANOPARTICLE-POLYMER COMPOSITES

2.1 Contribution of Authors and Co-Authors

Manuscript in Chapter 2

Author: Alec Rose

Contributions: Collected and analyzed all modeling results. Assisted in writing and editing manuscript.

Co-Author B. Ryan Latterman

Contributions: Assisted in experimental background and design and assisted in editing manuscript.

Co-Author: David R. Smith

Contributions: Assisted with data interpretation and edited manuscript.

Co-Author: Philip Sullivan

Contributions: Assisted with data interpretation and in writing and editing manuscript.

2.2 Manuscript Information Page

Alec Rose, Ryan Latterman, David R. Smith, and Philip Sullivan
Applied Physics Letters
Status of Manuscript:
____Prepared for submission to peer-reviewed journal
____Officially submitted to a peer-reviewed journal
____Accepted by a peer-reviewed journal
_X_ Published in a peer-reviewed journal

Publisher: AIP Publishing
Date of Submission: 6 May 2013
Date Accepted: 25 June 2013
Volume 103, July 2013, 031102
The following chapter has been published in Applied Physics Letters (vol. 103) and appears in this thesis/dissertation with the journal's permission.

CHAPTER 2

LOWER POLING THRESHOLDS AND ENHANCED POCKELS COEFFICIENTS IN NANOPARTICLE-POLYMER COMPOSITES

2.3 Abstract

In this chapter, we investigate computationally the electromagnetic response of composite media made from high aspect ratio nanoparticle arrays. The shape and local ordering of the nanoparticles can be used to both confine and enhance the local electric fields induced in response to static and propagating fields. When such nanoparticle arrays are hybridized with electrooptic polymers and subjected to a poling field, we show that the nanoparticles can enable variant tensor orientations and lower poling thresholds. From an effective medium perspective, we find that the Pockels coefficients of the nanoparticle-polymer composites can be enhanced by more than an order of magnitude.

2.4 Introduction

Materials exhibiting extraordinarily large second-order nonlinear optical susceptibilities have long been of interest for applications involving frequency conversion and electro- optic modulation.[1-4] Recently, it has been shown that metamaterials, i.e., nanostructured arrays of sub-wavelength

polarizable elements, may be designed to not only adopt but greatly enhance the optical properties of interspersed nonlinear dielectrics. When carefully designed with the aid of recently developed theoretical methods, nonlinear metamaterials (NLMMs) are predicted to support exotic and widely reconfigurable optical phenomena.

Engineered organic nonlinear optical dielectrics (ONLOs) are particularly attractive for facile introduction of large low-loss optical nonlinearities into these micro or nano-patterned NLMM structures. ONLOs may be easily processed using solution-casting techniques, in contrast to crystalline $\chi^{(2)}$ materials such as $LiNbO_3$, allowing for simple and effective back-filling of prefabricated features as small as several nanometers via capillary action.[5-7] However, unlike spontaneously polarized crystalline materials, the vast majority of ONLOs are initially isotropic. Therefore, a nonzero $\chi^{(2)}$ is most commonly introduced via electric field poling processes that align the constituent nonlinear molecules (chromophores). The magnitude of the resulting $\chi^{(2)}$ is proportional to, and necessarily limited by, the magnitude of the poling field that may be applied before damage occurs due to dielectric breakdown.[4,8] The $\chi^{(2)}$ tensor orientation that results from DC electric field poling is also solely dictated by the direction of the applied field. Taking the Pockels effect as an example, it is often assumed for typical materials that $r_{33} \approx 3r_{13}$, while the off-diagonal elements are weak by comparison. As a

result, voltage-induced coupling between orthogonal polarizations is limited. It follows that poling methods and thresholds are in fact significant factors in achieving highly efficient $\chi^{(2)}$-based devices. In this chapter, we introduce the concept of using NLMMs to structurally modify the poling thresholds and tensors of an effective medium, computationally exploring the example of a gold nanorod-ONLO composite array (figure 2.1).

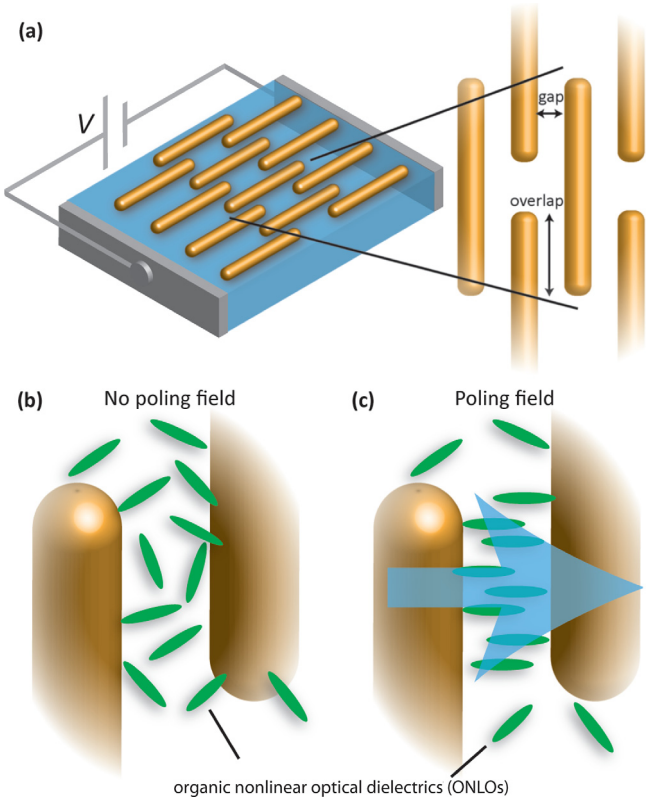


Figure 2.1. Sketch of a Pockels cell composed from a nanoparticle-ONLO composite, with variable dimensions indicated (a). The gap size is controlled by the extent of the ONLO around the nanorod, while we define the overlap as the percentage of the nanorod that coincides transversely with its nearest neighbors. Illustration of polymer ordering before (b) and after (c) a poling field is applied to the medium.

2.5 Inhomogeneous Fields In Metamaterials

Within an inhomogeneous medium, the local fields can vary quite dramatically from the macroscopic and applied fields, both in magnitude and direction.[9-11] While field concentration has been a driving force in the search for metamaterials and plasmonic media with enhanced nonlinear coefficients,[12-17] control over field orientation has received less attention. However, it is this control of the directionality of the local fields that allows access to effective properties of fundamentally different natures than the constitutive materials. For example, effectively nonlinear magnetic susceptibilities have been demonstrated in metamaterials composed of metals and dielectrics through structurally supported circulating currents.[18-21] Furthermore, a variety of nonlinear magneto-electric susceptibilities have been predicted and demonstrated in composites as a direct consequence of local overlap of the fields induced by both magnetic and electric incident fields.[22-24] In effect, manipulating the directionality of the local fields in metamaterials can supplement the overall enhanced coefficients while offering additional degrees of functionality and flexibility.

Metamaterials not only can lead to effective magnetic and magneto-electric behavior but can also control the anisotropy of optical properties. If we assume a metamaterial with negligible magnetism and losses, we can employ a recently developed coupled mode theory to relate the effective $\chi^{(2)}$ to

overlap integrals in the limit that the lattice constant is much smaller than a wavelength[22]

$$\chi_{ijk}^{(2)} = \frac{1}{V_0}\int\int\int_{V_0} dV \vec{\vec{\chi}}^{(2)}(\vec{r}) : \vec{e}_j(\vec{r})\vec{e}_k(\vec{r}) \cdot \vec{e}_i(\vec{r}), \qquad (1)$$

Where $\overrightarrow{e_n}(\vec{r})$ is the electric field of the Bloch mode with macroscopic polarization and frequency indexed by n, and the integral is performed over a single unit-cell with volume V_0. If the Bloch modes were nothing more than simple plane waves, as in a homogeneous medium, then it is clear that the effective susceptibility would be a simple volume average of the local one, and only the (typically) weaker off-diagonal tensor elements could couple waves with orthogonal polarizations. However, due to the inhomogeneous nature of the metamaterial, the local electric fields can overlap despite the orthogonality of the macroscopic fields, leading to great flexibility in the effective nonlinear tensors. The consequences of equation (1) are most evident in electro-optics, indicating that a simple poling voltage in an inhomogeneous metamaterial can lead to strong coupling of originally orthogonal polarizations. When one of these polarizations is associated with the metamaterial's internal resonance, the overall effect can be quite dramatic. Moreover, an applied poling field or voltage can likewise induce local fields that are much stronger, or even differently oriented, than the applied field,

leading to poling thresholds and configurations that are distinct from a simple bulk medium.

2.6 Pockels Coefficients of a Model Gold Nanorod Array

As a demonstrative example, consider the simple idealized nanoparticle array shown in figure 2.2(a), consisting of gold nanorods 65 nm in length and 8 nm in diameter, and coated in ONLO (ϵ = 2.19). These nematic-like (alternating) gold nanorods are loosely based on those in Refs. 25 and 26 and are known to support a polarization sensitive plasmonic resonance.[27] Using a transfer-matrix based nonlinear retrieval method, we show

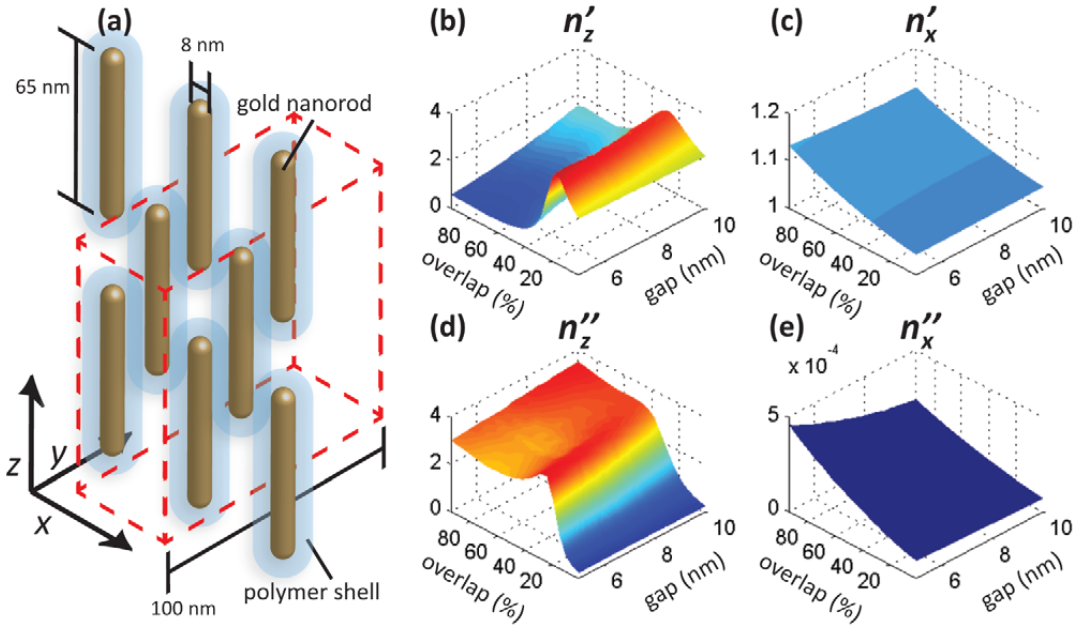


Figure 2.2. (a) Illustration of the nanorod-polymer array, with the basic rectangular unit-cell indicated by the dashed red box. Plot of the real (b), (c) and imaginary (d), (e) parts of the effective indices for both polarizations.

that this class of metamaterial supports a set of non-zero Pockels coefficients at telecommunication wavelengths that are both distinct in orientation and enhanced in magnitude compared to the ONLO alone. By changing the interstitial spacing (gap) and overlap between nearest neighbors, along with the choice of poling orientation, we demonstrate a continuum of nonlinear tensor configurations and strengths. Ultimately, metamaterials with this degree of control over the effective nonlinear tensor can lead to Pockels cells with reduced dimensions and poling thresholds. In the linear regime, fields normally incident on the sur- face of such a structure can be decomposed into two orthogo- nal polarizations, corresponding to the electric field parallel ($\hat{z}$) and transverse ($\hat{x}$) to the rod axis. For light with wave- length λ = 1530 nm, as in typical telecommunications sys-tems, we can describe the anisotropic interaction through effective complex indices of refraction, $n_j = n_j' + in_j''$, applying the well-known set of retrieval equations[28] to the results of finite-element simulations (COMSOL Multiphysics). We simulate a single unit-cell, defined by the dashed red box in figure 2.2(a), using periodic boundary conditions along the transverse boundaries and assuming a lattice constant of 100 nm in the direction of propagation ($\hat{y}$). The resulting effective indices are displayed in figure 2.2(b). As expected, for certain combinations of gap and overlap, the $\hat{z}$ polarization excites the dominant plasmonic resonance at λ = 1530 nm, as evidenced by the strong

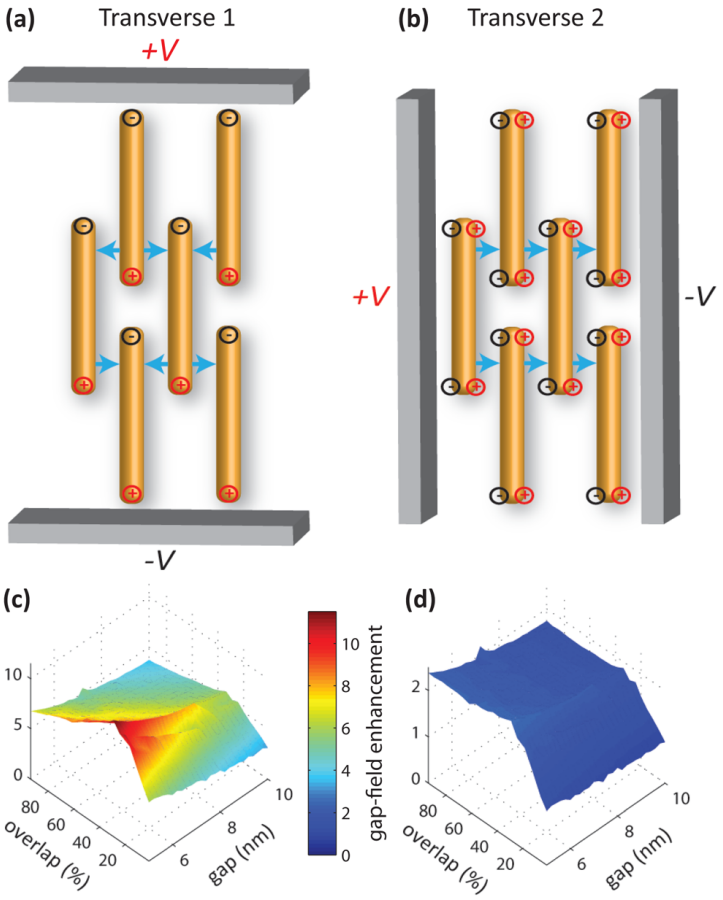


Figure 2.3. Schematic of the local fields (a), (b) and estimate of the local field enhancement in the gaps between nanorods (c), (d) for the two transverse poling configurations.

peak in absorption (n_z''). At the same time, the $\hat{x}$ polarization exhibits near transparency ($n_x \approx 1$). However, it is interesting to note that despite such large anisotropy, both polarizations will tend to excite significant electric fields in the gaps between adjacent nanorods, dominantly oriented transverse to the rod surfaces. This is illustrated in figure 2.3 for DC fields: while the macroscopic fields drive charge buildup in the individual nanorods, the overlap between nearest neighbor nanorods focuses the energy into these

gaps, regardless of polarization. In addition, this analysis immediately reveals the potential for lowering the effective poling thresholds in such a structure. Confinement of energy in small gaps must be accompanied by local field enhancement, and so macroscopic poling fields can be reduced while still achieving the required field strengths to pole the ONLO located within the gaps. As a rough measure of this factor in poling threshold reduction, we plot the local electric field at the center-point between two nanorods, normalized by the applied field, as a function of gap and overlap in figure 2.3(b) for both transverse poling configurations. Both configurations display poling threshold reductions, while the local directionality of the second-order material is now a function of the applied field *and* the local structure.

In calculating the effective nonlinear coefficients of the nanorod metamaterial, we turn to the recently developed transfer-matrix based retrieval method,[29,30] which has shown success in determining the susceptibilities related to second harmonic generation and self-phase modulation in similar structures.[15,31] In particular, we investigate the Pockels effect, in which a propagating field is modified by the presence of a strong DC or slowly varying electric field. However, a similar method could be applied to determine effective wave-mixing coefficients.

Again using finite-element simulations via COMSOL Multiphysics, we first simulate the poling field by applying a voltage in either of the transverse poling configurations. To simplify and generalize our results, we assume the

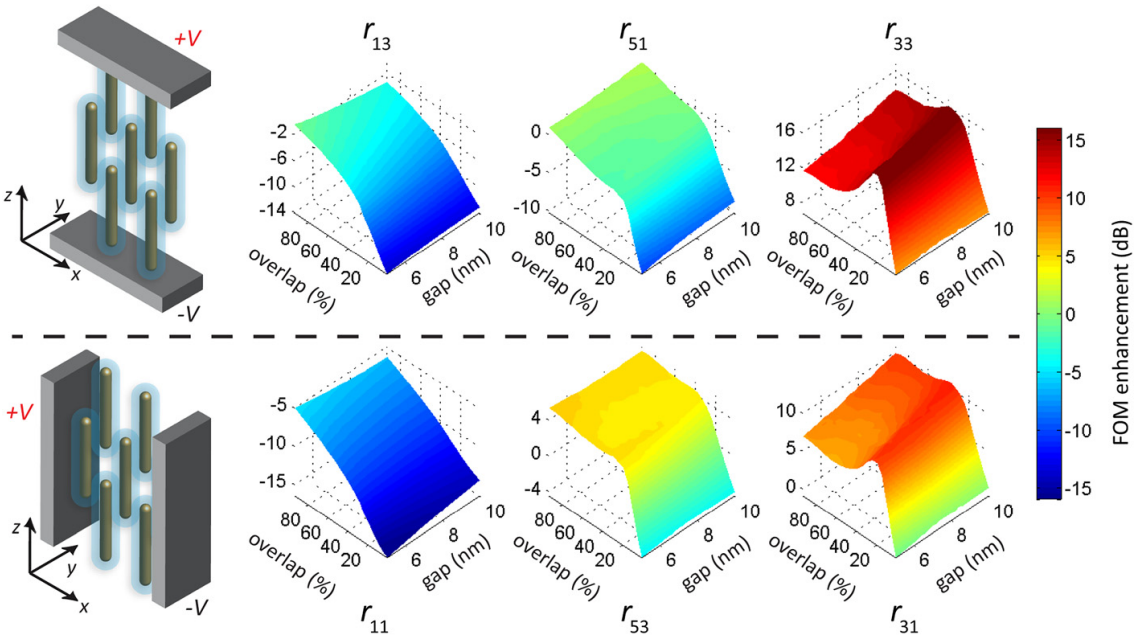


Figure 2.4. Magnitude of the Pockels coefficient figures of merit for the gold nanorod-ONLO array, $(n_i n_j)^{3/2} r_{ijk}$, normalized by the figure of merit for the ONLO itself, in dB. The plots are separated by row, corresponding to the two transverse poling configurations, shown schematically: poling field along $\hat{z}$ (top row) and poling field along $\hat{x}$ (bottom row).

ONLO will orient itself completely in the direction of the local poling field and only consider the local nonlinear susceptibility along this axis. Next, we use the product of propagating and DC fields to excite the ONLO according to its local nonlinear tensor, collecting the re-radiated fields at the entrance and exit planes of the simulation, as in reference 15. The nonlinear retrieval method is applied to this result to give the effective nonlinear susceptibility, and the process is repeated for all possible permutations of poling and propagating polarizations. From the nonlinear susceptibilities, we can calculate the Pockels coefficients according to $r_{ijk} = \frac{\epsilon_0^2}{\epsilon_i \epsilon_j} \chi_{ijk}^{(2)}$. For comparison,

we consider electrooptic modulation of the refractive indices, proportional to the material figure of merit $(n_i n_j)^{3/2} r_{ijk}$.[32] The magnitudes of these figures of merit are normalized by $n^3 r_{33}$ of the ONLO alone and plotted in figure 2.4, according to the usual contracted index notation, for all non-zero elements in the two transverse poling configurations.

As expected, the coefficients r_{33} and r_{31} are largest in magnitude, enhanced by more than an order of magnitude for the geometries that support plasmonic resonances close to the operational wavelength, λ = 1530 nm. The coefficients r_{51} and r_{53}, though weaker, are interesting from an additional perspective: r_{51} and r_{53} represent the ability of a DC field to induce coupling between the two originally orthogonal polarizations. In this way, the transparency of the $\hat{x}$ polarized wave can be switched off by forcing it to couple to the inherently lossy plasmonic resonance of the nanorods. This differs drastically from a homogeneous medium, which would need to employ an ONLO that itself had large off-diagonal tensor elements, limiting the choice of materials and overall efficiency.

2.7 Conclusion

In nonlinear metamaterials, the engineered interaction of multiple waves and even DC fields gives access to an unprecedented number of degrees of freedom in the manipulation and enhancement of electromagnetic

phenomena. Using the example of gold nanorods hybridized with ONLOs, we have demonstrated the ability of metamaterials to combine nonlinearity with massive anisotropy, reduce poling thresholds by an order of magnitude, and exhibit different and enhanced effective nonlinear tensor elements compared to the constituent materials. This analysis can be extended beyond electro-optics to general three- and four-wave mixing as well. In particular, the massive anisotropy and off-diagonal tensor elements make the proposed structure a potential candidate for mirrorless birefringence-phase-matched optical parametric oscillation, as described in reference 31.

2.8 References

1. Burland, D., Miller, R. & Walsh, C. Second-order nonlinearity in poled-polymer systems. *Chem. Rev.* **94,** 31–75 (1994).

2. Dalton, L. Theory-inspired development of organic electro-optic materials. *Thin Solid Films* **518,** 428–431 (2009).

3. Dalton, L. *et al.* From molecules to opto-chips: organic electro-optic materials. *J. Mater. Chem.* **9,** 1905–1920 (1999).

4. Dalton, L. R., Sullivan, P. A. & Bale, D. H. Electric field poled organic electro-optic materials: state of the art and future prospects. *Chem. Rev.* **110,** 25–55 (2010).

5. Baehr-Jones *et al.* Optical modulation and detection in slotted Silicon waveguides. *Opt. Express* **13,** 5216 (2005).

6. Hochberg, M. *et al.* Terahertz all-optical modulation in a silicon-polymer hybrid system. *Nat. Mater.* **5,** 703–9 (2006)

7. Wang, X. *et al.* Effective in-device r_33 of 735 pm/V on electro-optic polymer infiltrated silicon photonic crystal slot waveguides. *Opt. Lett.* **36,** 882 (2011).

8. Huang, S. *et al.* Advanced Materials **24**, OP42 (2012), ISSN 1521-4095.

9. Sipe, J.E., & Boyd, R. W. Nonlinear susceptibility of composite optical materials in the Maxwell Garnett model. *Phys. Rev. A* **46,** 1614–1629 (1992).

10. Fischer, G. *et al.* Enhanced Nonlinear Optical Response of Composite Materials. *Phys. Rev. Lett.* **74,** 1871–1874 (1995).

11. Boyd, R., Gehr, R., Fischer, G. & Sipe. Nonlinear optical properties of nanocomposite materials. *Pure Appl. Opt. J. European Opt Soc. Part A* **5,** 505–512 (1996).

12. Pendry, J. B., Holden, A. J., Robbins, D. J. & Stewart, W. J. Magnetism from conductors and enhanced nonlinear phenomena. *IEEE T. Microw. Theory* **47,** (1999).

13. Bouhelier A., Beversluis M., Hartschuh A. & Novotny L. Near-Field Second-Harmonic Generation Induced by Local Field Enhancement. *Phys. Rev. Lett.* **90,** (2003).

14. Soljacic, M. & Joannopoulos J. D. Enhancement of nonlinear effects using photonic crystals. *Nat. Mater.* **3,**211–219 (2004).

15. Rose, A., Larouche S., & Smith, D. R. Quantitative study of the enhancement of bulk nonlinearities in metamaterials. *Phys. Rev. A* **84**, 053805 (2011).

16. Wurtz, G. A. *et al.* Designed ultrafast optical nonlinearity in a plasmonic nanorod metamaterial enhanced by nonlocality. *Nat. Nanotechnol.* **6,** 107–11 (2011).

17. Ciracì, C., Poutrina E., Scalora M., & Smith, D. R. *Phys. Rev. B* **85**, 201403 (2012).

18. Zharov, A., Shadrivov, I. & Kivshar, Y. Nonlinear Properties of Left-Handed Metamaterials. *Phys. Rev. Lett.* **91,** (2003).

19. O'Brien, S., McPeake, D., Ramakrishna, A., & Pendry, J. B. Near-infrared photonic band gaps and nonlinear effects in negative magnetic metamaterials. *Phys. Rev. B* **69,** (2004).

20. Klein, M.W., Enkrich, C., Wegener, & M.,Linden, S. Second-Harmonic Generation from Magnetic Metamaterials. *Science* **313,** 502–504 (2006).

21. Larouche, S., Rose, A., Poutrina, E., Huang, D. & Smith, D. Experimental determination of the quadratic nonlinear magnetic susceptibility of a varactor-loaded split ring resonator metamaterial. *Appl. Phys. Lett.* **97,** 011109 (2010).

22. Rose, A., Larouche, S., Poutrina, E., & Smith, D. R. Nonlinear magnetoelectric metamaterials: Analysis and homogenization via a microscopic coupled-mode theory. *Phys. Rev. A* **86**, 033816 (2012).

23. Rose, A., Huang, D. & Smith, D. R. Demonstration of nonlinear magnetoelectric coupling in metamaterials. *Appl. Phys. Lett* **101,** 051103 (2012).

24. Rose, A., Huang, D. & Smith, D. R. Nonlinear Interference and Unidirectional Wave Mixing in Metamaterials. *Phys. Rev. Lett.* **110,** (2013).

25. Liu, Q. *et al.* Self-alignment of plasmonic gold nanorods in reconfigurable anisotropic fluids for tunable bulk metamaterial applications. *Nano Lett.* **10,** 1347–53 (2010).

26. Thorkelsson, K., Mastroianni, A. J., Ercius, P. & Xu, T. Direct nanorod assembly using block copolymer-based supramolecules. *Nano Lett.***12,** 498–504 (2012).

27. Vigderman, L., Khanal, B. P. & Zubarev, E. R. Functional gold nanorods: synthesis, self-assembly, and sensing applications. *Adv. Mater.* **24,** 4811–41, 5014 (2012).

28. Smith, D. R., Vier, D., Koschny, T. & Soukoulis, C. Electromagnetic parameter retrieval from inhomogeneous metamaterials. *Phys. Rev. E* **71,** (2005).

29. Larouche, S. & Smith, D. R. A retrieval method for nonlinear metamaterials. *Opt. Commun.* **283,** 1621–1627 (2010).

30. Rose, A., Larouche, S., Huang, D., Poutrina, E. & Smith, D. Nonlinear parameter retrieval from three- and four-wave mixing in metamaterials. *Phys. Rev. E* **82,** (2010).

31. Rose, A. & Smith, D. Overcoming phase mismatch in nonlinear metamaterials [Invited]. *Opt. Mater. Express* **1,** 1232 (2011).

32. Boyd, R. W. Nonlinear Optics (Academic Press, Burlington, MA, 2008).

CHAPTER 3

SYNTHESIS OF THIOL-FUNCTIONALIZED, RAFT POLYMERS WITH DIELS-ALDER REACTIVITY

3.1 Introduction

In order to harness the predicted field enhancements of ordered nanorods, methods that allow gold nanorods (GNRs) to self assemble into the optimized structures discussed in Chapter 2 were explored. Studies have shown that ordered liquid crystalline phases can result from high concentrations of a variety of rod shaped nanoparticles (TiO_2, SnO_2, ZnO, and CdTe) functionalized with diblock copolymers.[1,2] A polymer shell increases the mobility of highly concentrated nanorod solutions and allows for a size-tunable spacer between the rods. This chapter describes the synthesis of gold reactive polymers with the goals of solubilizing them in organic solutions, introducing Diels-Alder functionality, and increasing their mobility at high concentrations.

Typically, GNRs are synthesized in aqueous solutions and stabilized by charged surfactants. The resulting nanoparticle surface charge restricts the ability to use the particles in organic environments or electronic devices. Useful methods have been developed to solubilize aqueous solutions of gold nanoparticles in organic solutions by replacing the typical surfactant (CTAB)

used to stabilize them with alkanethiols. This functionalization also mitigates the surface charge problems and has been shown to yield nearly zero zeta potentials.[3] Some solubilization methods are more complex than others, but a promising approach uses a relatively simple two-step process.[3] Thiol-terminated polyethylene glycol (PEG-SH) serves as an intermediate stabilization layer that makes the nanoparticles soluble in both water and in organic solvents. The PEG-SH functionalized nanoparticles are then redispersed in a solvent such as tetrahydrofuran and left to react with solutions of thiol-terminated alkanes. The details of this functionalization process will be discussed in Chapter 4.

In this thesis gold nanorods were solubilized using thiol-functionalized copolymers synthesized by the RAFT (reversible addition-fragmentation chain transfer) technique. Originally developed in 1998 by a team at Australia's federal science agency, CSIRO[4], the RAFT process has since gained tremendous popularity worldwide[5-7] for its ability to produce monodisperse polymers with engineered functionality. In a typical free-radical initiated polymerization, polymer chains are formed very rapidly when monomer concentration is high leading to high molecular weight chains in the early stages of the reaction. New polymer chains are also terminated when a radical from one chain reacts with a radical on another. This kind of uncontrolled polymerization leads to broad molecular weight distribution and very little control towards a target molecular weight. Because RAFT is a

living free-radical method, the majority of termination events are eliminated allowing for the control of molecular weight at low polydispersity with the added utility of the RAFT agent being the end group of the polymer chains produced.

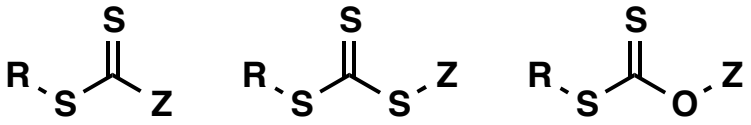


Figure 3.1. General structures of common RAFT agents. R is a designed to be both a good leaving group and an efficient free radical reinitiating group. Z should activate the thiocarbonyl towards radical addition.

The RAFT process includes all of the same reagents and conditions used in conventional free-radical polymerization but with the crucial addition of a RAFT chain transfer agent. The general structure of a RAFT agent is shown in figure 3.1 where R is usually an alkyl group that is responsible for reinitiating polymer growth. Z can vary depending on the choice of monomer used in the polymerization and is responsible for activating the double bond in the RAFT agent for radical addition. In this thesis the chosen RAFT agent was a trithicarbonate, a reagent that is especially suitable for acrylate monomers.[8]

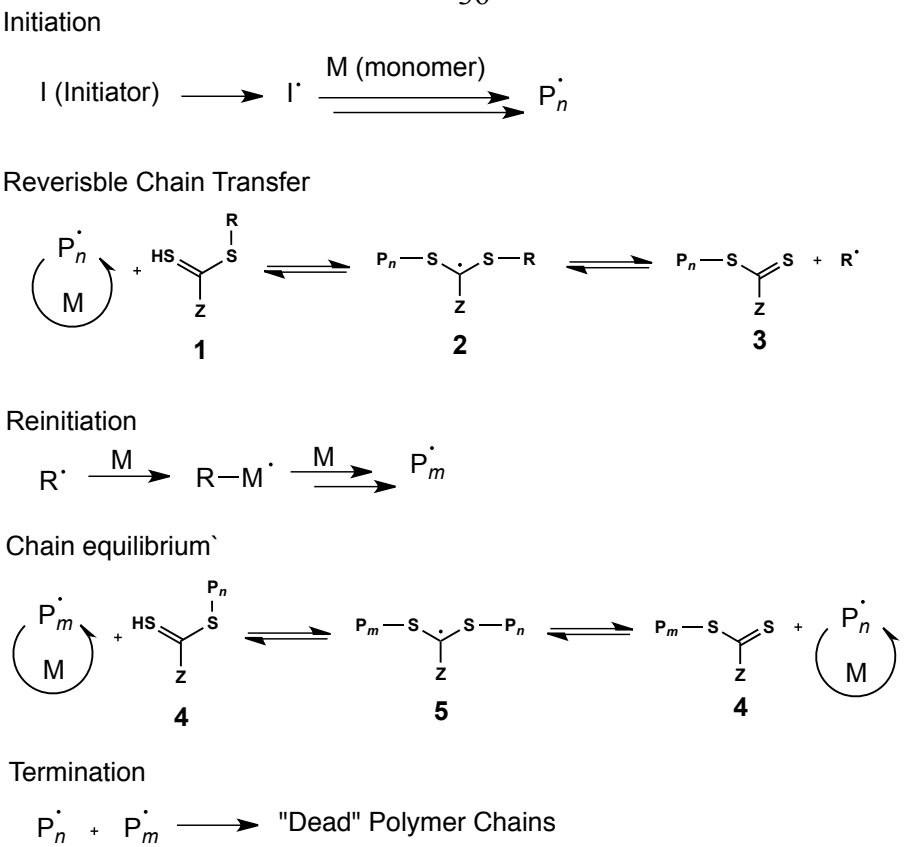


Figure 3.2. Generally accepted RAFT mechanism.

All benefits of the RAFT process originate from the addition of a RAFT agent and the unique mechanism resulting from it. Depicted in figure 3.2, the mechanism begins with initiation, just as in a typical free-radical polymerization, with a radical produced via an initiator. This radical reacts with a certain amount of monomer to produce an oligomeric radical, $P_n^{\cdot}$. Because the RAFT agents are designed to be reactive, most or nearly all of the added RAFT agent (1) reacts reversibly with the oligomeric radicals, $P_n^{\cdot}$, to form the intermediate radical (2) that can undergo fragmentation to produce a dormant polymer chain (3) along with another radical, $R^{\cdot}$. At this point, reinitiation occurs where additional monomer reacts with the new

radical, R·. Polymer chains will then grow larger as more monomer is added, but crucially, these new chains react with the RAFT agent-capped dormant chains (4) in the step labeled "chain equilibrium" in figure 3.2. Because the radical is tied up in this equilibrium reaction, termination events are limited, all polymer chains theoretically have the same probability of reacting with a radical, and all of the unique aspects of the RAFT process (low polydispersity, control over molecular weight, RAFT end groups on polymer chains) are observed.

In summary, the RAFT polymerization technique was chosen for this work because of the flexibility it offers with respect to monomer choice, and critically, RAFT allows for facile assembly of block copolymers. RAFT offers the ability to produce polymeric materials with gold-reactive and Diels-Alder reactivity at multiple blocks. Additionally, the RAFT process produces polymers with polydispersities lower than 1.2. In relation to the metamaterial structure proposed in Chapter 2, such capabilities allow for consistent and tunable gap lengths[9] between functionalized gold nanorods while introducing attachment points for nonlinear optical dyes.

3.2 Synthesis of Thiol-Functionalized PMMA

Figure 3.3 shows the first example of a gold-reactive polymer synthesized in this work and a depiction of GNRs functionalized with thiol polymers. First, methyl methacrylate was polymerized using azobisisobutyronitrile (AIBN) as the radical initiator and 2-cyano-2-propyl dodecyl trithicarbonate as the RAFT agent. As noted previously, the type of RAFT agent used should be one that is compatible with a desired class of monomer. Many RAFT agents work well with acrylic monomers available from commercial sources and we chose one that was adaptable to a variety of different monomer classes. This first block of PMMA was not used as a functional center but rather as robust block that

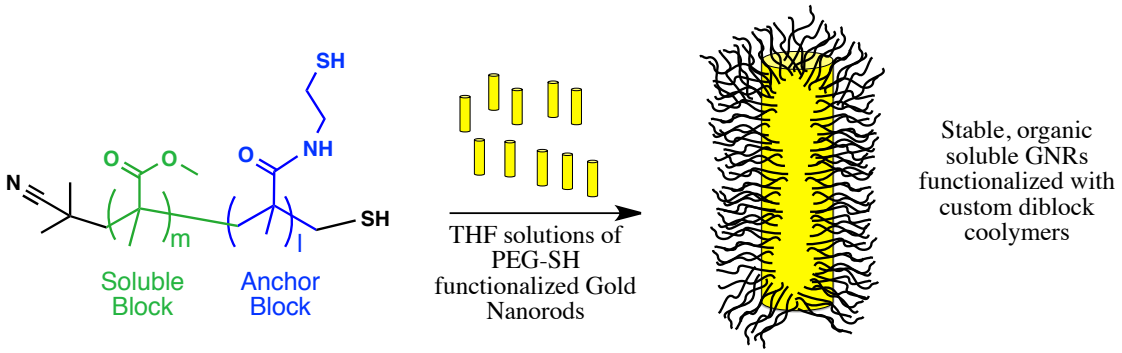


Figure 3.3. Summary of GNR functionalization process. GNRs coated in mPEG-SH react with thiol-containing polymer to produce stable organic solutions of GNRs.

contributes to high solubility in organic solvents. The first block is also referred to as the macroinitiator. It contains the RAFT agent at the end of

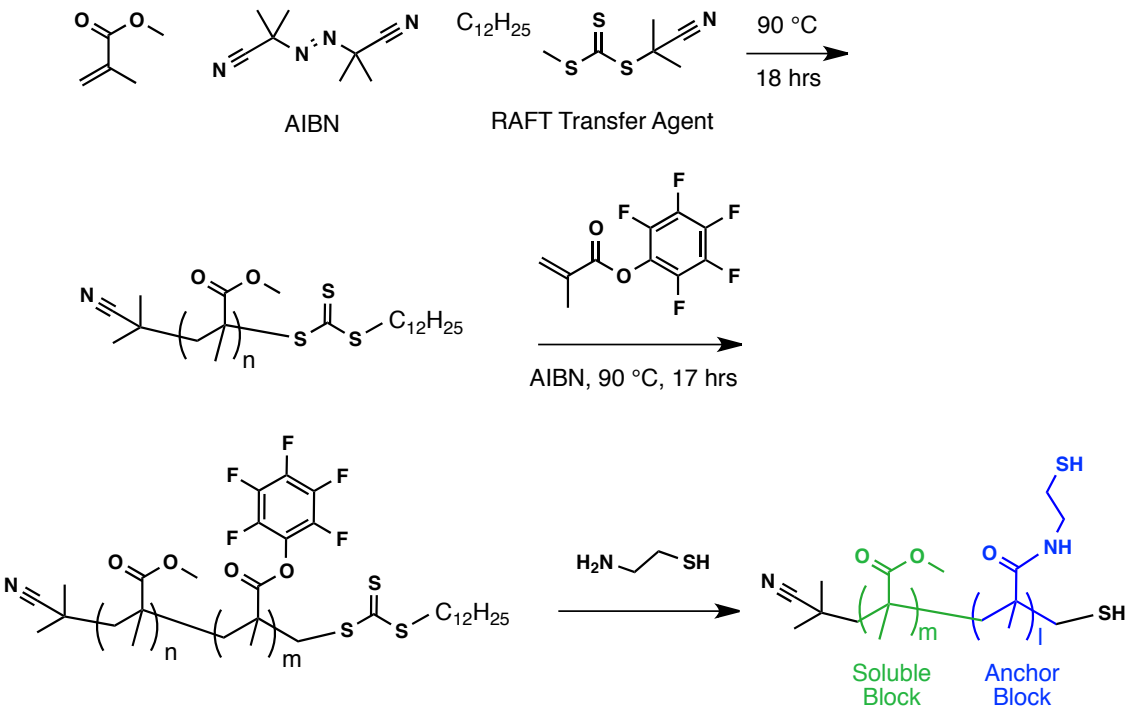


Figure 3.4. Synthesis of thiol-containing diblock copolymer

the chain and acts as the initiation site for additional polymerization with another monomer of choice and the same radical source (AIBN).

Pentafluorophenyl methacrylate was polymerized with the PMMA macroinitator to introduce the second polymer block. Pentafluorophenyl methacrylate was chosen because of its stability during polymerization and its ability for post-functionalization using nucleophiles.[10-12] After isolating the PMMA-co-PPFMA diblock, treating it with cysteamine produced the gold-reactive diblock copolymer, depicted in figure 3.4 as the final product of the synthesis scheme. This simple diblock copolymer was the first candidate used to functionalize GNRs and solubilize them in organic solvents. Chapter 4 will discuss the GNR functionalization process in detail.

3.3 Synthesis of Furan and Anthracene Polymer Derivatives: Scaffolds for Introduction of Nonlinear Organic Dyes

After the synthesis of the basic PMMA/Cysteamine diblock, efforts were focused towards the synthesis of polymers that contained Diels-Alder reactivity. Much research has focused on the utility of polymerizing Diels-Alder functional groups. Attachment of a desired compound can be achieved post-polymerization or the polymer may be reversibly or irreversibly cross-linked by the addition of an external linker molecule.[13-17] We intended to use similar chemistry to attach maleimide-functionalized chromophores to GNRs using Diels-Alder functional groups previously engineered into the polymers

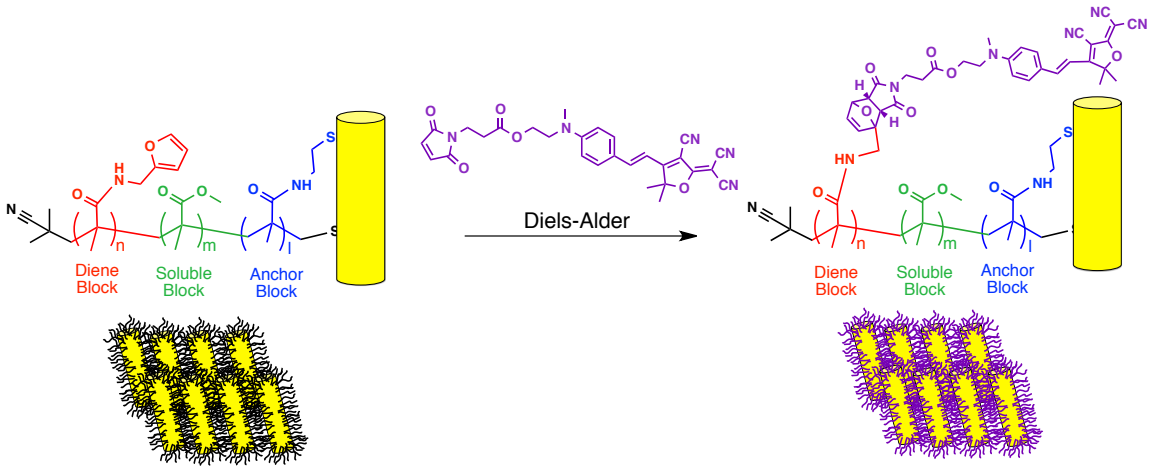


Figure 3.5. Ideal GNR-dye hybrid after Diels-Alder reaction between functionalized GNR and nonlinear organic dye.

attached for solubilizing the GNRs in organic solvents. This strategy was designed so that a furan monomer or an anthracene monomer would be effective candidates to introduce dienes in the polymer while maleimide

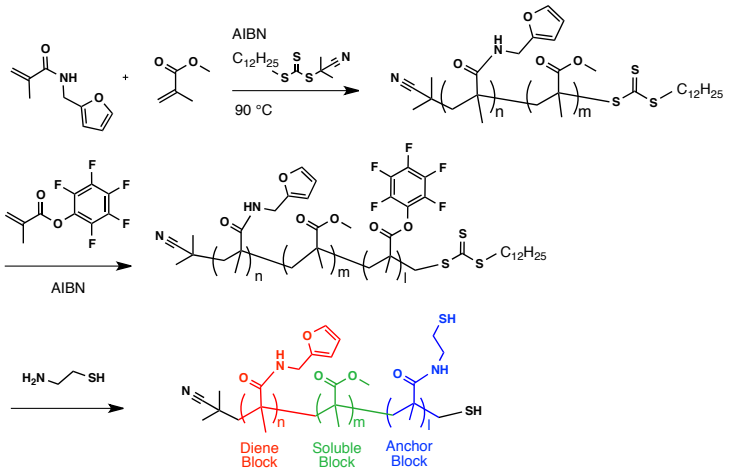


Figure 3.6. Synthesis of methacrylamide version of gold-reactive polymer that also contains Diels-Alder functionality.

functionality would be introduced as the dieonophile on nonlinear organic chromophores. Figure 3.5 depicts an ideal hybrid of dye, gold nanorod and polymer using a furan-containing polymer. Furan functionality provides a reversible Diels-Alder adduct while anthracene provides an irreversible adduct. Both furan[18,19] and anthracene[20,21] polymers were derived from methacrylate monomers and have literature precedence for successful polymerization. We again used acrylic monomers because they are well suited for the chosen RAFT agent.

3.3.1 Synthesis of Furan Polymer Derivative

The first candidate for furan functionality was produced from furfuryl methacrylamide. This monomer was synthesized from furfuryl amine and methacryloyl chloride. Methyl methacrylate and furfuryl methacrylamide were then polymerized together at a specified molar ratio using the typical

RAFT protocol to form a random copolymer (RL64, 65). With Diels-Alder reactivity introduced, pentafluorophenyl methacrylate was polymerized with RL64 followed by replacement of the pentafluorophenyl group with cysteamine to produce a gold-reactive, furan-containing polymer, shown in figure 3.3. Eventually, furfuryl methacrylamide was replaced by furfuryl methacrylate because of commercial availability and low cost. Furfuryl methacrylamide was similarly polymerized together with methyl methacrylate but at a specified molar ratio of sixty percent furfuryl

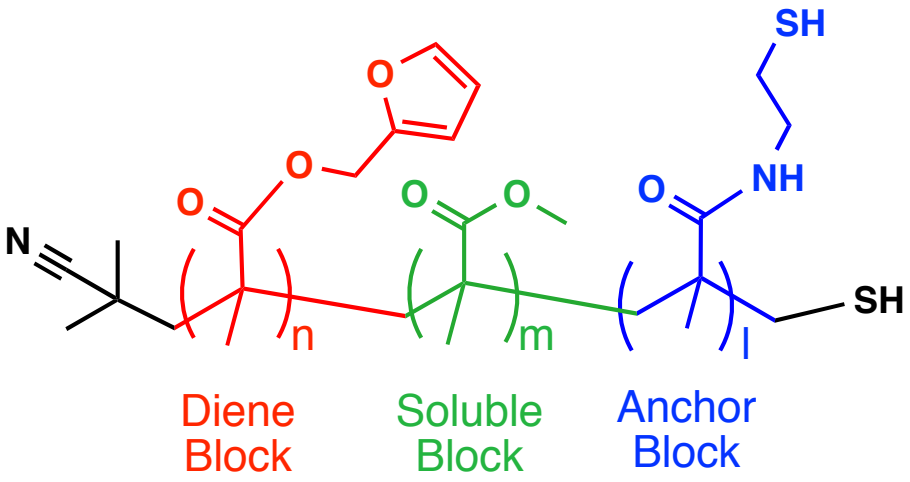


Figure 3.7. Revised version of gold-reactive, furan-containing polymer using furfuryl methacrylate rather than furfuryl methacrylamide.

methacrylate to 40 percent methyl methacrylate. ^{1}H NMR indicated the molar ratio to be very close to what was predicted with 38 percent of the polymer consisting of methyl methacrylate. The copolymer of PMMA and poly(furfuryl methacrylate) was then polymerized with pentafluorophenyl

methacrylate and treated with cysteamine to produce the gold-reactive furfuryl methacrylate polymer derivative depicted in figure 3.7

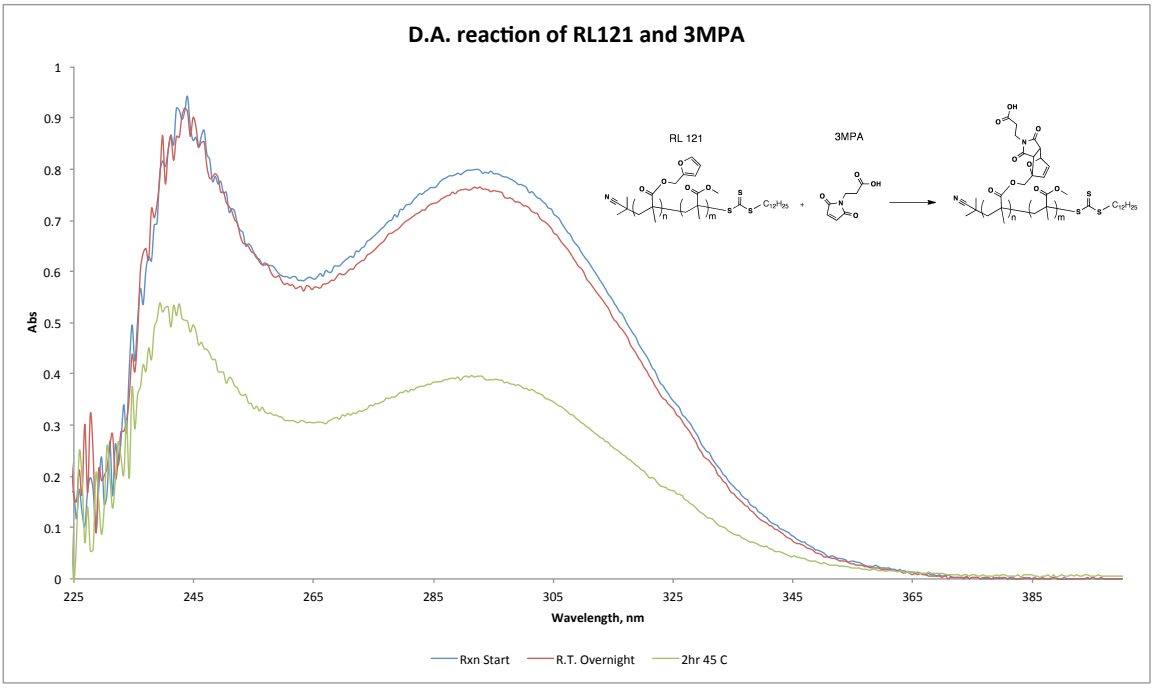


Figure 3.8. Diels-Alder reaction between furan-containing RL121 and 3MPA. As the Diels-Alder reaction proceeds, the distinct absorption peak of RL 121 at 290 nm decreases dramatically.

In order to investigate the feasibility of Diels-Alder reactivity, one equivalent (relative to furan monomer) of RL121 was left to react at room temperature overnight with two equivalents of 3-(maleimido)propionic acid (3MPA). 3MPA was used in place of a full dye in order to simplify the absorption spectrum and quickly test the Diels-Alder capabilities of a furan-containing polymer. The furan group on RL121 has a distinct absorption near 290 nm due to its aromatic structure. As a Diels-Alder reaction proceeds, the absorption at 290 nm of the furan group should start to

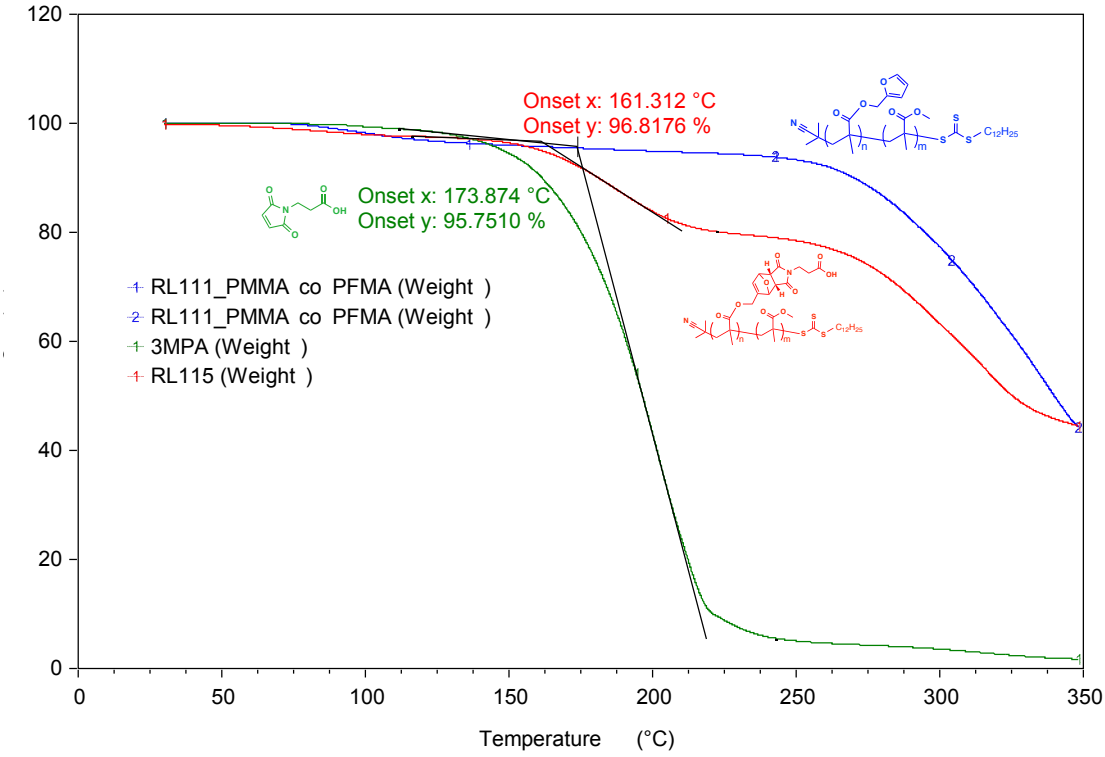


Figure 3.9. TGA of Diels-Alder adduct RL115. Pure 3MPA has a distinct decomposition temperature near 170 °C while pure PMMA-co-PFMA shows 275 °C. The Diels-Alder adduct of 3MPA and PMMA-co-PFMA shows loss of mass at 160 °C and 275 °C indicating the loss of 3MPA in a retro Diels-Alder reaction.

decrease as the conjugation is broken after the formation of a Diels-Alder adduct.[22] Very little absorption change was observed after reacting overnight at room temperature. However, after heating the same reaction mixture for two hours at 45 °C, a large decrease in absorbance was observed, as shown in Figure 3.8, indicating successful Diels-Alder adduct formation. The additional heat needed for this reaction to proceed is not unusual, as the formation of a Diels-Alder adduct between furan and maleimide is still favorable up to 60°C.[22,25,26]

3.3.1a Thermogravimetric Analysis of Diels-Alder Adducts. Thermogravimetric analysis (TGA) was used in further studies to investigate the Diels-Alder reaction between 3MPA and PMMA-co-PFMA polymer. TGA allows for the precise measurement of mass loss as a compound is heated at a specified rate and is often used to study the thermal stability of polymers. The adduct of 3MPA and PMMA-co-PFMA (RL115)

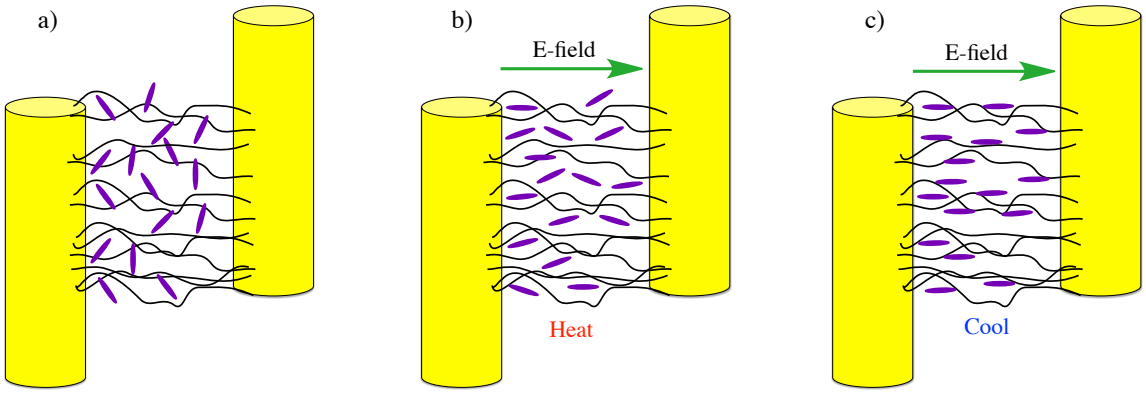


Figure 3.10. An schematic illustration showing ideal poling of a GNR-polymer-dye hybrid. After functionalizing gold GNRs with polymer and dye, an electric poling field can be used to orient the dyes accentrically in order to produce a non-linear active material. Furthermore, using a reversible Diels Alder adduct may increase chromophore mobility during the heating step.

was analyzed by TGA and compared to the results of pure 3MPA and PMMA-co-PFMA. Figure 3.9 shows the mass percent vs. temperature of these three compounds. Pure 3MPA has a reasonably sharp onset of mass loss near 170 °C. The Diels-Alder adduct shows a similar but broader onset temperature. This result may indicate that the 3MPA is being detached from the polymer via a retro-Diels Alder reaction.[23] The adduct also shows mass

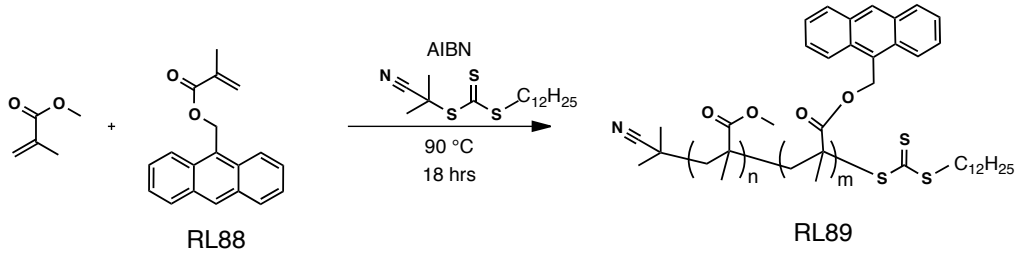


Figure 3.11. RAFT Co-polymerization of methyl methacrylate and 9-Anthracenylmethyl methacrylate

loss similar to that of pure PMMA-co-PFMA. These results further support the hypothesis that a Diels-Alder reaction between a maleimide-containing dye and a furan-containing polymer should be successful. The furan monomer was chosen because of its ease of synthesis and the fact that a reversible Diels-Alder reaction maybe be beneficial during the poling process. Detailed in figure 3.10, as the GNR-polymer-dye hybrid is heated to the polymer glass transition temperature, the nonlinear dyes should become mobile and are able to reorient parallel to the DC poling field axis. The temperature increase will also induce a retro Diels-Alder reaction, further mobilizing the chromophores. As the temperature is decreased, the dyes may covalently attach back onto the polymers, now oriented accentrically.[17] Diels-Alder reversibility may also be eliminated in case such back reactions become difficult to control. To achieve this capability, tuned electron density diene monomers, such as the more reactive 9-anthrylmethyl methacrylate were synthesized to replace the furan monomer and will be discussed in the next section.

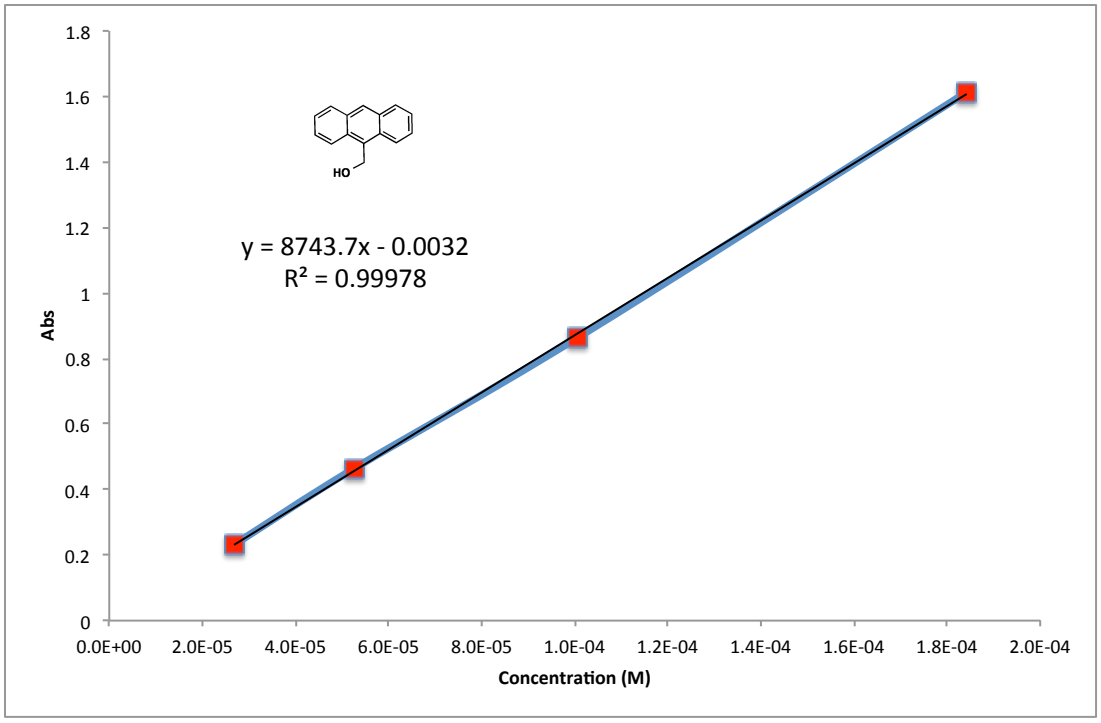


Figure 3.12. Calibration curve using 9-Anthracene methanol. Absorption was monitored at 367 nm.

3.3.2 Anthracene Polymer Derivative

9-Anthracene methanol was reacted with methacryloyl chloride to produce 9-Anthracenylmethyl methacrylate (RL 88). In the typical fashion, RL88 was polymerized, in the presence of a RAFT agent, with methyl methacrylate to produce a random copolymer of poly(methyl methacrylate) and poly(9-Anthracenylmethyl methacrylate) (PAnMMA) (RL89). The synthesis scheme is given in figure 3.11. In order to calculate how much organic dye we could attach to the polymer, a calibration curve for the anthracene group was made using solutions of 9-Anthracene methanol as seen in figure 3.12. Using this curve, data showed that RL89 consisted

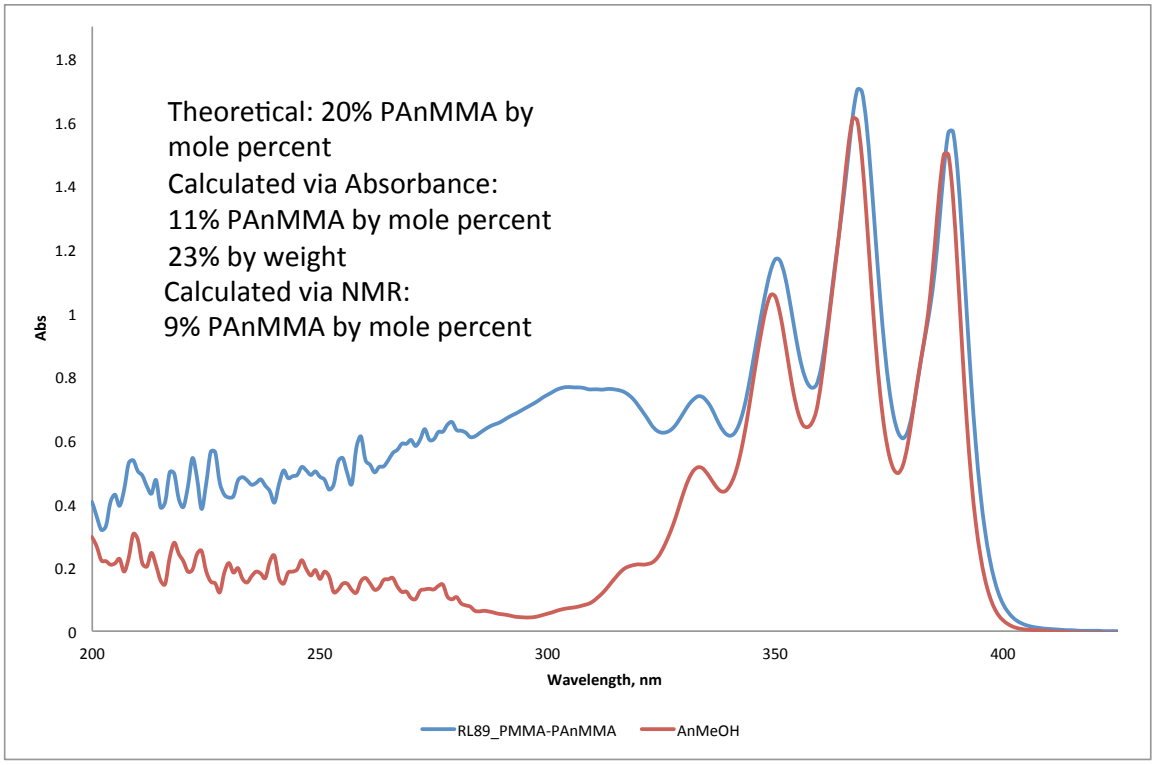


Figure 3.13. Absorption spectra of PMMA-co-PAnMMA compared to that of 9-Anthracene methanol.

of 11% 9-Anthracenylmethyl methacrylate by mole percent, approximately half of the theoretical value of 20%. By NMR, 9-anthracenylmethyl methacrylate content was calculated to be 9%. Figure 3.13 summarizes these data and shows the absorption spectra of RL89 polymer compared to 9-Anthracene methanol in tetrahydrofuran.

Similar to the furan derivative, the Diels-Alder reaction between an anthracene group and a maleimide group was be monitored using UV/visible absorption. A slight molar excess of 3MPA was dissolved in dioxane with RL89 and left to react for two hours at 90 °C. Figure 3.14 displays the distinctive absorption profile of the anthracene functional group decreasing

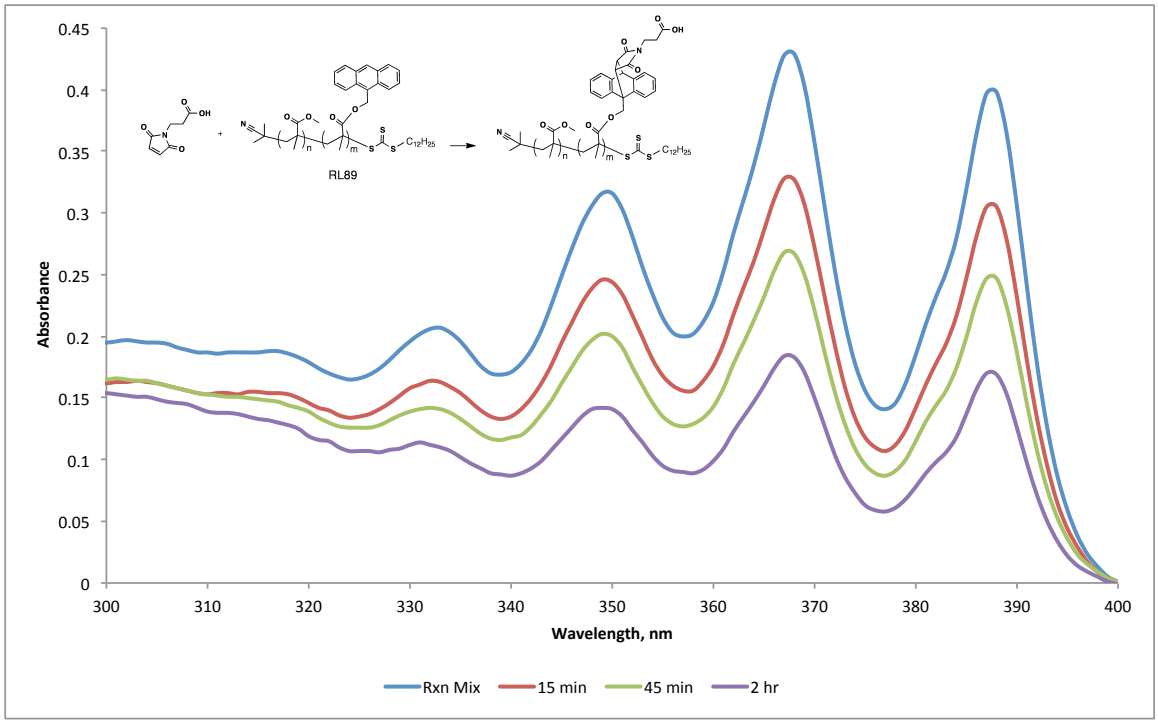


Figure 3.14. Diels-Alder reaction of 3MPA with copolymer of poly(methyl methacrylate) and poly(9-Anthracenylmethyl methacrylate). After reacting for 2 hours at 90 °C, a significant loss of anthracene absorption is observed.

as the reaction progresses. These results indicate that an organic dye functionalized with a maleimide group should be a promising candidate for a Diels-Alder reaction with PAnMMA. Ideally, both the furan and anthracene polymer derivatives could be attached to gold nanorods and then allowed to react with maleimide-containing nonlinear dyes to form the desired hybrid described in the modeling results from Chapter 2 of this thesis.

3.4 Synthesis of Gold-Reactive Polymer Derived From a Lipoic Acid Monomer

The first strategy to synthesize gold-reactive polymers involved post-functionalization by converting an already polymerized pentafluorophenyl ester into an acrylamide using cysteamine. This method was chosen because of the literature precedent that produced RAFT polymers and successful post-functionalization results.[1,2,11] However, after functionalization with cysteamine, the resulting polymer at times became an insoluble gel. The likely reason for this result was that a disulfide linkage formed in the presence of O_2, leading to an insoluble cross-linked network. Even when care

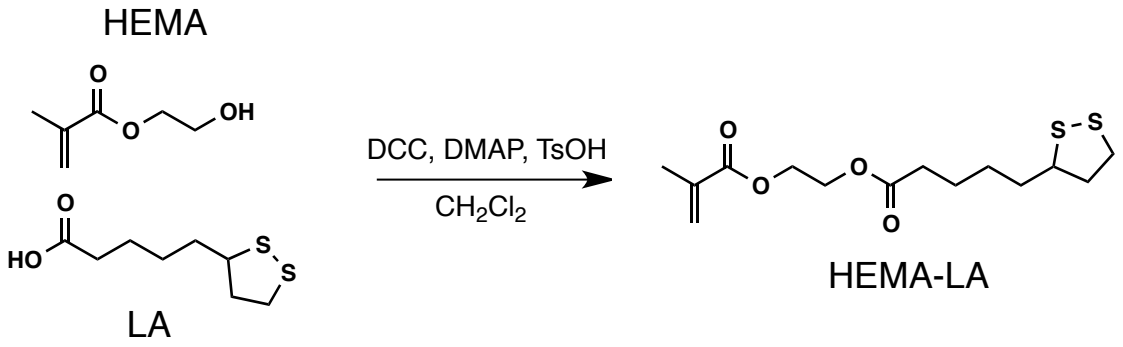


Figure 3.15. Synthesis of gold-reactive monomer, HEMA-LA. Lipoic acid and hydroxyethyl methacrylate were coupled using *N,N'*-dicyclohexylcarbodiimide and 4-dimethylaminopyridine as a catalyst

was taken to keep oxygen out of the reaction, on rare occasions the resultant product was no longer soluble and usable for GNR functionalization. To

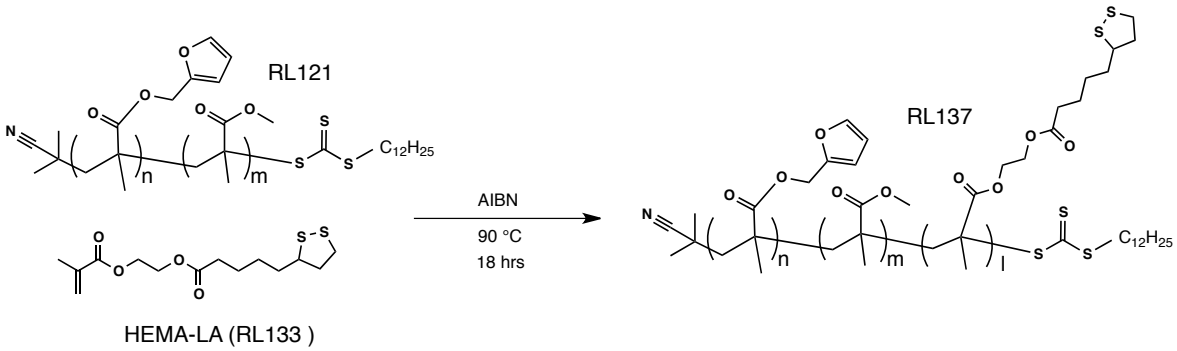


Figure 3.16. Synthesis of RL137. HEMA-LA monomer is polymerized from the RAFT end group on RL121 to produce a novel polymer with Diels-Alder reactivity and a gold-reactive anchor block.

avoid these issues, and to avoid reliance on a post-functionalization strategy, an alternative gold-reactive polymer was sought in the literature. Chen, *et al.* used the RAFT technique and copolymerized a charged monomer and the methacrylate monomer derived from lipoic acid to produce water-soluble gold-reactive polymers. Lipoic acid contains a disulfide bond that, under RAFT conditions, is stable during polymerization and because it is already reduced, poses much less risk for crosslinking during the reaction or during storage afterwards. To produce the desired monomer, lipoic acid (LA) and hydroxyethyl methacrylate (HEMA) were coupled using *N,N′*-dicyclohexylcarbodiimide as shown in figure 3.15. The resulting monomer, HEMA-LA, was polymerized with RAFT terminated PMAA-*co*-PFMA (**RL137**) to generate the novel Diels-Alder and gold-reactive polymer shown in figure 3.16. Attempts at functionalizing gold-nanorods with this and other thiol-containing polymers will be discussed in Chapter 4.

3.5 Conclusion

In this chapter, thiol-containing polymers were prepared with the goal of functionalizing gold nanorods. The polymer shell will solubilize gold nanorods in organic environments such as solvents or viscous polymer sultions. Additional polymers were also prepared that contain Diels-Alder reactive groups. Functionalizing gold nanorods with these polymers allows for attachment points for nonlinear organic chromophores. The Diels-Alder reactivity of both furan and anthracene polymer derivatives was studied using UV/visible absorption spectroscopy and thermogravimetric analysis. The results show that the polymers should be reactive towards organic compounds containing maleimide groups. Functionalizing organic chromophores with maleimide groups should allow for attachment to gold nanorods coated in Diels-Alder polymers.

Chapter 4 will discuss efforts towards the synthesis of gold nanrods and the methods required to functionalize them with the thiol-containing polymers described in this chapter.

3.6 Experimental Section

3.6.1 Materials and General Procedures

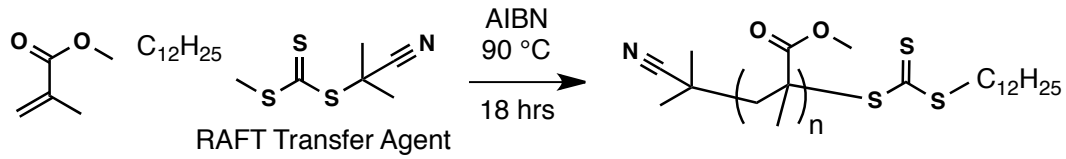
Methyl methacrylate (Aldrich) was purified by distillation at 50 °C under reduced pressure to remove the radical inhibitor. The inhibitor was

extracted from Pentafluorophenyl methacrylate (Aldrich, 95%) with activated charcoal and Azobisisobutyronitrile (AIBN) (Aldrich, 98%) was recrystallized from methanol before use. 2-cyano-2-propyl dodecyl trithicarbonate (Aldrich, 97%) and Cysteamine (Aldrich, >98%) were used as received. THF was dried over sodium metal and benzophenone.

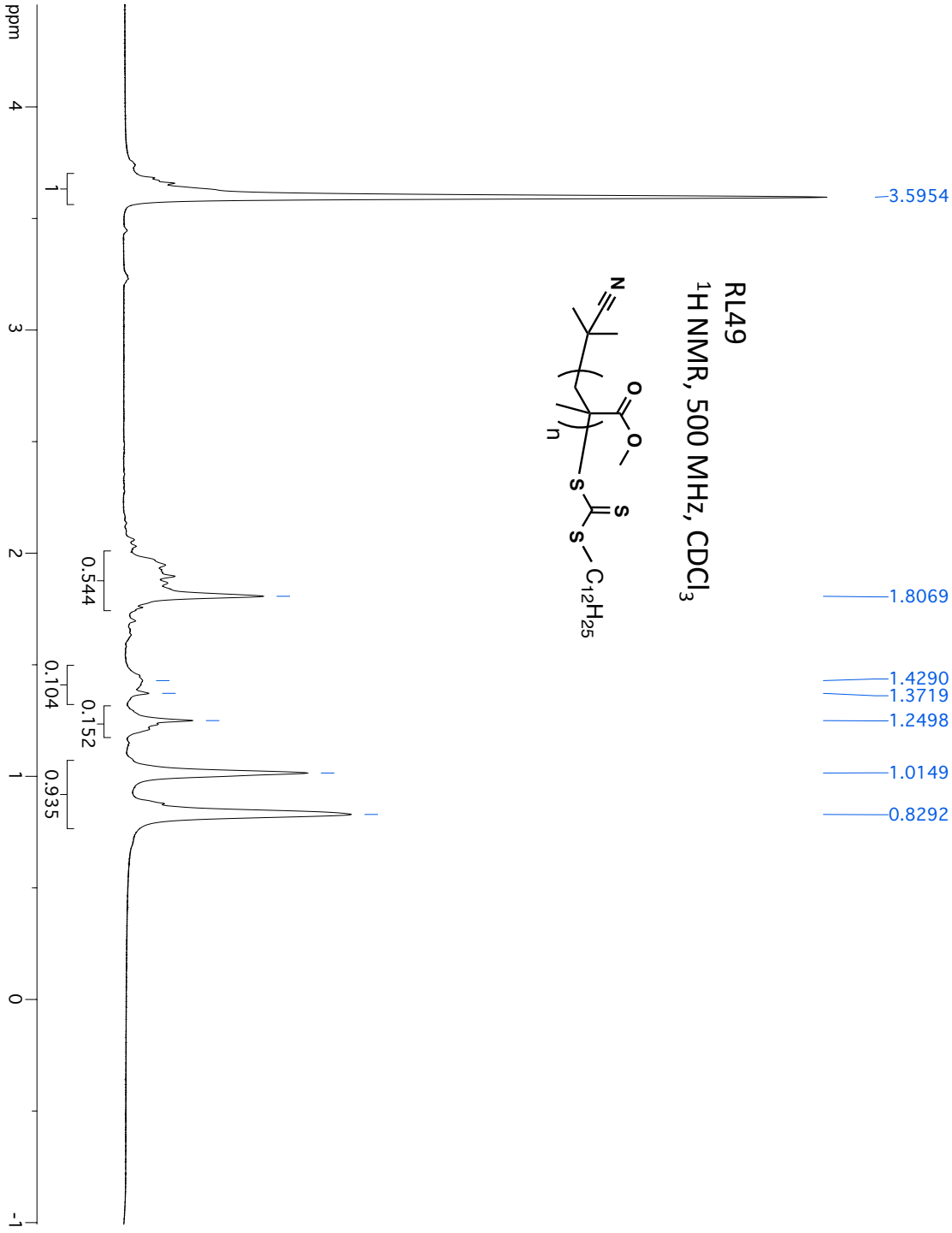
^{1}H NMR spectra were recorded on a Bruker DRX500 (500 MHz, 1H) or a Bruker DRX300 (300 MHz, 1H). Chemical shifts (δ) are reported in ppm, employing the solvent resonance as the internal standard. Splitting patterns are designated as: s (singlet), d (doublet), t (triplet), dd (doublet of doublets), m (multiplet), and bs (broad singlet). Coupling constants (J) are reported in hertz (Hz). Ultraviolet-Visible (UV-Vis) spectra were recorded on a Shimadzu UV-2101PC or an Ocean Optics USB2000+. MALDI was obtained on a Bruker MALDI-TOF. Thermogravimetric analysis was performed using a TA Instruments Discovery TGA. Typical experiments were run at 20°C per minute. Uv/Vis spectra were obtained using either an Ocean Optics USB2000+ or a Shimadzu UV2400.

3.6.2 Experimental Procedures and Spectra

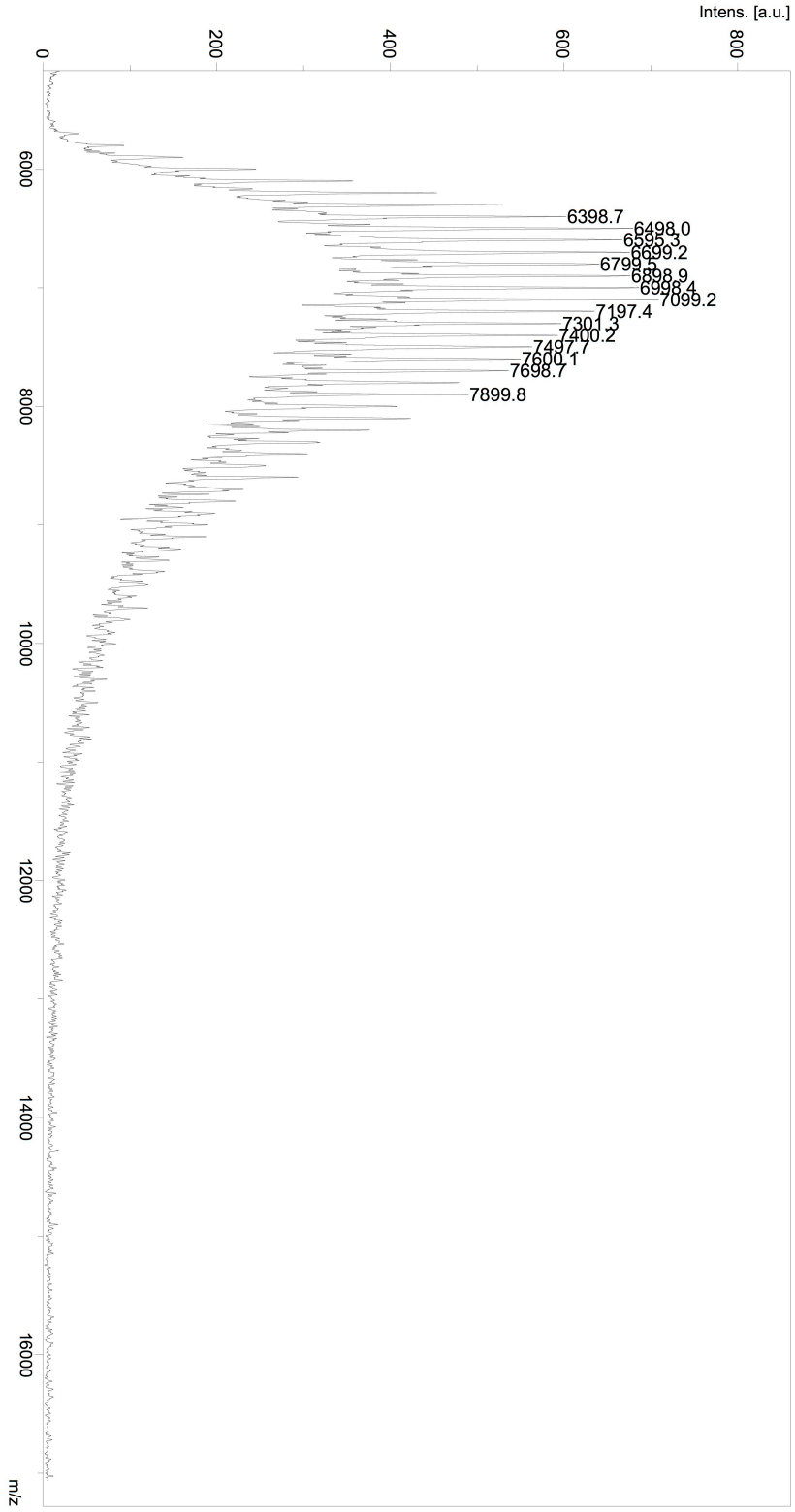
Synthesis of poly(methyl methacrylate) macroinitiator (RL49)



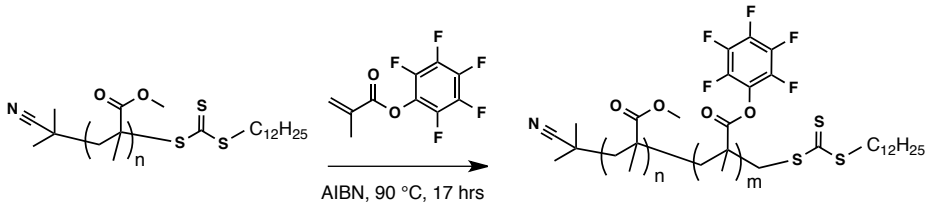
A Schlenk tube was charged with methyl methacrylate (5.0 g, 1 eq), 2-cyano-2-propyl dodecyl trithiocarbonate (RAFT agent) (350.0 mg, 0.0203 eq) and azobisisobutyronitrile, (21.8 mg, 0.0026 eq) A small portion (~2 mL) of benzene was used to wash the sides of the tube. Oxygen was exchanged with nitrogen by 3 freeze-pump thaw cycles. After allowing the tube to warm to room temperature, the tube was placed in a 90 °C oil bath and allowed to react for 18 hours. The resulting polymer was dissolved in 5 mL THF and added dropwise to 500 mL of stirring methanol. The precipitated polymer was filtered, redissolved in THF, purified in the same manner two additional times, and dried under vacuum to yield 2.933 g (58%). ^{1}H-NMR (500 MHz; DMSO-d_6): δ 3.60 (s, 3H), 1.81 (m, 2H), 1.40 (m,), 1.25 (s, 1H), 1.01 (s, 1H), 0.83 (s, 2H).


RL49
^{1}H NMR, 500 MHz, CDCl$_3$
3.5954
1.8069
1.4290
1.3719
1.2498
1.0149
0.8292
1
0.544
0.104
0.152
0.935
ppm
4
3
2
1
0
-1

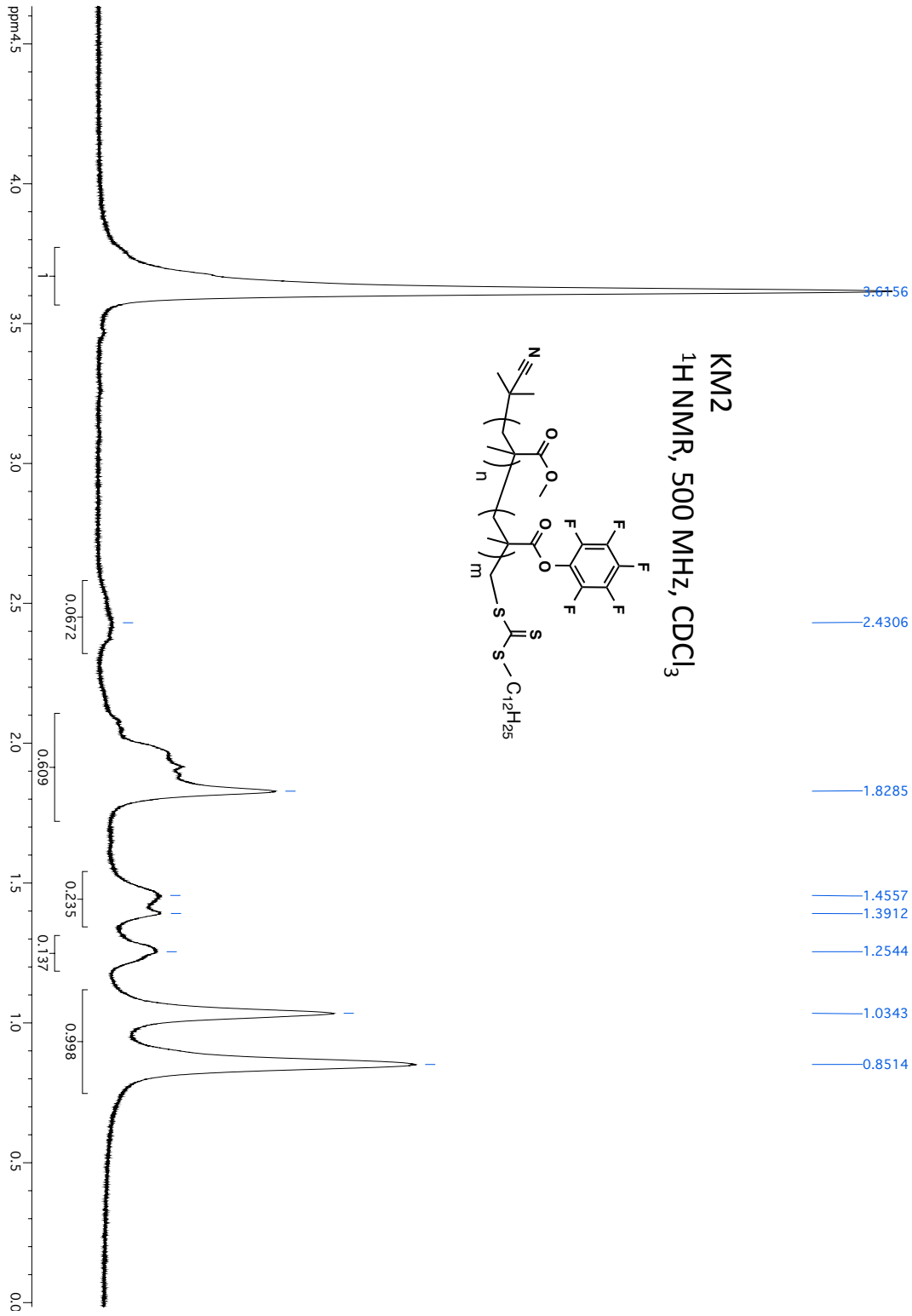
MALDI-TOF spectrum of RL 49



Synthesis of reactive diblock copolymer (KM2) (Figure 3.4)



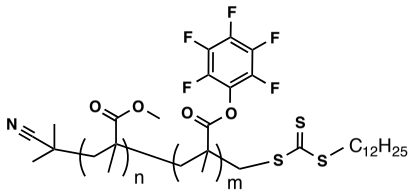
Schlenk tube was charged with 0.5 g of previously synthesized PMMA macroinitiator, 0.4182 (1.67 mmol) g of pentafluorophenyl methacrylate, and 1 mg azobisisobutyronitrile. After three pump-thaw cycles, the tube was placed in a 90 °C oil bath and left to react overnight. The resulting diblock copolymer was purified by precipitating dissolving in ~ 2 mL of THF and precipitating in hexanes three times to yield 0.5373 g. ^{1}H-NMR (500 MHz; $CDCl_3$): δ 3.62 (s, 3H), 2.43 (s,), 1.83 (m, 2H), 1.42 (m, 1H), 1.25 (s,), 1.03 (s, 1H), 0.85 (s, 2H). ^{19}F NMR (282 MHz; $CDCl_3$): δ -150.8, -156.7, -161.9

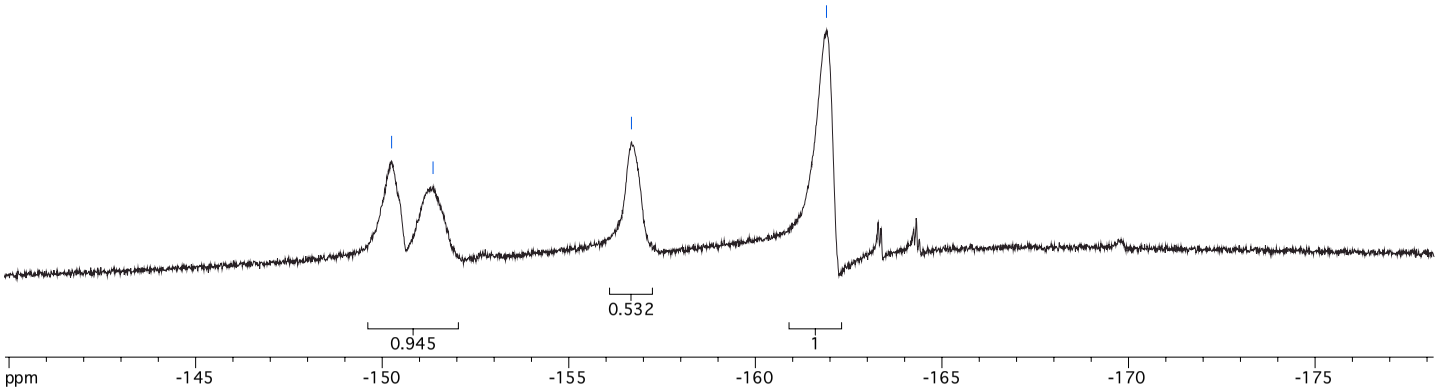

KM2
^{1}H NMR, 500 MHz, $CDCl_3$
3.6156
2.4306
1.8285
1.4557
1.3912
1.2544
1.0343
0.8514
0.0672
0.609
0.235
0.137
0.998
ppm

150.2519
151.3625
156.6795
161.9062

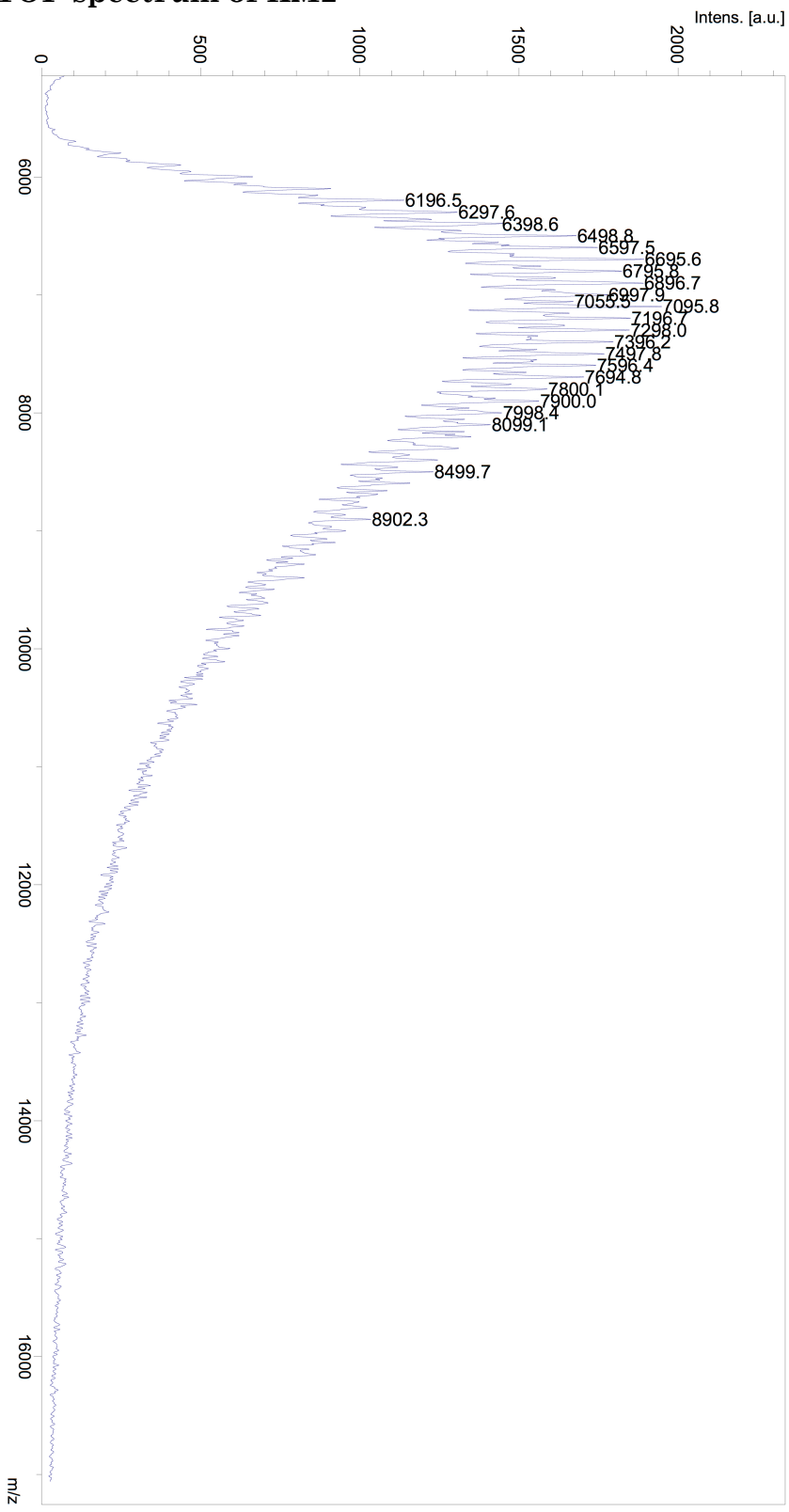
KM2

^{19}F NMR, 300 MHz, $CDCl_3$

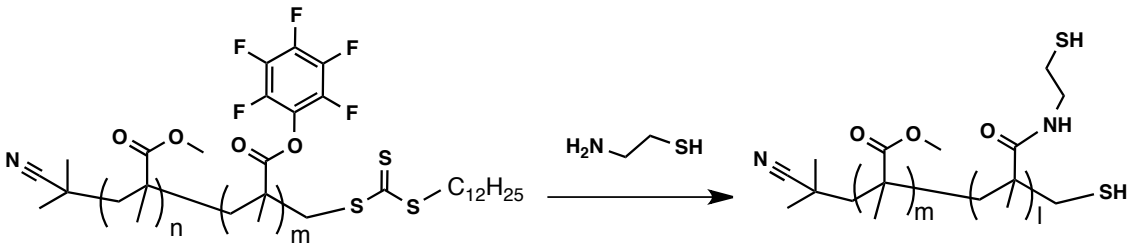




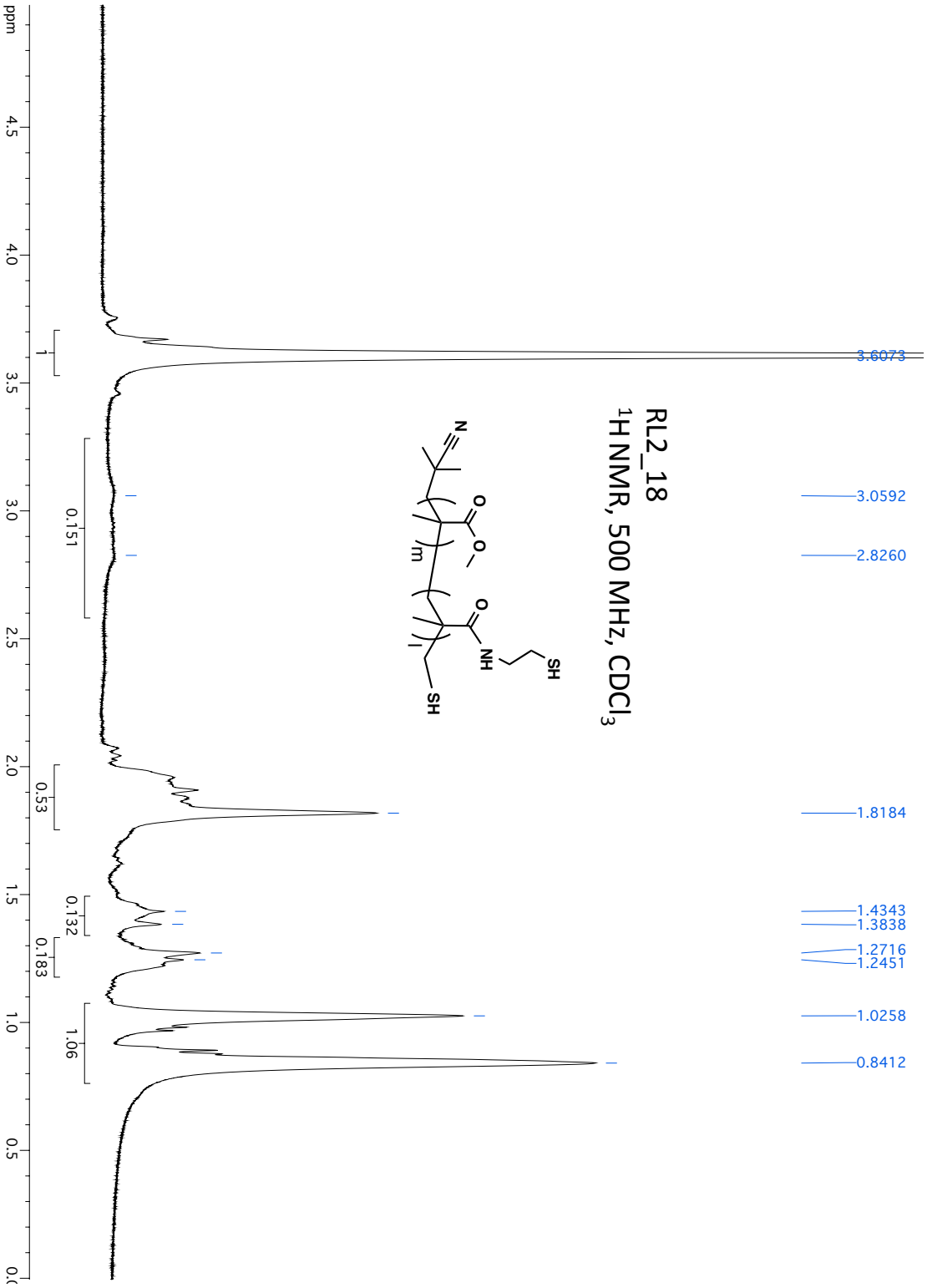
MALDI-TOF spectrum of KM2



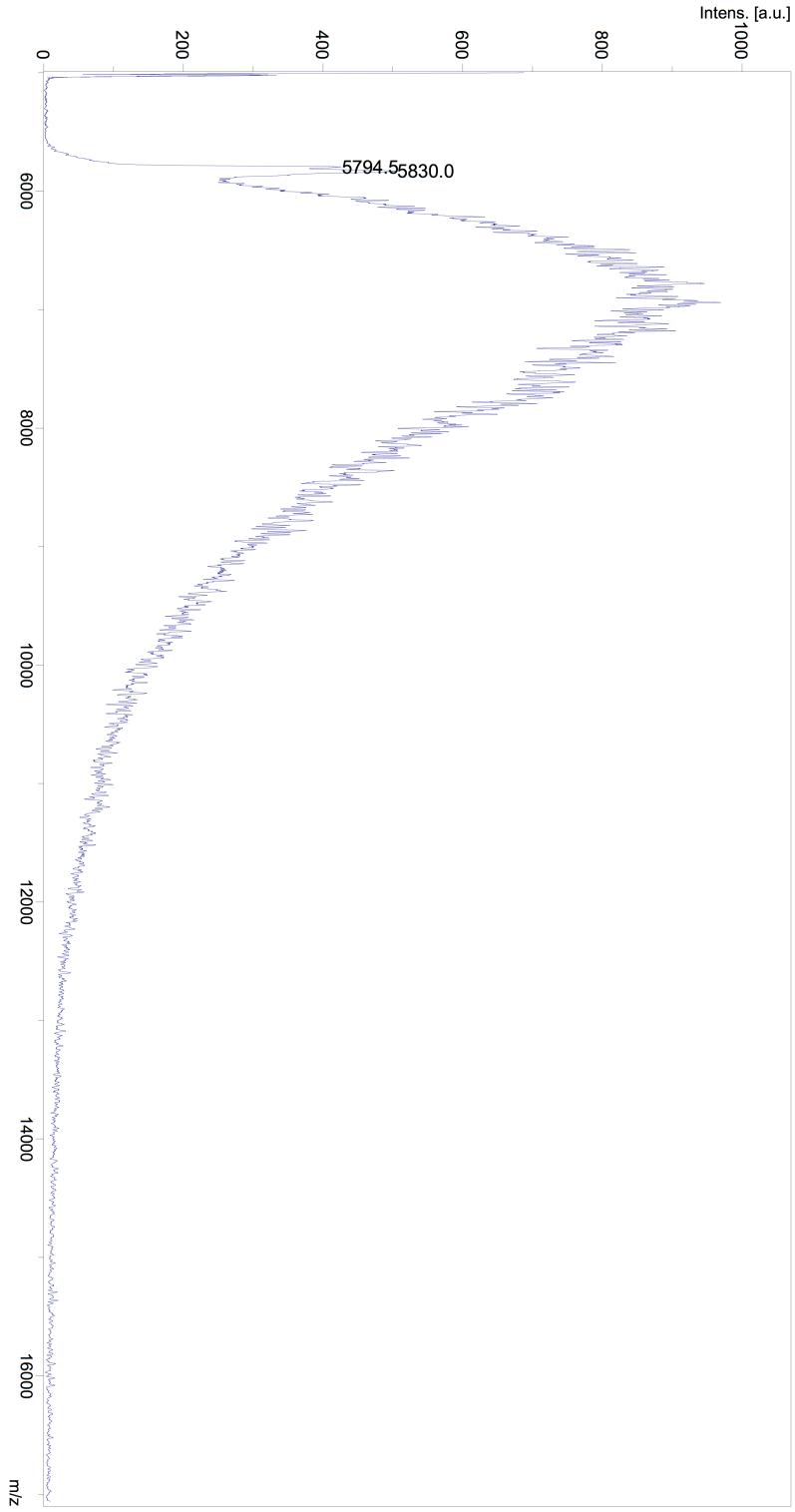
Conversion of diblock to poly(methyl methacrylate-b-cysteamine methacrylamide) (RL2_18) (Figure 3.4)



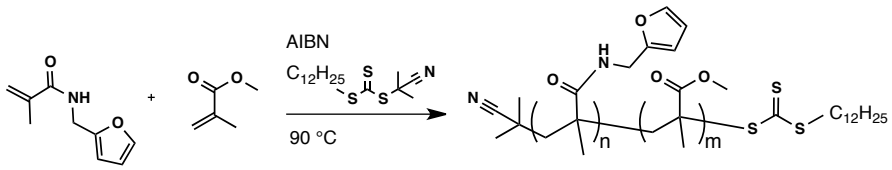
0.5495 g of reactive diblock (KM_2), 0.12 g (1.19 mmol) triethylamine, and 92.00 mg (1.19 mmol) cysteamine were dissolved in a 10 mL round-bottom flask. A small amount of heat was applied to help dissolve the reactants and stirred overnight at room temperature under N_2 atmosphere. The product was added drop-wise to 300 mL of stirring hexanes and collected. 0.4560 g were isolated. ^{1}H-NMR (500 MHz; $CDCl_3$): δ 3.61 (s, 3H), 2.94 (m,), 1.82 (m, 2H), 1.41 (m,), 1.26 (m, 1H), 1.03 (s, 1H), 0.84 (s, 2H).


RL2_18
^{1}H NMR, 500 MHz, CDCl$_3$
ppm
4.5
4.0
3.5
3.0
2.5
2.0
1.5
1.0
0.5
1
0.151
0.53
0.132
0.183
1.06
3.6073
3.0592
2.8260
1.8184
1.4343
1.3838
1.2716
1.2451
1.0258
0.8412
N
O
O
m
O
NH
SH
l
SH

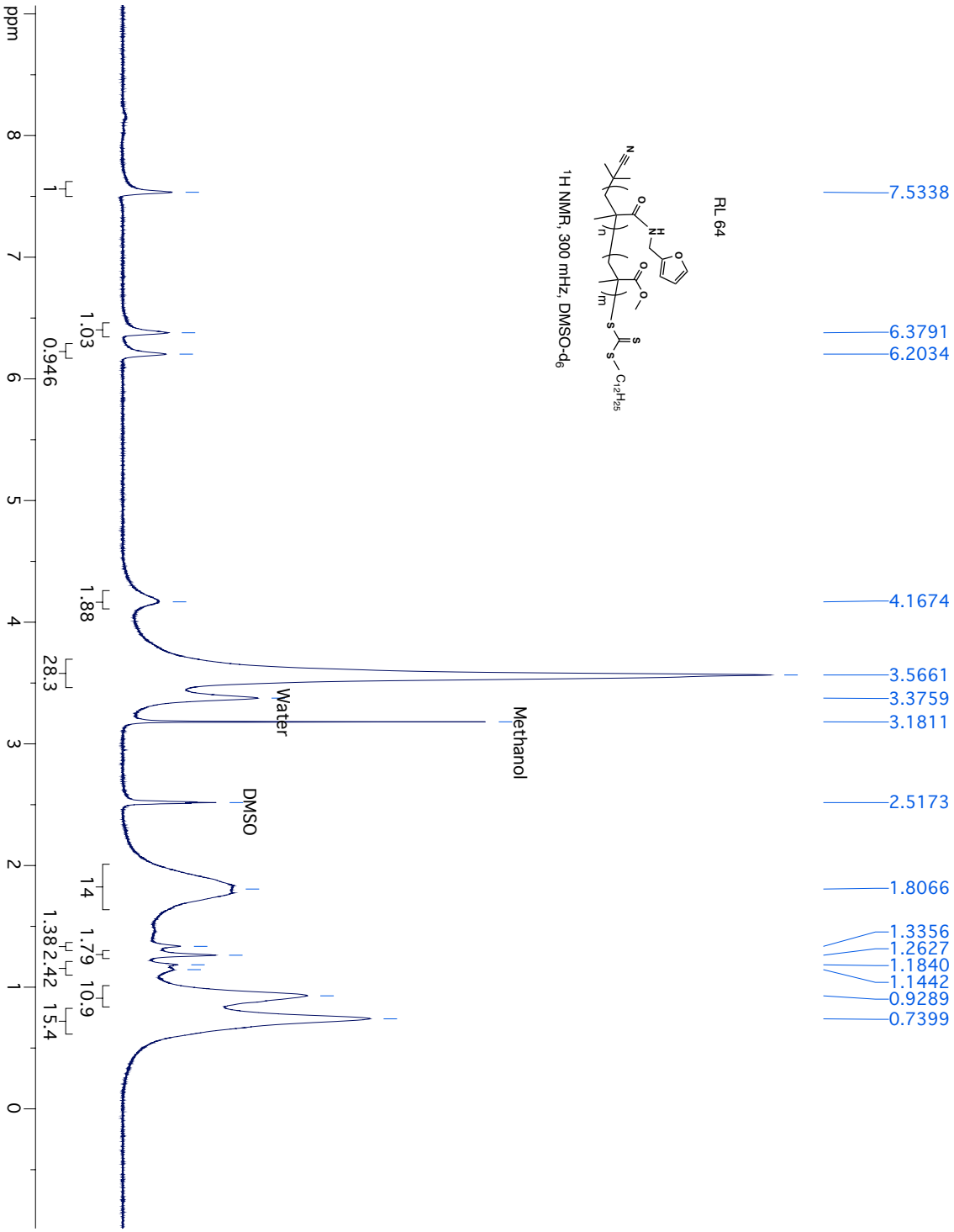
MALDI-TOF spectrum of RL2_18



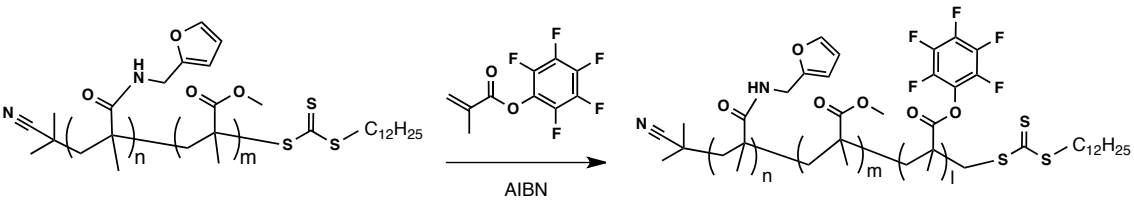
RL64 – Synthesis of poly(methyl methacrylate-co-furfuryl methacrylamide)



Methyl methacrylate (3.770 g, 5 eq), furfuryl methacrylamide (1.2443g, 1 eq), RAFT agent (0.3456 g, 0.022 eq) and azobisisobutyronitrile (19.8 mg) were dissolved in 2 mL benzene and placed in a Schlenk flask. After 3 freeze pump thaw cycles, the flask was filled with nitrogen, sealed, placed in a 90 °C oil bath and left to react for 18 hours. The reaction mixture was diluted with 2 mL tetrahydrofuran and precipitated in 500 mL stirring methanol three times. 1.2260 g (24% yield) of pale yellow polymer was isolated after drying under vacuum. ^{1}H-NMR (300 MHz; DMSO-d_6): δ 7.53 (s, 1H), 6.38 (s, 1H), 6.20 (s, 1H), 4.17 (s, 2H), 3.57 (s, 28H), 1.81 (s, 14H), 1.34 (s, 1H), 1.26 (s, 2H), 1.16 (d, J = 12.0 Hz, 2H), 0.93 (s, 11H), 0.74 (s, 15H).

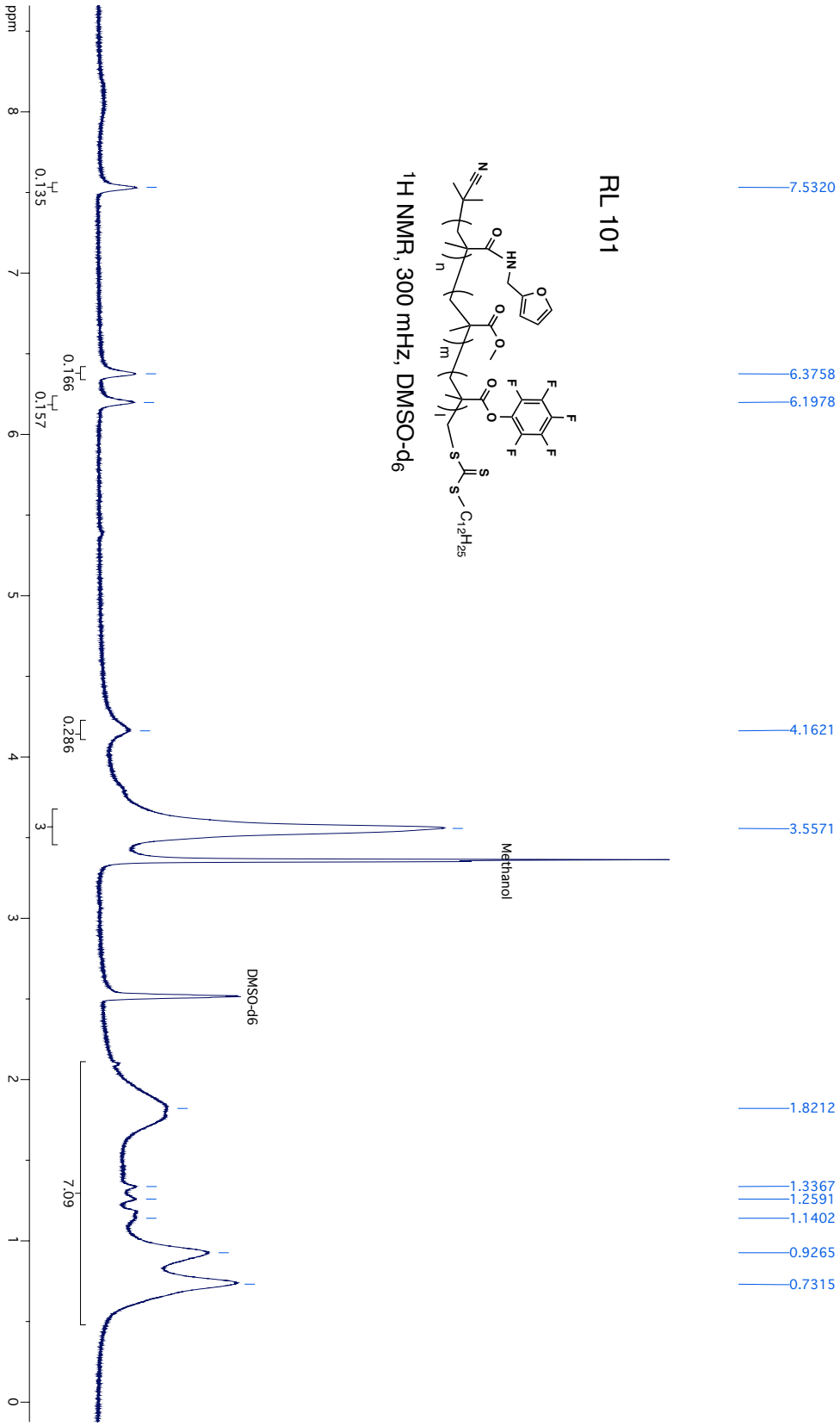

RL 64
^{1}H NMR, 300 mHz, DMSO-d_6
ppm
Water
Methanol
DMSO
7.5338
6.3791
6.2034
4.1674
3.5661
3.3759
3.1811
2.5173
1.8066
1.3356
1.2627
1.1840
1.1442
0.9289
0.7399
1
1.03
0.946
1.88
28.3
14
1.79
1.38
2.42
10.9
15.4

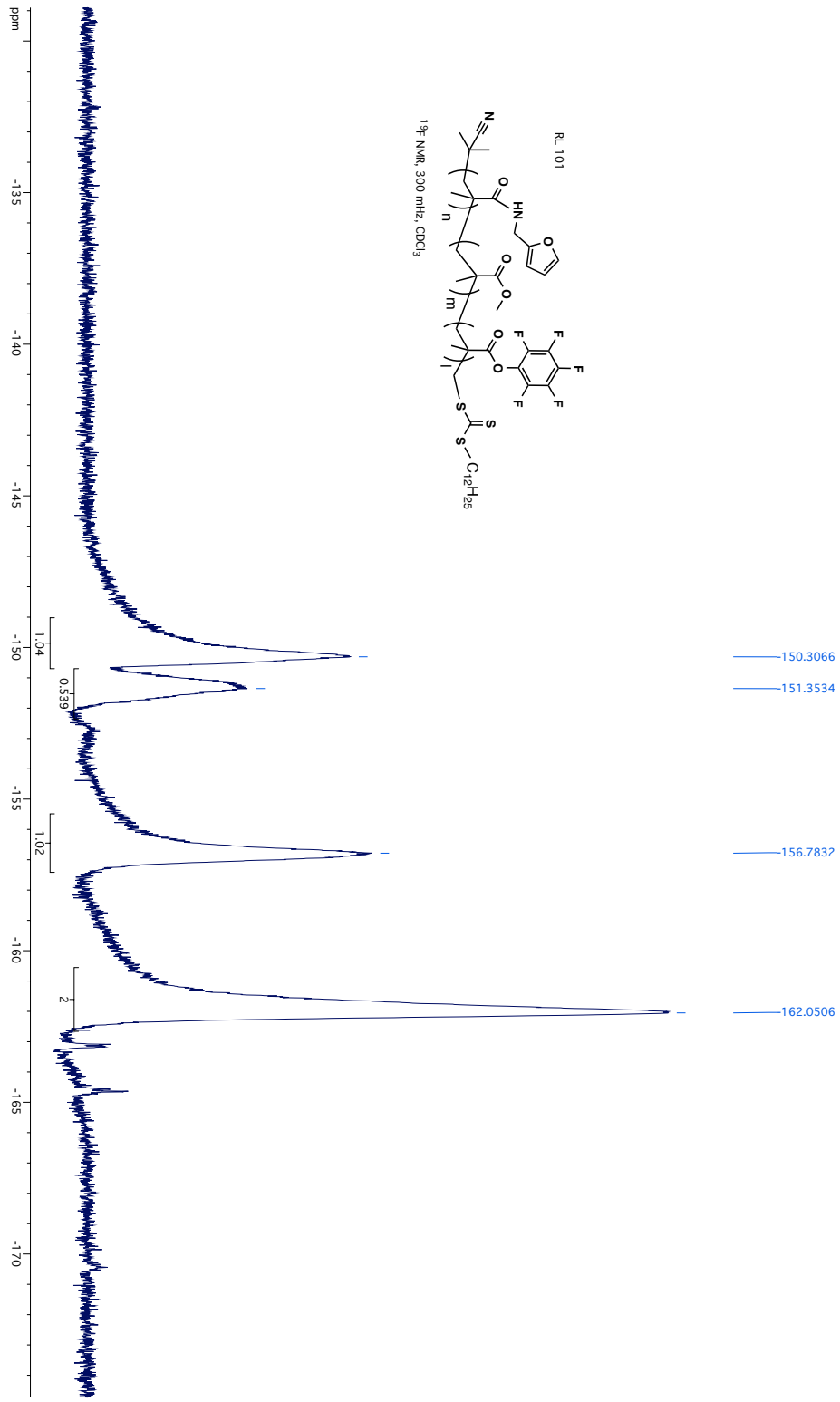
RL101 - PMMA-co-PFMA-b-PFPHMA



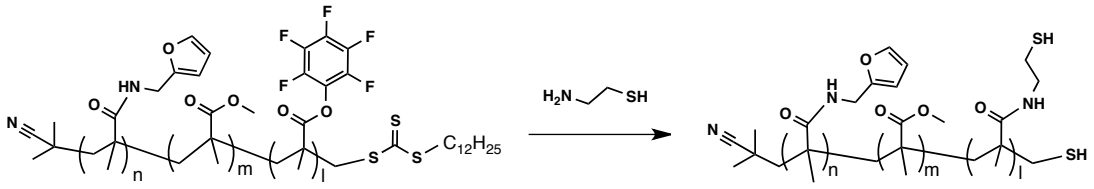
Compound	Molar Mass (g/mol)	To Add (g)	To Add (mL)	mmol	eq.	Actual (g)	Actual mmol
Pentafluorophenyl methyl methacrylate	252.14	0.8	1.0638	3.173	1	0.8001	3.173
RL64		0.8				0.8258	
AIBN	164.21	0.003		0.018	0.0058	0.0032	0.019
Dioxane			3				

Pentafluorophenyl methyl methacrylate (0.8001 g, 1 eq), RL64 (0.8258 g),) and azobisisobutyronitrile (3.2 mg, 0.006 eq) were dissolved in 3.3 mL dioxane and placed in a Schlenk flask. After 3 freeze pump thaw cycles, the flask was filled with nitrogen, sealed, placed in a 90 °C oil bath and left to react for 18 hours. The reaction mixture was diluted with 1 mL tetrahydrofuran and precipitated in 400 mL stirring hexanes. 1.1393 g (70% yield) of polymer was isolated after drying under vacuum. ^{1}H-NMR (300 MHz; $CDCl_3$): δ 7.53 (s,), 6.38 (s,), 6.20 (s,), 4.16 (s,), 3.56 (s, 3H), 1.82-0.73 (m, 7H). ^{19}F NMR (282 MHz; CDCl3): δ -150.3, -151.4, -156.8, -162.1

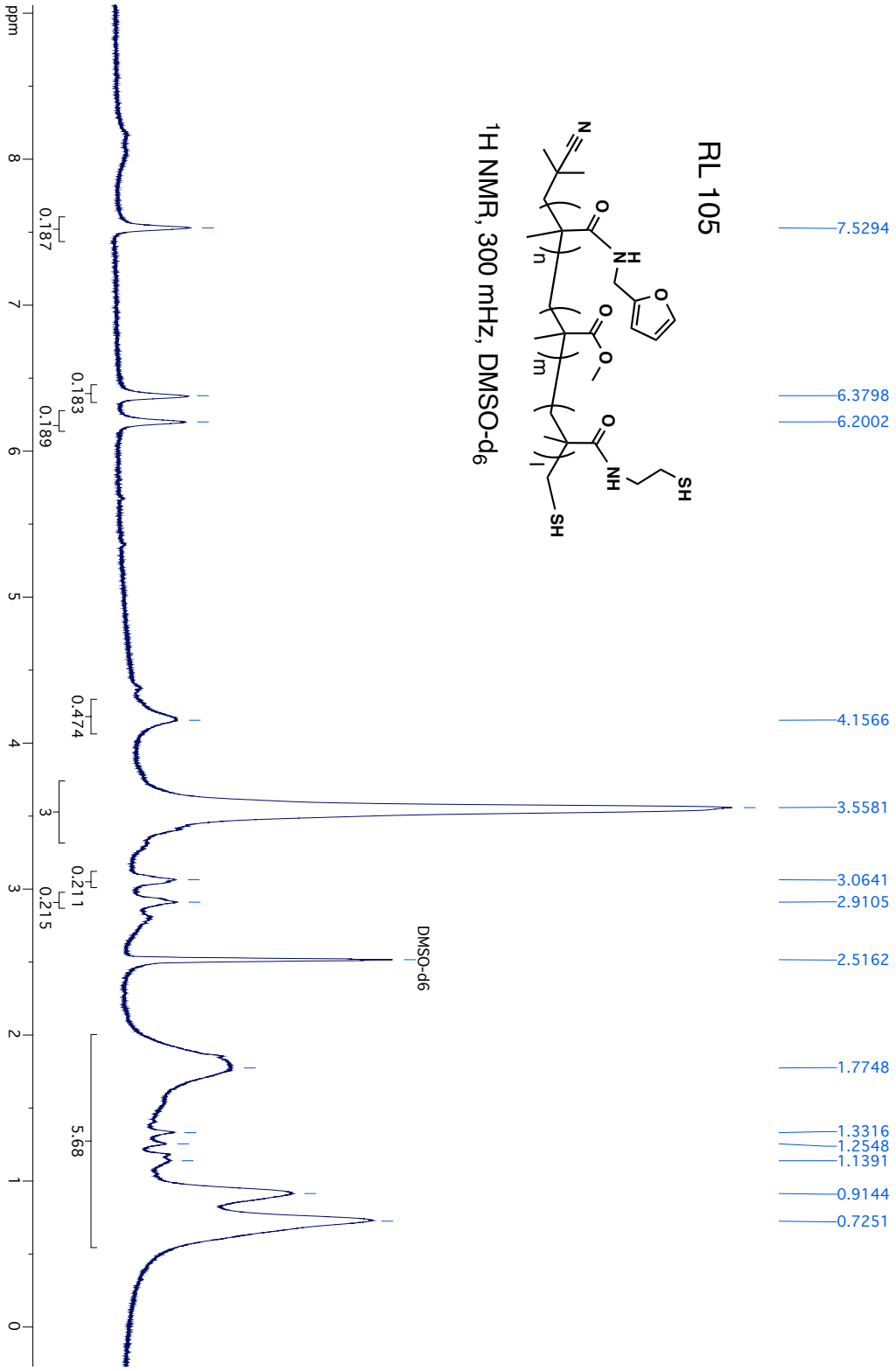

RL 101
^{1}H NMR, 300 mHz, DMSO-d$_6$
ppm
0.135
0.166
0.157
0.286
3
7.09
Methanol
DMSO-d6
7.5320
6.3758
6.1978
4.1621
3.5571
1.8212
1.3367
1.2591
1.1402
0.9265
0.7315


RL 101
^{19}F NMR, 300 mHz, $CDCl_3$
ppm
-135
-140
-145
-150
-155
-160
-165
-170
1.04
0.539
1.02
2
150.3066
151.3534
156.7832
162.0506

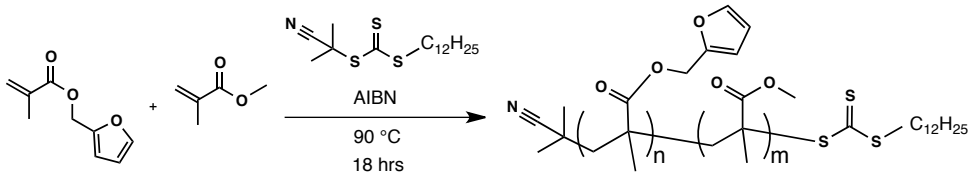
RL 105 - PMMA-co-PFMA-b-cysteamine methacrylamide



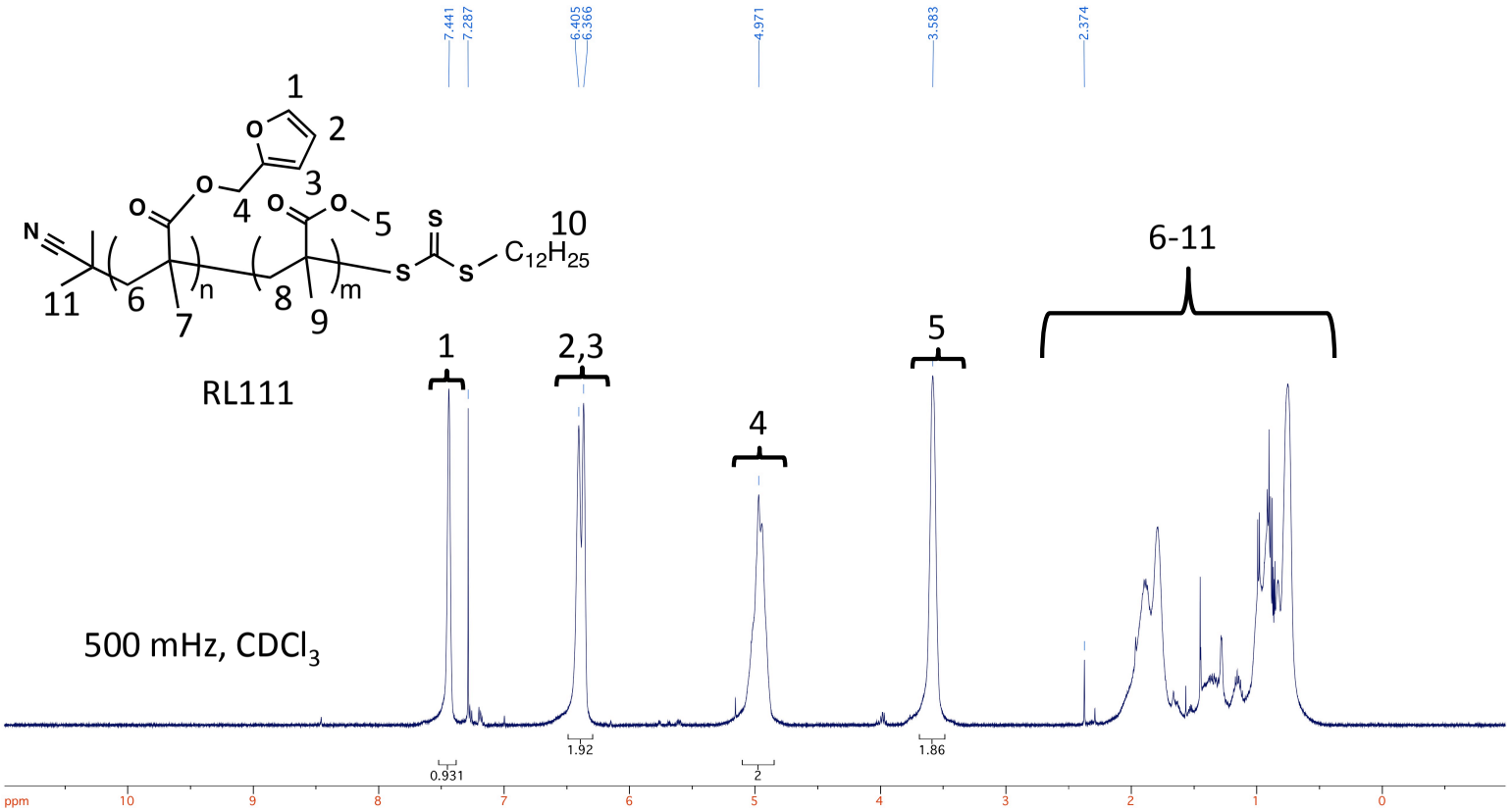
Cysteamine (49.4 mg) and triethylamine (65.4 mg) were dissolved in 3 mL tetrahydrofuran followed by the addition of RL101 (0.3019 g). Cysteamine does not fully dissolve at the start of the reaction. After stirring overnight under nitrogen atmosphere, the reaction mixture was added dropwise to 400 mL stirring hexanes. 0.2962 of polymer was isolated after drying under vacuum. ^{1}H-NMR (300 MHz; DMSO-d_6): δ 7.53 (s,), 6.38 (s,), 6.20 (s,), 4.16 (s,), 3.56 (s, 3H), 3.06 (s,), 2.91 (s,), 1.77-0.73 (m, 6H).


RL 105
^{1}H NMR, 300 mHz, DMSO-d$_6$
7.5294
6.3798
6.2002
4.1566
3.5581
3.0641
2.9105
2.5162
1.7748
1.3316
1.2548
1.1391
0.9144
0.7251
DMSO-d6
0.187
0.183
0.189
0.474
3
0.211
0.215
5.68
ppm

RL111 - poly(methyl methacrylate-co-furfuryl methacrylate)



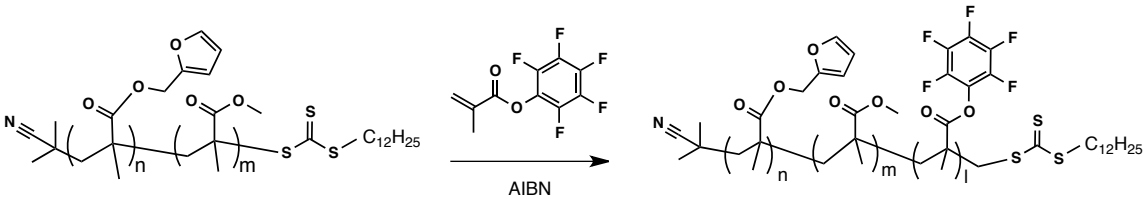
Methyl methacrylate (0.4253 g, 0.69 eq), furfuryl methacrylate (1.0177 g, 1 eq), RAFT agent (0.013 g, 0.0036 eq) and azobisisobutyronitrile (4.7 mg, 0.0047 eq) were dissolved in 1.5 mL benzene and transferred to a Schlenk flask. After 3 freeze pump thaw cycles, the flask was filled with nitrogen, sealed, placed in a 95 °C oil bath and left to react for 18 hours. The reaction mixture was diluted with 2 mL tetrahydrofuran and precipitated in 500 mL stirring hexanes to afford a very sticky, viscous product. The polymer was dissolved in redissolved in 5 mL tetrahydrofuran and precipidated again in 400 mL stirring hexanes. 0.8085 g (56% yield) of polymer was isolated after drying under vacuum. ^{1}H NMR (500 MHz; $CDCl_3$): δ 7.44 (s, 1H), 6.39 (m, 2H), 4.97 (s, 2H), 3.58 (s, 2H), 1.88-0.90 (m, 10H).



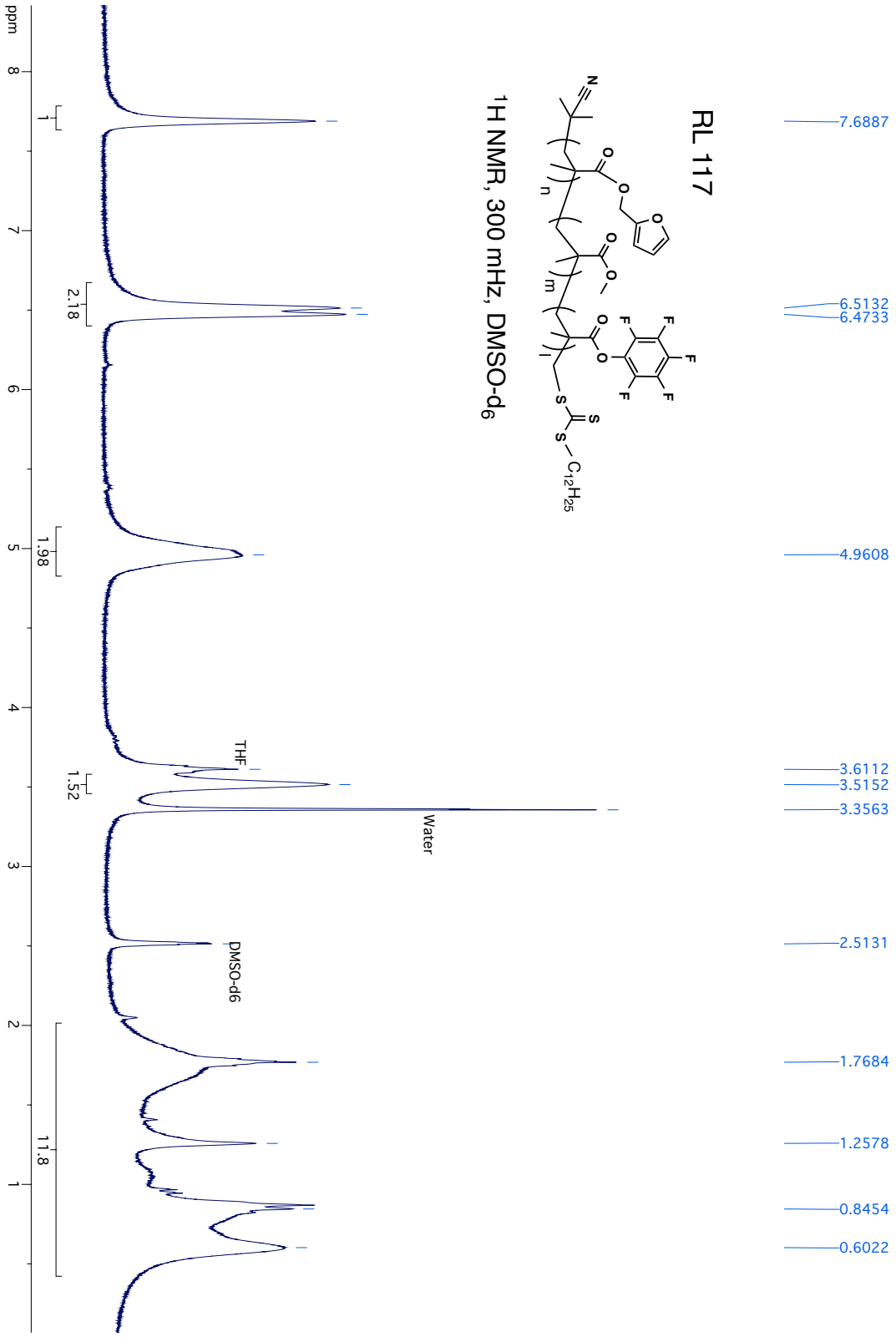
72

Mole Percent MMA/FMA	
Predicted	Actual
40.95%	38.22%

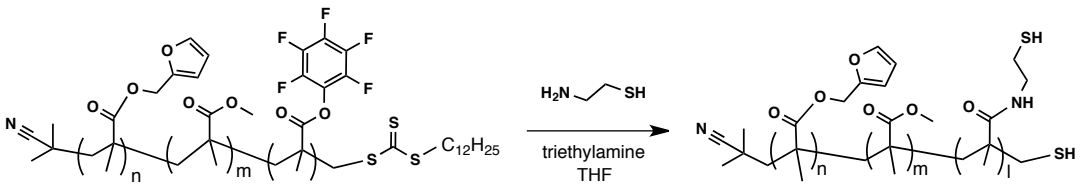
Synthesis of RL117



Pentafluorophenyl methyl methacrylate (0.1948 g, 1 eq), RL111 (0.4959 g), and azobisisobutyronitrile (2.0 mg, 0.0158 eq) were dissolved in 3 mL dioxane and placed in a Schlenk flask. After 3 freeze pump thaw cycles, the flask was filled with nitrogen, sealed, placed in a 90 °C oil bath and left to react for 18 hours. The reaction mixture was precipitated in 400 mL stirring hexanes. 0.4461 g (65% yield) of polymer was isolated after drying under vacuum. ^{1}H-NMR (300 MHz; DMSO-d_6): δ 7.69 (s, 1H), 6.49 (d, J = 12.0 Hz, 2H), 4.96 (s, 2H), 3.52 (s, 2H), 1.12 (m, 12H).


RL 117
^{1}H NMR, 300 mHz, DMSO-d$_6$
7.6887
6.5132
6.4733
4.9608
3.6112
3.5152
3.3563
2.5131
1.7684
1.2578
0.8454
0.6022
THF
Water
DMSO-d6
2.18
1.98
1.52
11.8
ppm

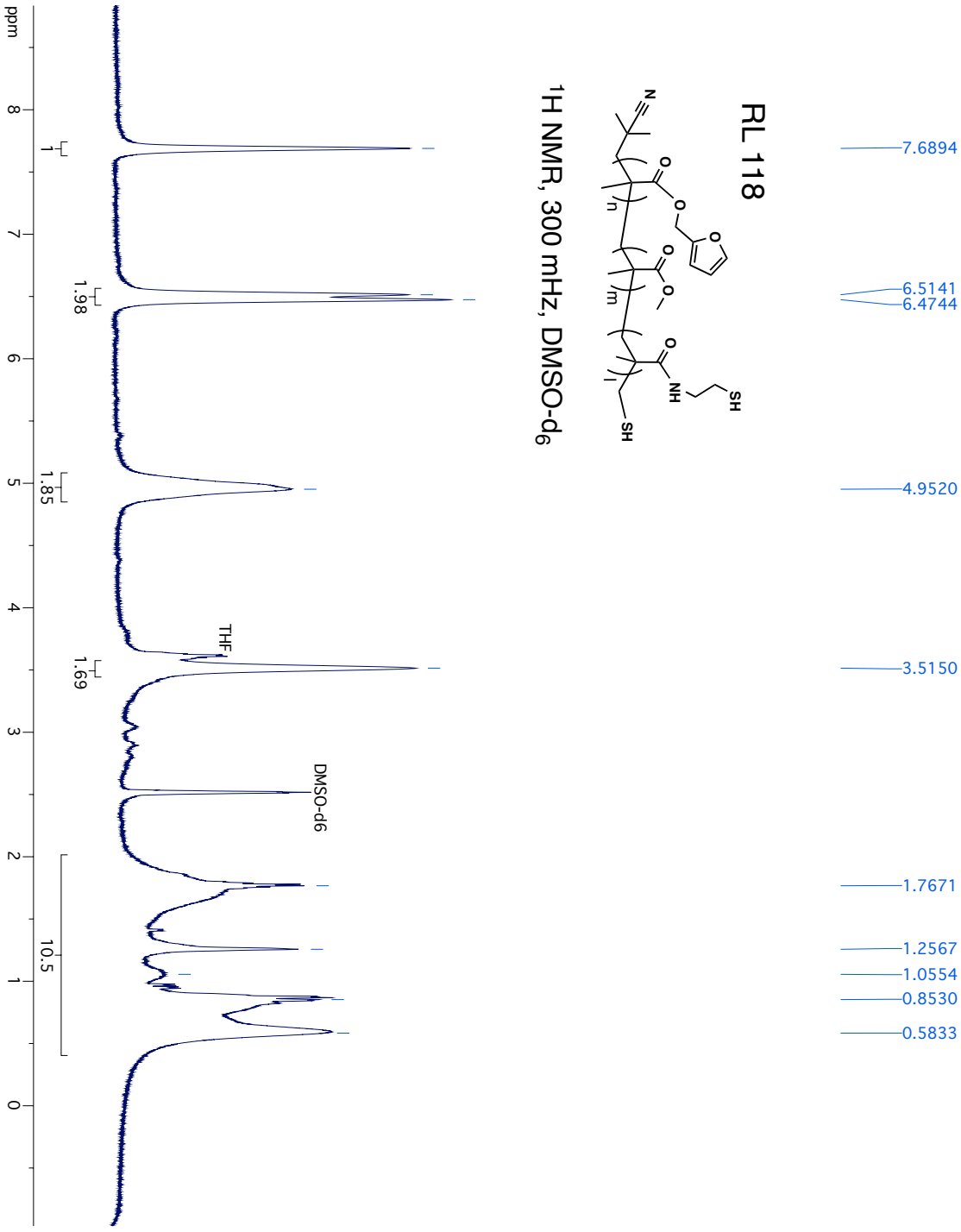
Synthesis of RL118



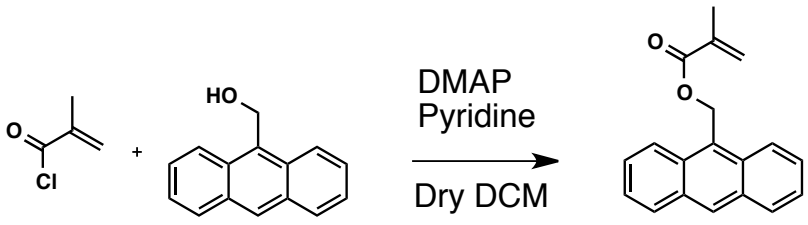
0.245 g of RL118, 45.0 mg of triethylamine, and 25.0 mg cysteamine were dissolved in a 10 mL round-bottom flask. A small amount of heat was applied to help dissolve the reactants and stirred overnight at room temperature under N_2 atmosphere. The product was added drop-wise to 300 mL of stirring hexanes and collected. 64.2 g were isolated.

^{1}H-NMR (300 MHz; DMSO-d_6): δ 7.69 (s, 1H), 6.49 (d, J = 11.9 Hz, 2H), 4.95 (s, 2H), 3.51 (s, 2H), 1.77-0.58 (m, 11H).

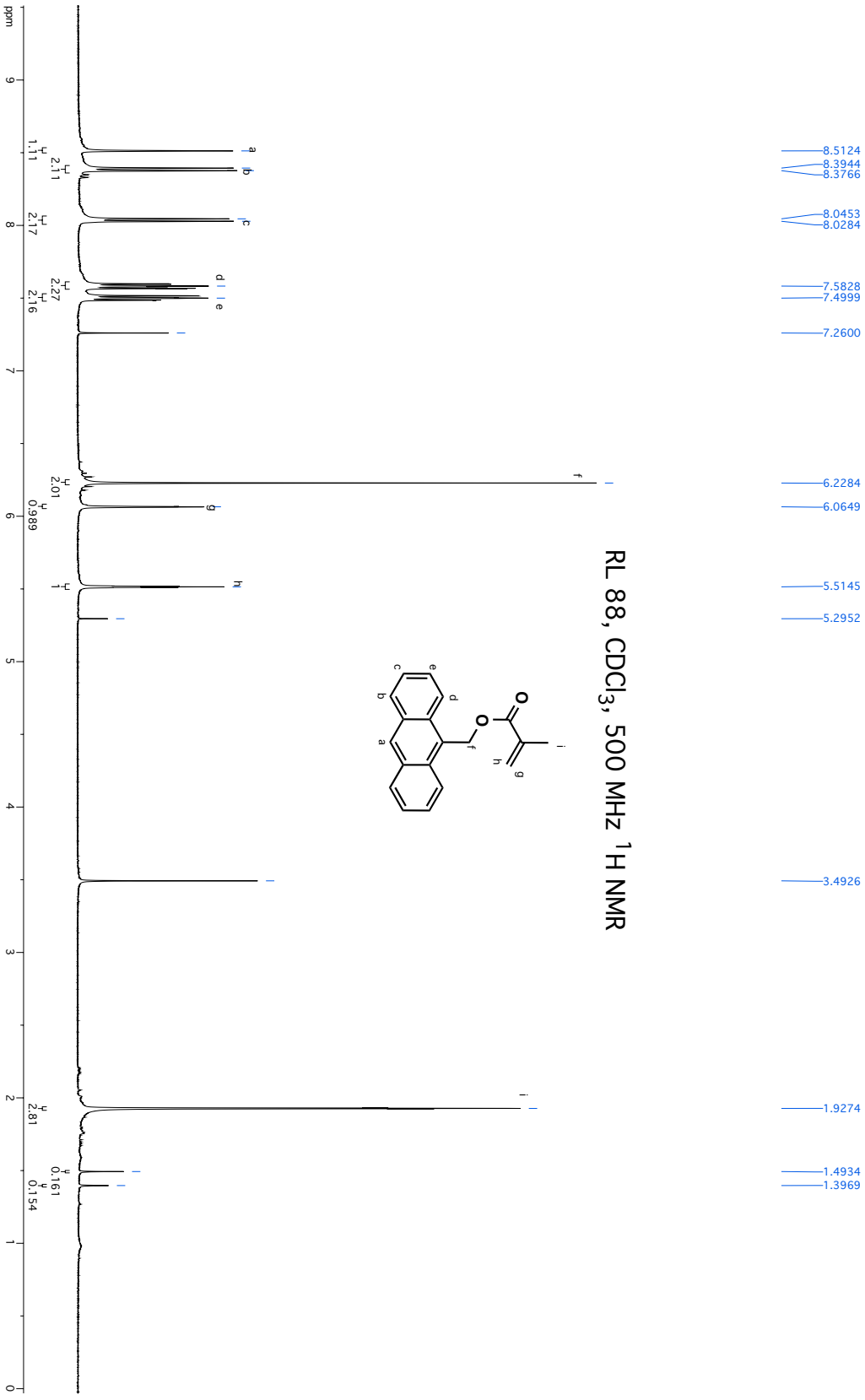
RL118 ^{1}H NMR


RL 118
^{1}H NMR, 300 mHz, DMSO-d$_6$
ppm
1.98
1.85
1.69
10.5
THF
DMSO-d6
7.6894
6.5141
6.4744
4.9520
3.5150
1.7671
1.2567
1.0554
0.8530
0.5833

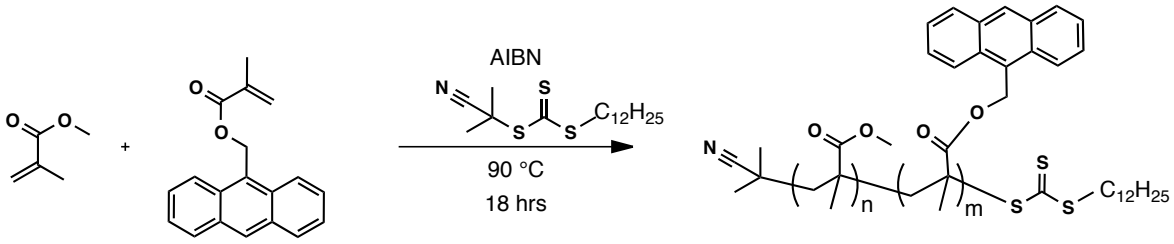
Synthesis of 9-Anthracenylmethyl methacrylate (RL88)



9-anthracene methanol (1.9821 g, 1 eq) and 4-dimethylaminopyridine (8.0 mg) were added to a 50 mL round bottom flask. 30 mL of dry dichloromethane and pyridine (1.136 g, 1.5 eq) were then added via syringe. After cooling in an ice bath, methacryloyl chloride (1.104 g, 1.1 eq) was added dropwise. The reaction mixture became homogenous after 30 minutes and was then washed with 50 mL of water, 50 mL of saturated sodium chloride solution, extracted with dichloromethane, dried over magnesium sulfate and concentrated in vacuo. The crude product was purified by silica gel chromatography using 20% ethyl acetate in hexanes as the eluent to afford a yellow oil. Additionally, the final product was dissolved in a small amount of dichloromethane and precipitated in methanol to afford a white solid. (0.7877 g, 51% yield) ^{1}H-NMR (500 MHz; $CDCl_3$): δ 8.51 (s, 1H), 8.39 (d, J = 8.9 Hz, 2H), 8.04 (d, J = 8.4 Hz, 2H), 7.58 (t, J = 7.1 Hz, 2H), 7.50 (t, J = 7.0 Hz, 2H), 6.23 (s, 2H), 6.06 (s, 1H), 5.51 (s, 1H), 1.93 (s, 3H).

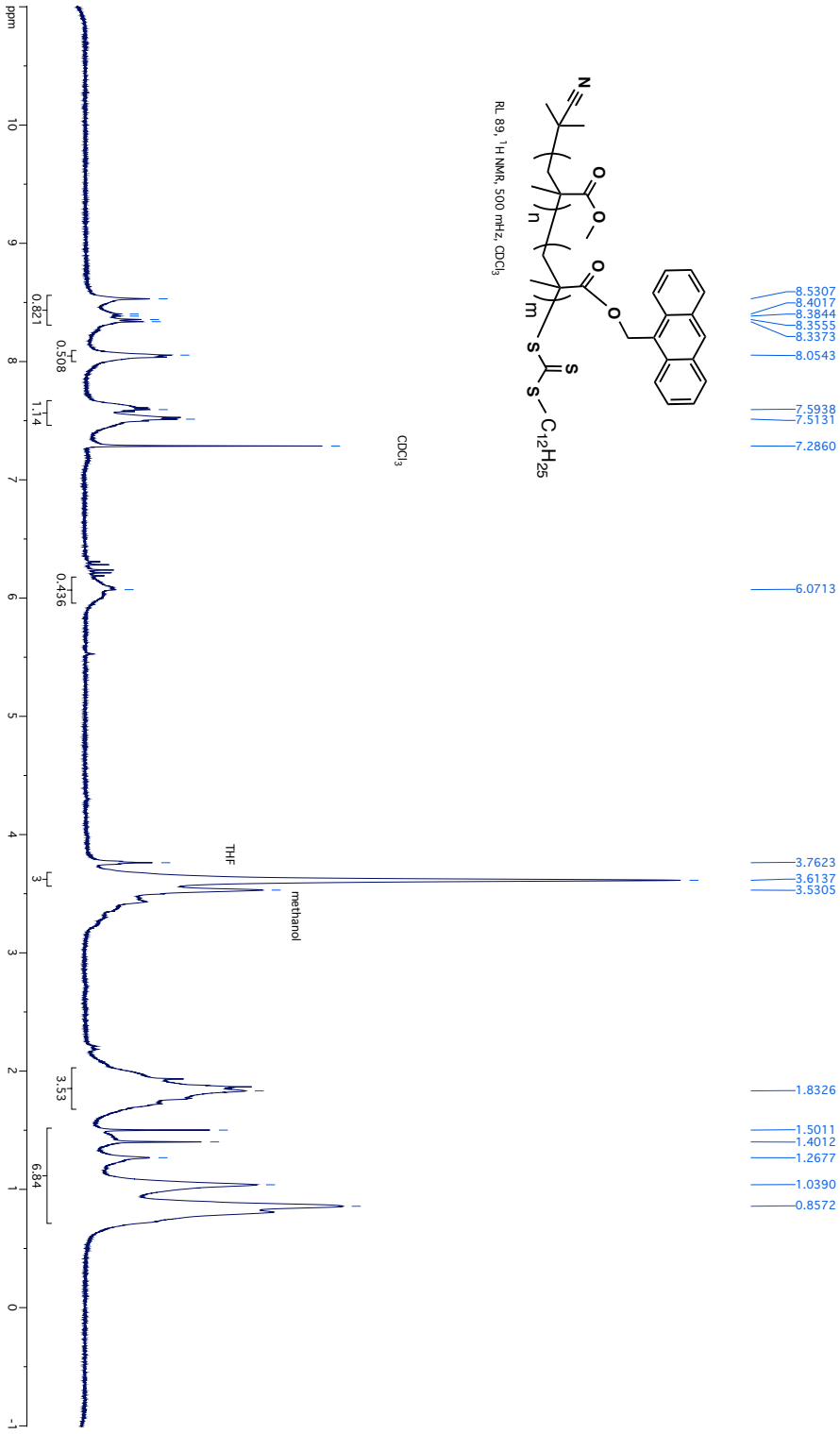

RL 88, CDCl3, 500 MHz 1H NMR
8.5124
8.3944
8.3766
8.0453
8.0284
7.5828
7.4999
7.2600
6.2284
6.0649
5.5145
5.2952
3.4926
1.9274
1.4934
1.3969
ppm

RL89 – Synthesis of RAFT terminated poly[(methyl methacrylate)-co-(9-anthracenylmethyl methacrylate)]

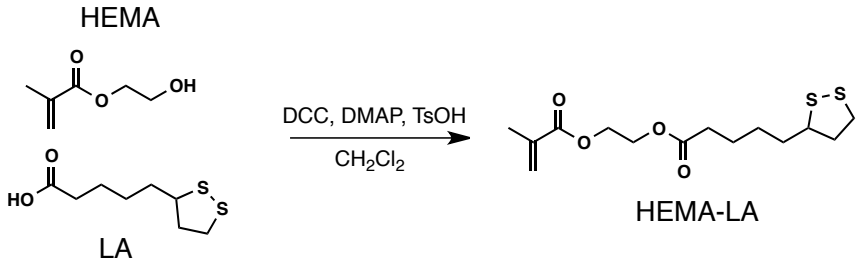


	Molar Mass (g/mol)	Density (g/mL)	To Add (g)	To Add (mL)	mmol	eq.	Actual (g)	Actual mmol	Actual eq.
Methyl Methacrylate	100.12	0.94	1	1.0638	9.988	1	0.94	9.3887	1.0000
AnMMA	276.33		0.5519		1.997	0.2000	0.551	1.9939	0.2124
RAFT Agent	345.63		0.0158		0.046	0.0038	0.013	0.03761	0.0033
AIBN	164.21		0.0047		0.029	0.0024	0.0043	0.02618	0.0023
Benzene				3					

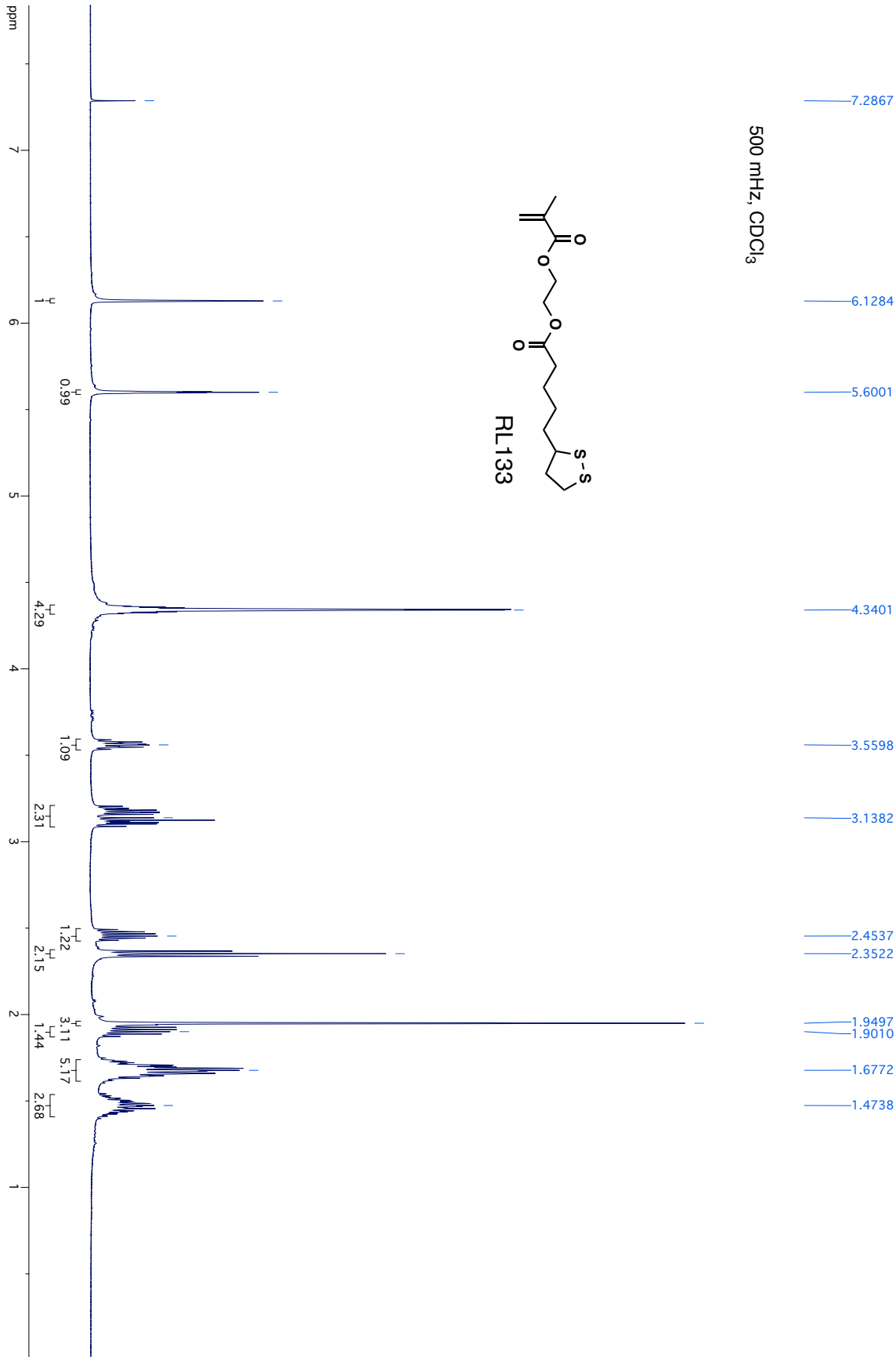
Methyl methacrylate (0.94 g, 1.0 eq), 9-Anthracenylmethyl methacrylate (0.551.g, 0.2 eq), RAFT agent (0.013 g, 0.0033 eq) and azobisisobutyronitrile (14.3 mg, 0.0023 eq) were dissolved in 3 mL benzene and placed in a Schlenk flask. After 3 freeze pump thaw cycles, the flask was filled with nitrogen, sealed, placed in a 90 °C oil bath and left to react for 21 hours. The reaction mixture was added dropwise to 500 mL of stirring methanol and dried under vacuum. 1.0886 g isolated (70% yield).


RL 89, ^{1}H NMR, 500 mHz, $CDCl_3$
ppm
10
9
8
7
6
5
4
3
2
1
0
-1
0.821
0.508
1.14
0.436
3
3.53
6.84
$CDCl_3$
THF
methanol
8.5307
8.4017
8.3844
8.3555
8.3373
8.0543
7.5938
7.5131
7.2860
6.0713
3.7623
3.6137
3.5305
1.8326
1.5011
1.4012
1.2677
1.0390
0.8572
N
O
O
O
O
n
m
S
S
S
$C_{12}H_{25}$

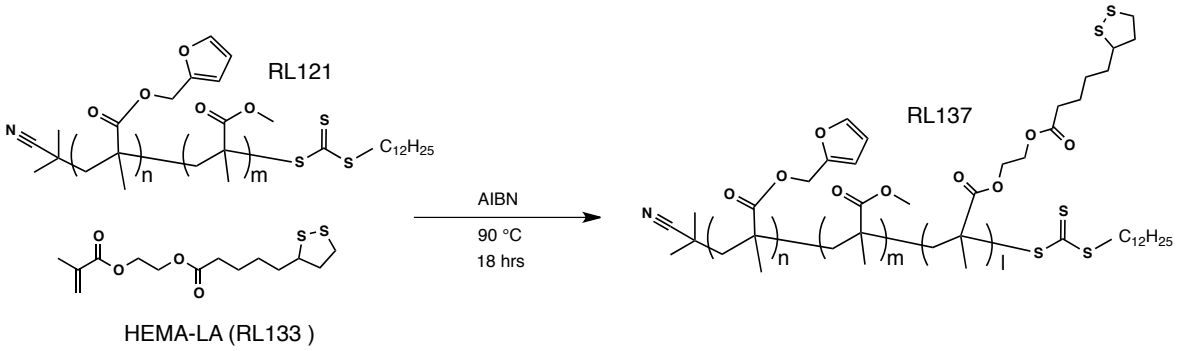
RL133 – Synthesis of HEMA-LA



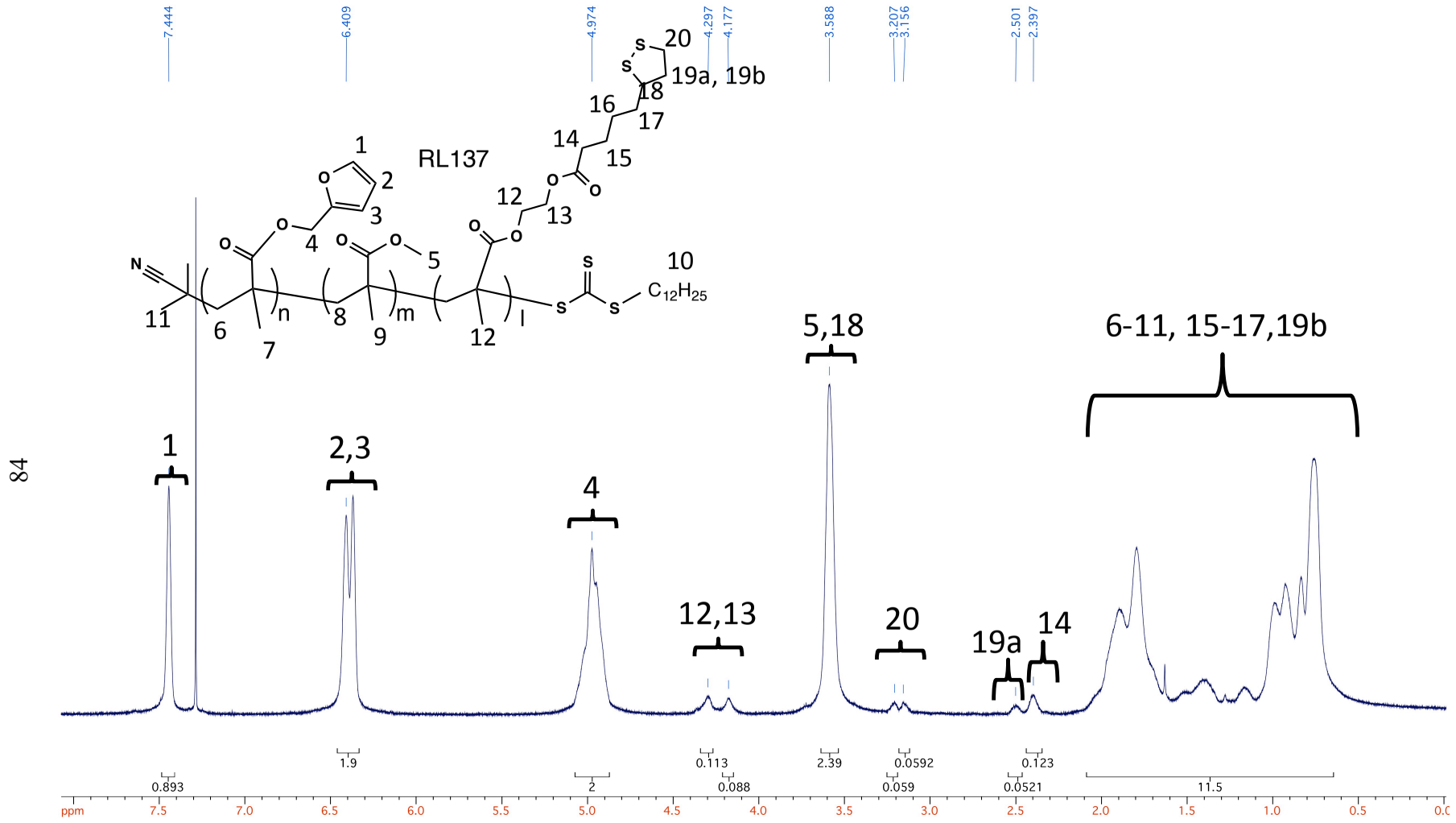
Hydroxyethyl methacrylate (1.387 g, 1.1 eq), lipoic acid (2.0 g, 1 eq), and p-Toluenesulfonic acid (0.1855 g, 0.1 eq) were dissolved in 15 mL of dry dichloromethane in a 50 mL round bottom flask. This mixture was stirred under nitrogen atmosphere and cooled to 0 °C. 10 mL of additional dichloromethane was added to rinse the sides of the flask. 4-dimethylaminopyridine (.1180 g, 0.1 eq) and *N,N'*-dicyclohexylcarbodiimide (2.808 g, 1.4 eq) were added with an additional 5 mL dichloromethane to rinse the sides of the flask. The solution was stirred for 15 minutes at 0 °C and then allowed to stir overnight and warm to room temperature. Solid dicyclohexylurea byproduct was filtered after cooling the reaction flask and the reaction mixture was washed with two 15 mL portions of 1M HCl, 20 mL of saturated sodium bicarbonate and 30 mL of saturated sodium chloride solution. The organic layers were combined, concentrated via rotovaporation, dried over magnesium sulfate and purified via a silica gel column with 50% hexanes/50% ethyl acetate as the eluent. 2.00 g of yellow oil were isolated (65%). ^{1}H NMR matched literature values.[24]


500 mHz, CDCl3
RL133
7.2867
6.1284
5.6001
4.3401
3.5598
3.1382
2.4537
2.3522
1.9497
1.9010
1.6772
1.4738
ppm
1
0.99
4.29
1.09
2.31
1.22
2.15
3.11
1.44
5.17
2.68

RL137 – Polymerization of RL133 with RL121



2.035 g of RL121 was dissolved in 5 mL of dioxane with the aid of slight heat and sonication. 0.5013 g of RL133 was dissolved in 1 mL of dioxane and added to the solution of RL121 followed by 4.2 mg of AIBN. The reaction mixture was transferred to a Schlenk tube under N_2 atmosphere. After three freeze pump thaw cycles, the reactants were placed in a 90 °C oil bath and left to react overnight. The reaction mixture was diluted with 2 mL of THF and precipitated in 600 mL stirring hexanes. Yellow, think polymer was filtered, collected and dissolved in 10 mL of THF and precipitated in 500 mL of stirring methanol. 1.3841 g of white, fluffy polymer was collected. (55% yield). ^{1}H-NMR (500 MHz; DMSO-d_6): δ 7.44 (s, 1H), 6.39 (m, 2H), 4.97 (s, 2H), 4.30 (s,), 4.18 (s,), 3.59 (m, 2H), 3.21 (s,), 3.16 (s,), 2.50 (s,), 2.40 (s,), 1.90-0.76 (m, 12H).



84

500 mHz, $CDCl_3$

3.7 References

1. Zorn, M. *et al.* Liquid crystalline phases from polymer functionalised semiconducting nanorods. *J. Mater. Chem.* **18,** 3050–3058 (2008).

2. Meuer, Oberle, Theato, Tremel & Zentel. Liquid Crystalline Phases from Polymer-Functionalized TiO2 Nanorods. *Adv. Mater.* **19,** 2073–2078 (2007).

3. Thierry, B., Ng, J., Krieg, T. & Griesser, H. J. A robust procedure for the functionalization of gold nanorods and noble metal nanoparticles. *Chem. Commun.* 1724–6 (2009).

4. Chiefari, J. *et al.* Living Free-Radical Polymerization by Reversible Addition−Fragmentation Chain Transfer: The RAFT Process. *Macromolecules* **31,** 5559–5562 (1998).

5. Moad, G., Rizzardo, E. & Thang, S. Living Radical Polymerization by the RAFT Process. *Aust. J. Chem.* **58,** 379 (2005).

6. Moad, G., Rizzardo, E. & Thang, S. Living Radical Polymerization by the RAFT Process—A First Update. *Aust. J. Chem.* **59,** 669 (2006).

7. Moad, G., Rizzardo, E. & Thang, S. Living Radical Polymerization by the RAFT Process – A Second Update. *Aust. J. Chem.* **62,** 1402 (2009).

8. Moad, G., Rizzardo, E. & Thang, S. Material Matters **5.1**, 2 (2010).

9. Kang, Y. & Taton, T. Controlling shell thickness in core-shell gold nanoparticles via surface-templated adsorption of block copolymer surfactants. *Macromolecules* **38,** 146115-6121 (2005)

10. Eberhardt, M. & Théato, P. RAFT Polymerization of Pentafluorophenyl Methacrylate: Preparation of Reactive Linear Diblock Copolymers. *Macromol. Rapid. Comm.* **26,** 1488–1493 (2005).

11. Eberhardt, M., Mruk, R., Zentel, R. & Théato, P. Synthesis of pentafluorophenyl(meth)acrylate polymers: New precursor polymers for the synthesis of multifunctional materials. *Eur. Polym. J.* **41,** 1569–1575 (2005).

12. Gibson, M., Fröhlich, E. & Klok, H. Postpolymerization modification of poly(pentafluorophenyl methacrylate): Synthesis of a diverse water-soluble polymer library. *J. Polym. Sci. Part Polym. Chem.* **47,** 4332–4345 (2009).

13. Laita, Boufi & Gandini. The application of the Diels-Alder reaction to polymers bearing furan moieties. 1. Reactions with maleimides. *Eur. Polym. J.* **33,** 1203–1211 (1997).

14. Mansfeld, U., Pietsch, C., Hoogenboom, R., Becer, C. & Schubert, U. Clickable initiators, monomers and polymers in controlled radical polymerizations – a prospective combination in polymer science. *Polymer Chemistry* **1,** (2010).

15. Gacal *et al.* Anthracene−Maleimide-Based Diels−Alder 'Click Chemistry' as a Novel Route to Graft Copolymers. *Macromolecules* **39,** 5330–5336 (2006).

16. Kim, T.-D. *et al.* Ultralarge and Thermally Stable Electro-optic Activities from Diels–Alder Crosslinkable Polymers Containing Binary Chromophore Systems. *Advanced Materials* **18,** (2006).

17. Sullivan, P. *et al.* Tri-component Diels–Alder polymerized dendrimer glass exhibiting large, thermally stable, electro-optic activity. *J. Mater. Chem.* **17,** 2899–2903 (2007).

18. Kavitha, A. & Singha, N. Atom-Transfer Radical Copolymerization of Furfuryl Methacrylate (FMA) and Methyl Methacrylate (MMA): A Thermally-Amendable Copolymer. *Macromol. Chem. Physic.* **208,** 2569–2577 (2007).

19. Pramanik, N., Bag, D., Alam, S., Nando, G. & Singha, N. Thermally amendable tailor-made functional polymer by RAFT polymerization and 'click reaction'. *J. Polym. Sci. Part Polym. Chem.* **51,** 3365–3374 (2013).

20. Demetriou, M. & Krasia-Christoforou, T. Well-defined diblock copolymers possessing fluorescent and metal chelating functionalities as novel macromolecular sensors for amines and metal ions. *J. Polym. Sci. Part Polym. Chem.* **50,** 52–60 (2012).

21. Moon, B., Hoye, T. & Macosko, C. Synthesis and application of fluorescently labeled phthalic anhydride (PA) functionalized polymers by ATRP. *Polymer* **43,** 5501–5509 (2002).

22. Liu, X. *et al.* Kinetic study of Diels–Alder reaction involving in maleimide–furan compounds and linear polyurethane. *Polym. Bull.* **70,** 23192335 (2013).

23. Dispinar, T., Sanyal, R. & Sanyal, A. A Diels-Alder/retro Diels-Alder strategy to synthesize polymers bearing maleimide side chains. *J. Polym. Sci. A Polym. Chem.* **45,** 4545–4551 (2007).

24. Chen, X., Lawrence, J., Parelkar, S. & Emrick, T. Novel Zwitterionic Copolymers with Dihydrolipoic Acid: Synthesis and Preparation of Nonfouling Nanorods. *Macromolecules* **46,** (2013).

25. Gandini, A. The furan/maleimide Diels–Alder reaction: A versatile click–unclick tool in macromolecular synthesis. *Prog. Polym. Sci.* **38,** (2013).

26. Fan, M., Liu, J., Li, X., Zhang, J. & Cheng, J. Recyclable Diels–Alder Furan/Maleimide Polymer Networks with Shape Memory Effect. *Ind. Eng. Chem. Res.* **53,** (2014).

CHAPTER 4

SYNTHESIS AND FUNCTIONALIZATION OF GOLD NANORODS

4.1 Introduction

Gold nanorods (GNRs) offer a versatile route to the fabrication of tunable metamaterial structures. As discussed in Chapter 2, modeling results predict large field enhancements between ordered arrays of metallic (silver or gold) nanorods. GNRs were chosen for this application because of their relative ease of synthesis and tunable optical properties. Before the year 2001, GNRs were typically made from templates of porous alumina, polycarbonates or carbon nanotubes through either electrochemical or photochemical processes.[1-6] Now, GNRs are readily available from a large number of commercial sources and specific sizes or coatings can be requested such as thiol-terminated polyethylene glycol. However, commercial GNRs can vary in the amount of spherical impurities they contain. They are also quite expensive and are not offered at particularly high concentrations. The ability to synthesize GNRs in the lab and functionalize them at high concentrations was crucial to the goals of this thesis. At a high enough number density, rod-like materials tend to align along their longitudinal axis. The prospect of creating a self-assembled metamaterial, then, hinges on being able to produce high concentrations of pure rods at high aspect ratios.[7]

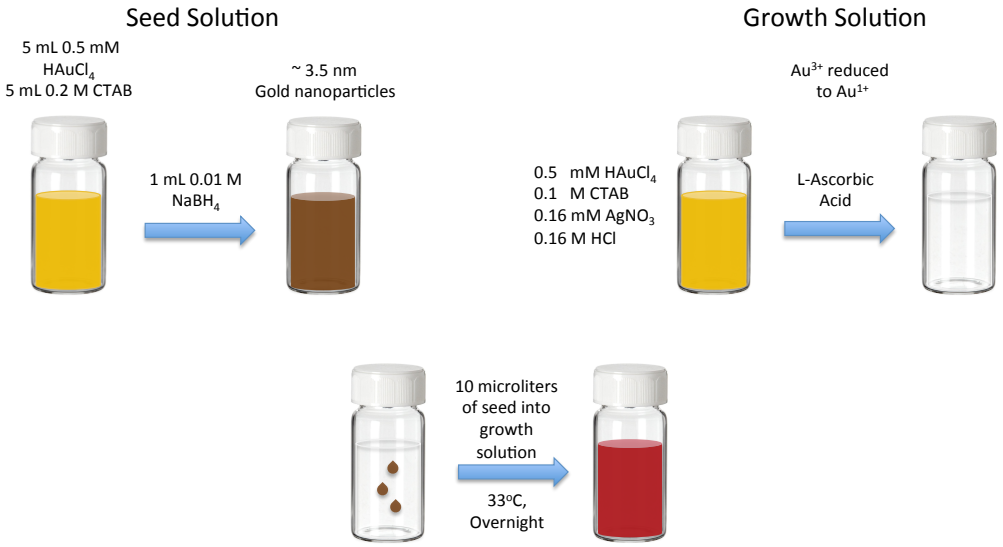


Figure 4.1. Typical small batch seed-mediated GNR synthesis. Seed crystals are made by reducing gold (III) chloride with a dilute solution of $NaBH_4$. Separately, a growth solution of Au^{3+} ions is reduced to a clear solution of Au^{+} ions with a weak reducing agent. A small volume of seed crystals is added to the growth solution and left to react overnight.

With this goal in mind, current methods in literature were researched and a variety of groups who have developed useful synthesis procedures were identified.

In 2001, a seed-mediated surfactant-based method was developed by Murphy *et al.*[8] and expanded upon in 2003 by El-Sayed *et al.*[9]. This so-called "seed-mediated" approach has been a popular synthesis method ever since because of its simplicity and versatility. Following this approach, seed crystals are first prepared by reducing an aqueous solution of a $HAuCl_4$ with sodium borohydride. A small amount of seed solution is added to a separate solution of gold (I) ions produced by reducing gold (III) ions with ascorbic acid. Figure 4.1 shows a typical seed-mediated GNR synthesis scheme.

Almost all seed-mediated approaches utilize aqueous solutions of a stabilizing surfactant, cetyltrimethylammonium bromide (CTAB), and Ag^+ ions as a template for crystal growth. While the mechanism is not fully understood, it is believed that CTAB along with Ag^+ ions preferentially bind to the {110} facets of the growing gold nanocrystals with predominant growth along the {100} facet, giving rise to anisotropic rod-shaped growth.[10,11]

Although the process may seem simple in principle, the formation of high yield, monodisperse high aspect ratio GNRs proved to be very challenging. The purity of rods produced is sensitive to temperature, pH, and final concentrations of reactants. Especially important is the concentration of $NaBH_4$ used when making the seed solution. The presence of too many seed crystals can lead to many sphere shaped deformities. Considerable effort in this thesis was focused on synthesizing pure, monodisperse rods having varied but well-defined aspect ratios. Early efforts in small batch nanorod synthesis will be presented and compared to results from large batch syntheses and illustrate dramatic differences in purity. After nanorod synthesis, the functionalization of GNRs will be discussed. The use of a thiol-containing block copolymer, that both solubilizes GNRs in organic solvents

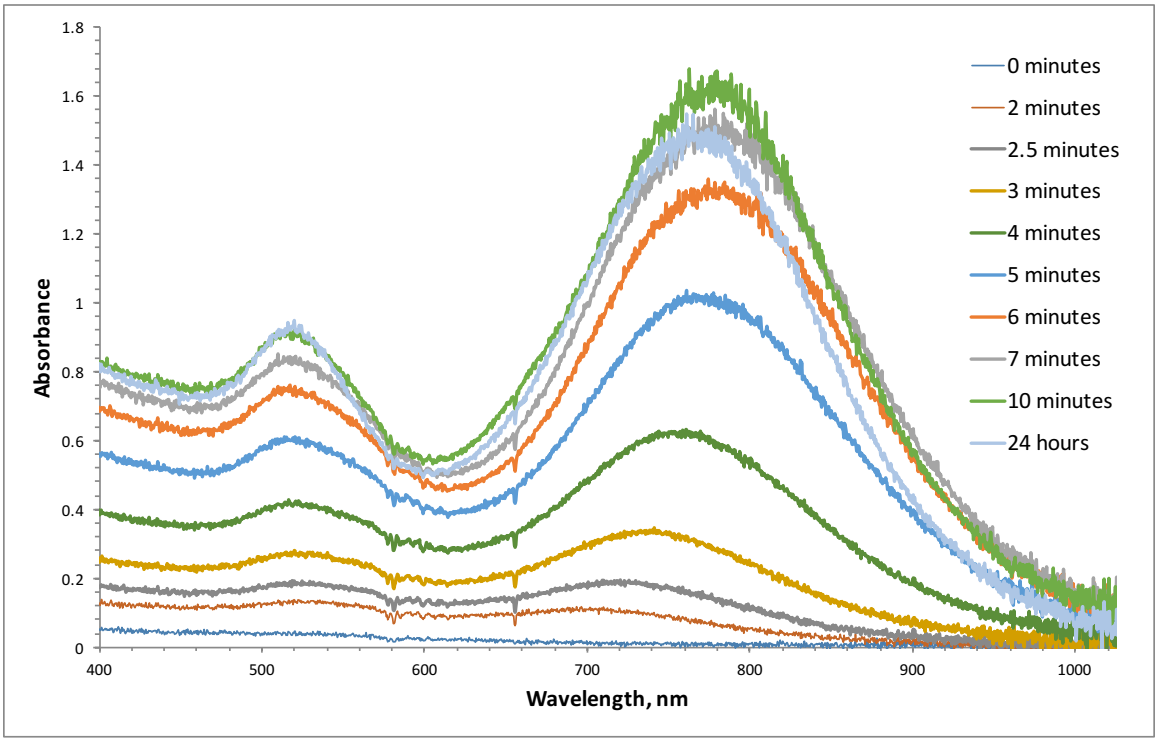


Figure 4.2. Absorption spectra of gold nanorod growth over time. These GNRs were synthesized using the basic small batch method shown in Figure 4.1. Growth typically ends after ten minutes.

and contains functionality for attaching nonlinear organic chromophores, is explored.

4.2 Synthesis of Gold Nanorods

4.2.1 Small Batch GNR Synthesis

In order to more easily test various literature methods, the first attempts at GNR synthesis began with a relatively small 20 mL sample volume. The basic synthesis is depicted in figure 4.1 and shows the typical substituents of the seed-mediated method. The small batch procedure produces nanorods

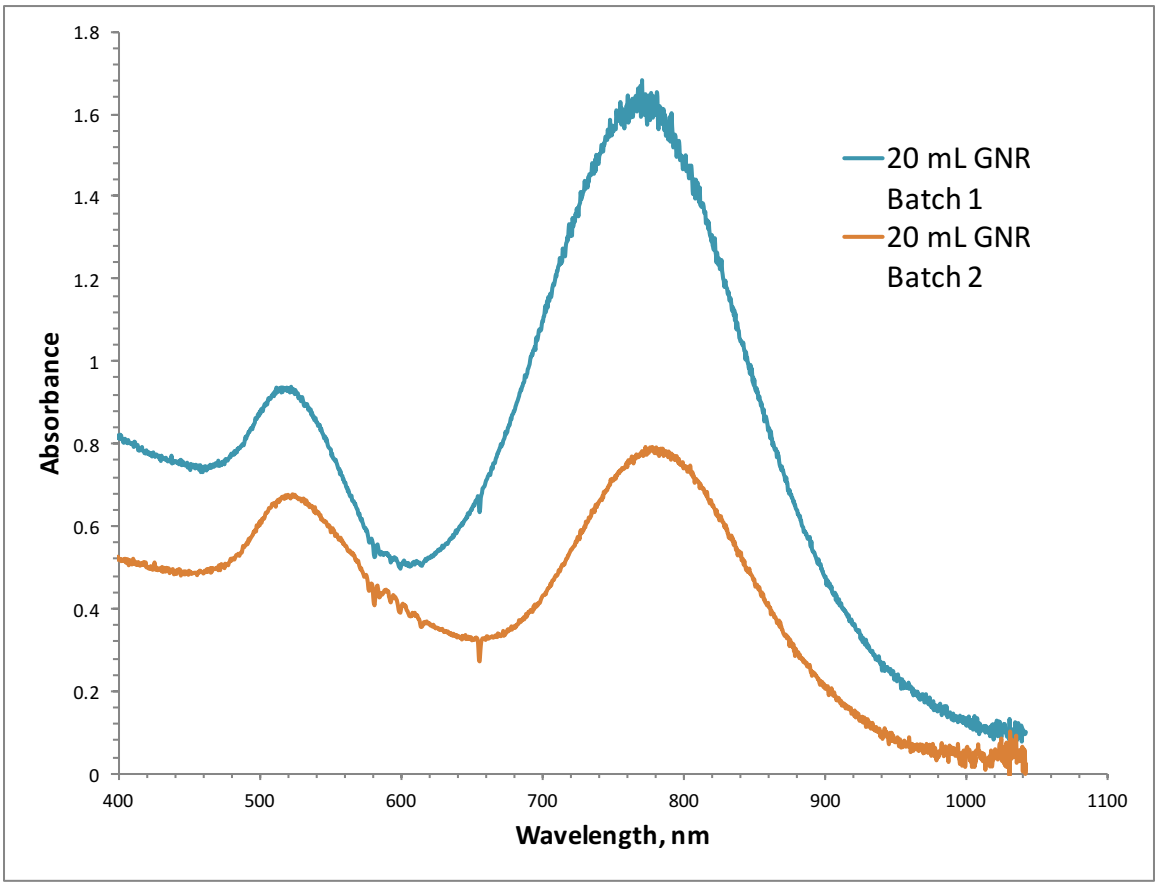


Figure 4.3. UV/Vis absorption spectra of two early batches of GNRs at a 20 mL scale. Both of these batches have large amounts of spherical impurities represented by absorbance near 500 nm. A pure batch of GNRs would have a large ratio of LSPR to TSPR absorbance.

very quickly. Figure 4.2 shows the absorption spectra overtime of a small batch of GNRs. Growth tends to end at around ten minutes. However, many unwanted spherical particles are present indicated by the large absorption near 500 nanometers.

When GNRs and other noble metal nanoparticles are exposed to light, the oscillating electromagnetic field induces an oscillation of free electrons in the metal. A maximum oscillation occurs at a frequency known as the

surface plasmon resonance (SPR) of the particle.[12,13] GNRs of certain sizes absorb visible light very strongly and exhibit two distinct SPR peaks called the transverse SPR (TSPR) and longitudinal SPR (LSPR). These two peaks make up the distinctive UV/Vis spectra of GNRs. The weak TSPR peak is always found close to 500 nm along with the SPR of spherical impurities. The ratio of rods to impurities can be estimated by comparing the intensity of the LSPR to the peak found near 500 nm. Figure 4.3 shows the absorption spectra of two small volume GNR batches with varying amounts of spherical impurities. These small batches were synthesized using a very basic procedure where only ascorbic acid is used to reduce gold (I) ions to gold (0). Typical seed-mediated synthesis uses 10% molar excess of ascorbic acid relative to gold chloride concentrations. Using more ascorbic acid leads to more spherical particles. According to Vigdermen *et al.*,[11] this result may be due to an increased reduction rate resulting and an increase of random nucleation events in the growth solution. Ye et al.[14] improved rod synthesis using aromatic additives that slowly reduced Au(III) to Au(0). Compounds such as 5-bromosalicylic acid and sodium oleate were found to offer slow reduction of gold ions. Ascorbic acid was still needed for successful rod formation but at a much lower concentration. Vigderman *et al*. were able to synthesize rods by replacing ascorbic acid with hydroquinone as the reducing agent. Importantly, the conversion of gold ions to rods was found to be near quantitative compared to a 15% conversion typical of more common seed

mediated syntheses. These new findings led us to believe that using additional additives had the potential to provide GNRs at higher purities. The following section discusses efforts towards this end.

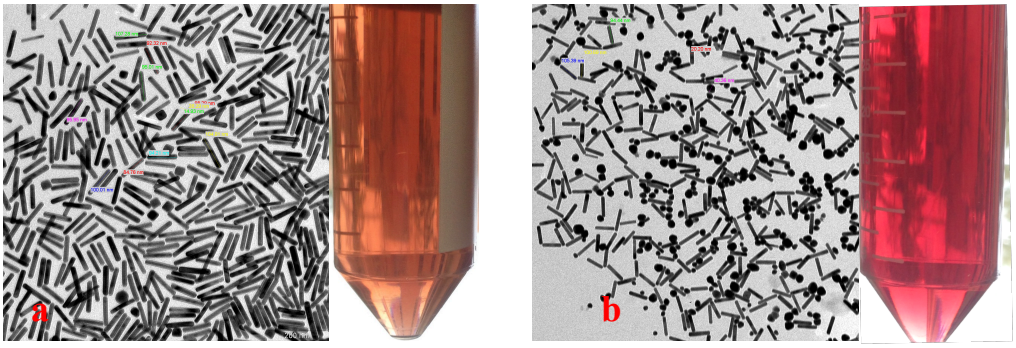


Figure 4.4. a) TEM image and photo of nearly monodisperse GNRs from synthesis conditions of Ye et al.[19,20] b) TEM image and photo of GNRs of similar size but with more spherical particles. Color difference is due to spherical impurities, not due to rod size difference.

4.2.2 GNR Synthesis Using Reductive Additives

Following a more recent procedure by Ye *et al.*[15], dramatic improvements in the yield of high aspect ratio rods was achieved. The improved procedure relies on the use of an additional surfactant, oleic acid. The oleic acid acts as a very mild reducing agent and replaces much of the ascorbic acid used in typical procedures. Less CTAB is needed as well, leading to the belief that the oleic acid also acts as a growth template in tandem with the CTAB. A slow and mild reduction of Au^{+} ions appears to be an important factor in the suppression of spherical impurities. Figure 4.4

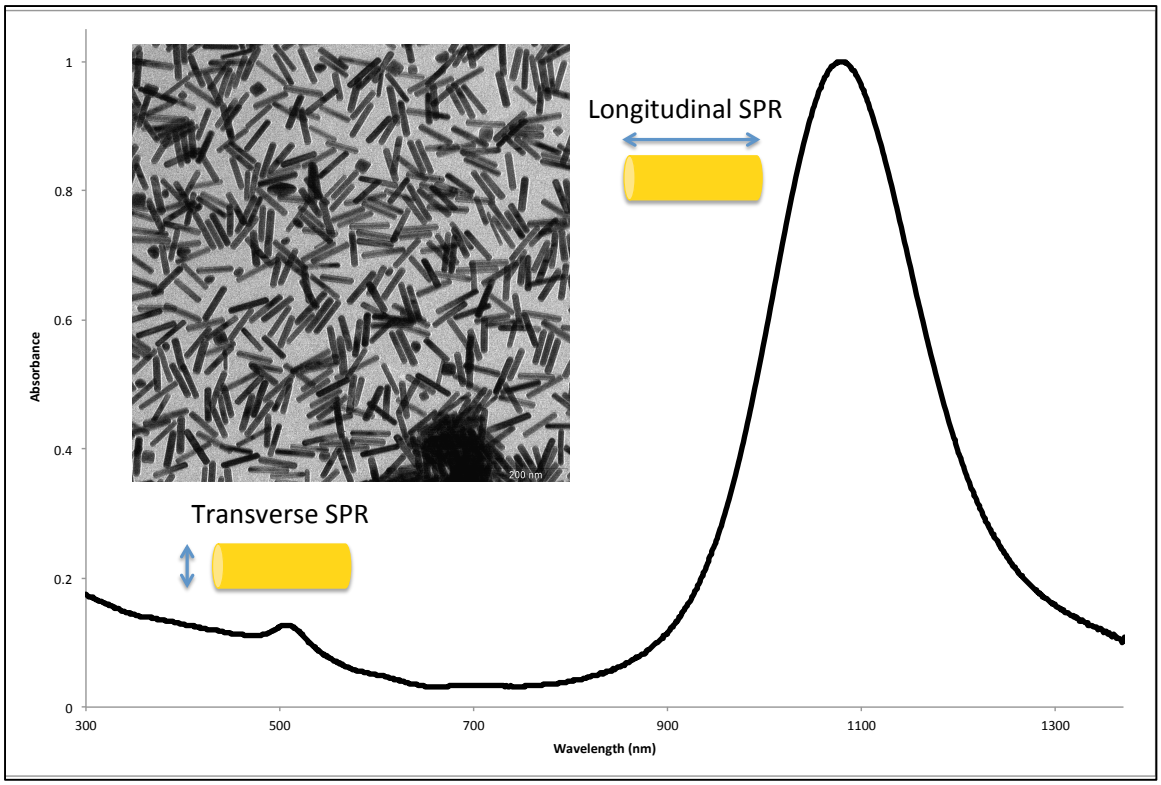


Figure 4.5. UV/Vis absorption spectrum of a sample of nearly monodisperse nanorods with aspect ratios of 6-7. Top left inset - TEM image showing small amount of spherical and cube shaped impurities.

shows the drastic color difference in solutions of pure rods and solutions containing many spherical impurities. The red hue in figure 4.4b illustrates the characteristic color of increased absorbance near 500 nm due to the presence of spherical impurities. Besides using oleic acid as an additive, Ye's method was prepared at a 500 mL scale with the advantages of producing more GNRs per batch and being less sensitive to fluctuations in reagent concentration between each batch. Generally, GNR synthesis procedures include specific instructions to use ultra pure water, fresh solutions, and aqua regia-cleaned glassware. These precautions were taken at first but it

was found that low impurity GNR batches could be produced without the need for such rigorous conditions. Figure 4.5 shows the absorption spectrum and resultant transmission electron micrograph of a typical batch of GNRs with a low amount of spherical impurities. Fresh ascorbic acid and sodium borohydride solutions were made and used for each batch while stock solutions of silver nitrate and gold chloride were kept at 0 ºC for weeks at a time before use. Although this method seems to be less sensitive to concentration fluctuations, we were not able to reproduce literature results until a crucial step was corrected. In the procedure from Ye's paper, the growth solution is produced by adding an aqueous solution of gold chloride to varying amounts of CTAB, sodium oleate and silver nitrate. We found that after the addition of gold chloride, enough time must be allowed for the sodium oleate to reduce the gold (III) ions to gold (I) ions, which was not noted in Ye's procedure. The solution starts as a pale yellow and eventually loses all color only after stirring for at least 45 minutes. Typically, the addition of ascorbic acid is responsible for this reduction step and resulting color change, but in this case sodium oleate is responsible. Confusingly, Ye's method still calls for the addition of ascorbic acid as the final step in the procedure, and indeed, does not successfully produce GNRs without it. After understanding the importance of sodium oleate as the main reducing agent, Ye's method became very reproducible and a variety of GNRs at different aspect ratios were accessed.

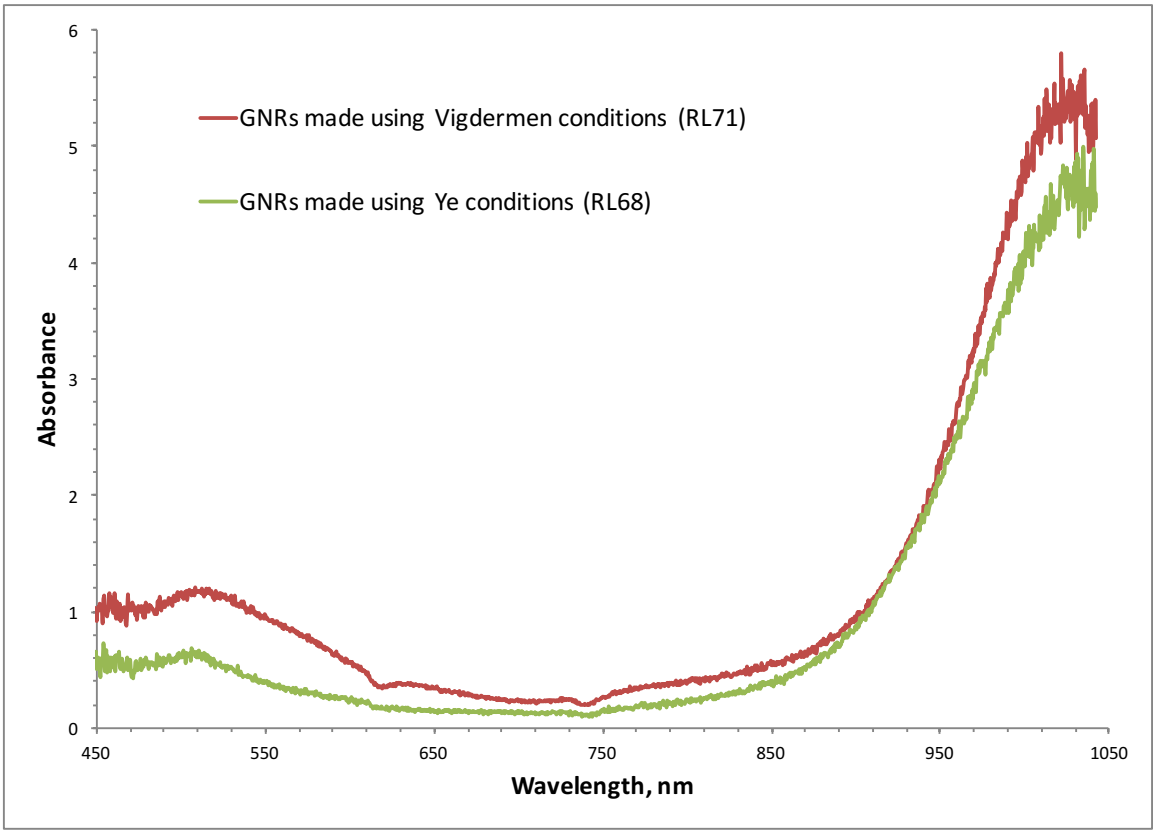


Figure 4.6. Absorption spectra of GNRs synthesized using Ye and Vigdermen conditions. Both batches were diluted by the same volume before obtaining absorption spectra. Vigdermen's method did not produce a drastically higher concentration of GNRs compared to Ye's method.

In an effort to find more efficient synthesis methods, Ye's method was compared to Vigdermen's where hydroquinone replaced ascorbic acid as the mild reducing agent. This method uses a large excess of hydroquinone relative to gold concentration, an approach that mitigates the effects of concentration fluctuations on overall yield and accuracy. Figure 4.6 includes the absorption spectra of two batches of GNRs made with Ye's method vs one made with Vigdermen's. Despite the advantages to using hydroquinone, we determined that Ye's method produced a similar concentration of GNRs.

Because Ye's method was reproduced without difficulty at a 500 ml scale, these conditions were chosen for future experiments.

4.3 Functionalization of Gold Nanorods With Thiol-Containing Polymers

4.3.1 Introduction

Because an aqueous, seed-mediated method of GNR synthesis was used, the resulting GNRs were coated in a charged surfactant and were not suitable for integration into polymer films or for the introduction of nonlinear organic molecules as proposed in Chapter 2. Aqueous GNRs can be successfully functionalized with a variety of thiol-containing compounds including cationic species,[16,17] porphyrins,[18] pseudorotaxanes,[19] perylenes[20], and water soluble diblock-copolymers.[21] In order to solubilize the GNRs in organic solvents, the use of a thiol-containing block copolymer, which both solubilizes GNRs in organic solvents and contains functionality for attaching nonlinear organic chromophores was proposed. A relatively simple two-step process[22,23] was investigated where thiol-terminated polyethylene glycol (PEG-SH) is used to replace the CTAB surfactant in aqueous solution. The resultant PEG-SH coated GNRs can be dispersed in an organic solution consisting of a high concentration of custom made thiol-containing polymer. The solution of new polymer competes for the gold surface and replaces the PEG-SH. The resulting product is stable in organic solvents and also

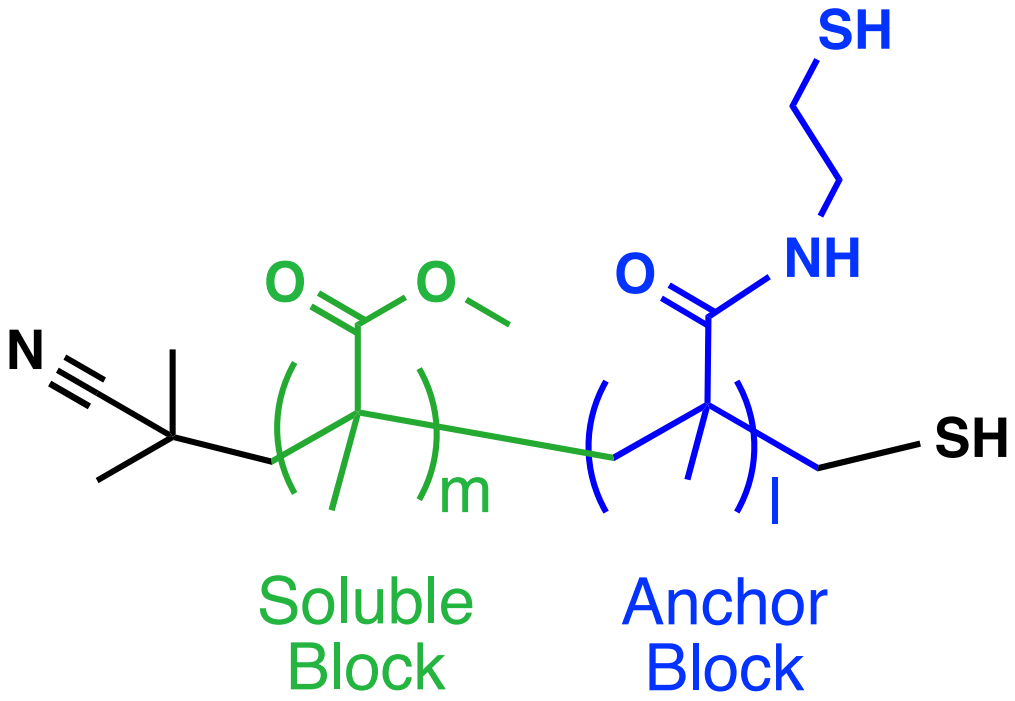


Figure 4.7. Gold reactive diblock co-polymer. Details of synthesis is found in Chapter 3.

contains any functionality included in the design of the thiol-containing polymer. Thefollowing sections will discuss the methods and characterization of functionalizing GNRs with a variety of thiol-containing polymers.

4.3.2 Functionalization of GNRs Using Thiol-Containing Poly(methyl methacrylate)

In order to develop repeatable and effective methods to functionalize GNRs at high concentrations, a simple polymer was synthesized that consisted of a poly(methyl methacrylate) block and a thiol-containing block. The synthesis of this polymer was discussed in Chapter 3 and can be seen in Figure 4.7, with a general depiction of the proses shown in Figure 4.8. The

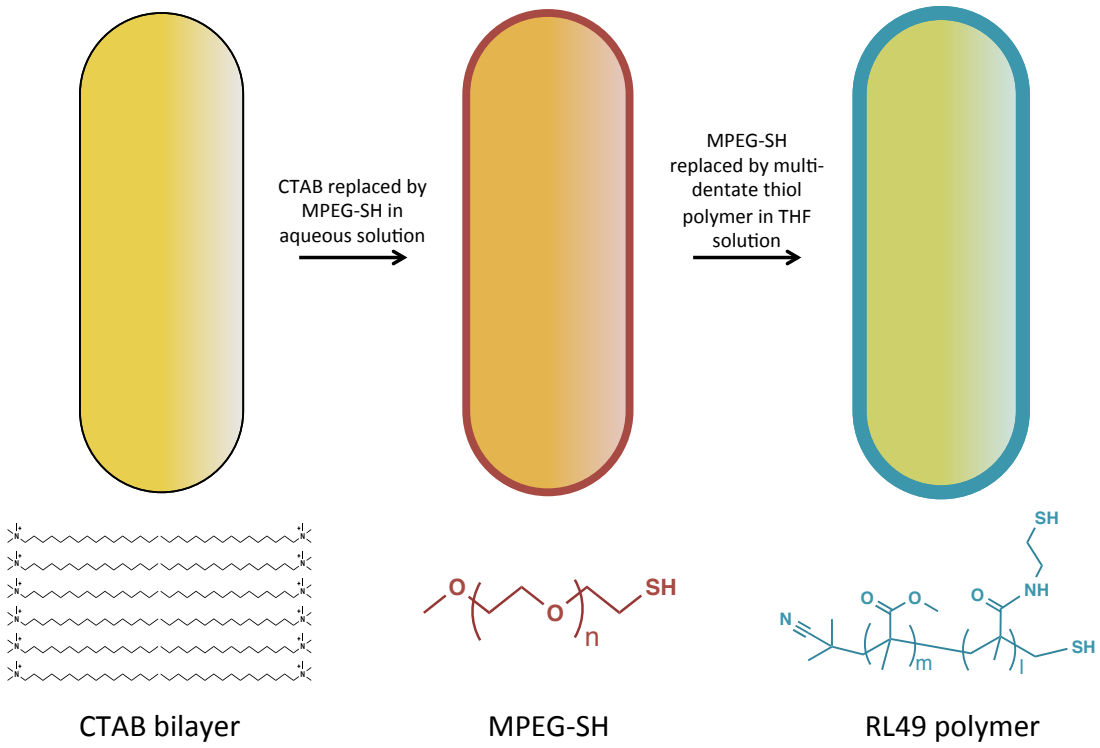


Figure 4.8. Overview of GNR functionalization. The CTAB bilayer is first replaced by MPEG-SH, a water-soluble polymer. MPEG-SH GNRs are then soluble in THF and are functionalized with a multi-dentate thiol-containing polymer.

methods of Thierry *et al.*[16] were used as a starting point but modified to adapt the method to higher concentrations of GNRs.

After GNRs are synthesized, the excess CTAB, sodium oleate and other reactants are removed by centrifugation. A typical GNR batch was prepared at a 500 mL scale. 168 mL were collected in 12 plastic falcon tubes each with a 14 mL capacity. After centrifugation, the supernatant containing undesired reactants was carefully removed and each pellet of GNRs was



Figure 4.9. Left: RL49 polymer-coated GNRs in THF. Right: Unstable CTAB coated GNRs in THF. Loss of color and precipitation occurs immediately after addition of THF.

redispersed in 1 mL of deionized water, centrifuged again and redispersed in a total of 6 mL of water. This highly concentrated solution of GNRs was used in the next reaction step without further purification. Additional centrifugation cycles were avoided as any more would reduce the residual CTAB concentration below the threshold for GNR stability.[23] 6 mL of a 1 mg/mL solution of thiol-terminated polyethylene glycol (5000 molecular weight) in water was prepared and added to a 14 mL falcon tube containing 6 mL of highly concentrated GNRs. After brief mixing and sonication, the mixture was allowed to react at room temperature overnight. The literature

called for a reaction time of a few hours, however, we found that an overnight reaction produced GNRs that were stable in organic solvents like tetrahydrofuran at a much more repeatable rate. After reacting overnight, the GNRs were purified by centrifugation and could then be redispersed in organic solvents. Although initially stable in organic solvents, PEG-SH coated GNRs were observed to precipitate out of solution after a week at room temperature. Therefore, these THF solutions of GNRs were immediately added to equivolume 5 mg/mL solutions of the multi-dentate thiol-containing polymer shown in figure 4.7. After 90 minutes of sonication, the solutions were left to react over night and then purified by centrifugation.

To demonstrate the drastic difference in solubility of GNRs before and after polymer functionalization, a concentrated pellet of CTAB coated GNRs was mixed with THF. Figure 4.9 shows the obvious incompatibility of CTAB-coated GNRs in organic solvents like THF. The GNRs immediately start to precipitate out of solution as shown by the dark grey pellet in the bottom of the centrifuge tube. Transmission electron micrograph images were taken of GNRs after functionalization with PEG-SH and the custom thiol-containing polymer. Figure 4.10 shows the TEM images of RL68 GNRs after functionalization with PEG-SH and RL49 thiol-polymer. Although the

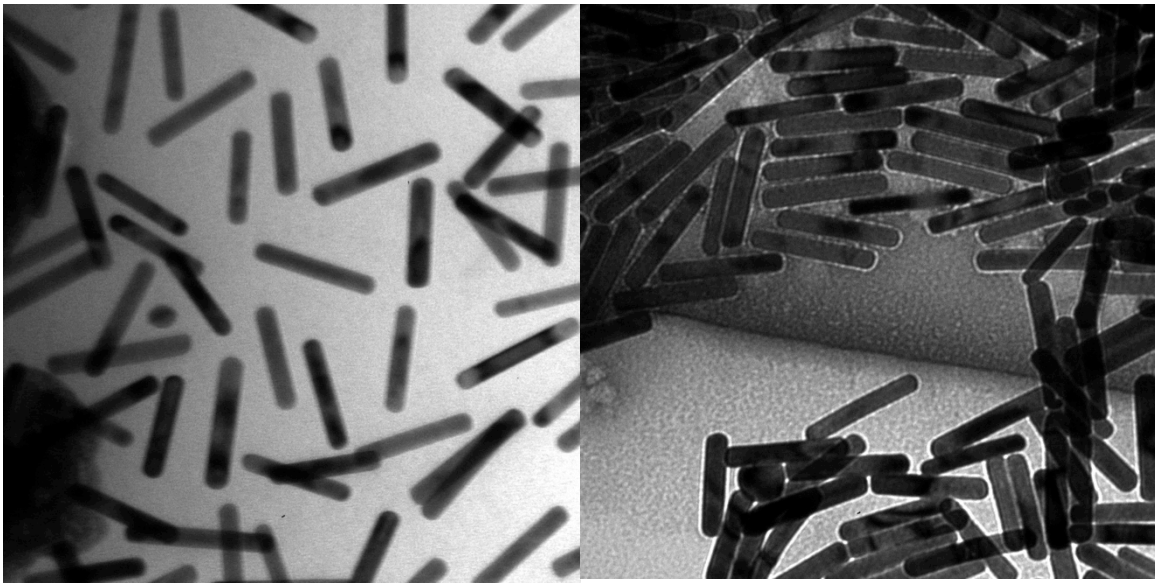


Figure 4.10. TEM images of GNRs. Left: Coated in RL49 polymer. Right: Coated in MPEG-SH.

polymer itself cannot be seen in these images, clearly the GNRs have remained stable and their shape has not been altered after the functionalization process. Solutions of GNRs functionalized with mono-dentate PEG-SH are only stable in organic solvents for approximately one week after which significant precipitation of GNRs is observed. The absorption spectrum of GNRs coated with a multi-dentate thiol polymer in acetone was collected two years after synthesis and is shown in Figure 4.11. No shape deformities can be seen in the spectrum and no precipitated GNRs were observed in the vial. The lack of precipitation indicates that GNRs coated in multi-dentate thiol-containing polymers are stable in organic solvents for long periods at room temperature.

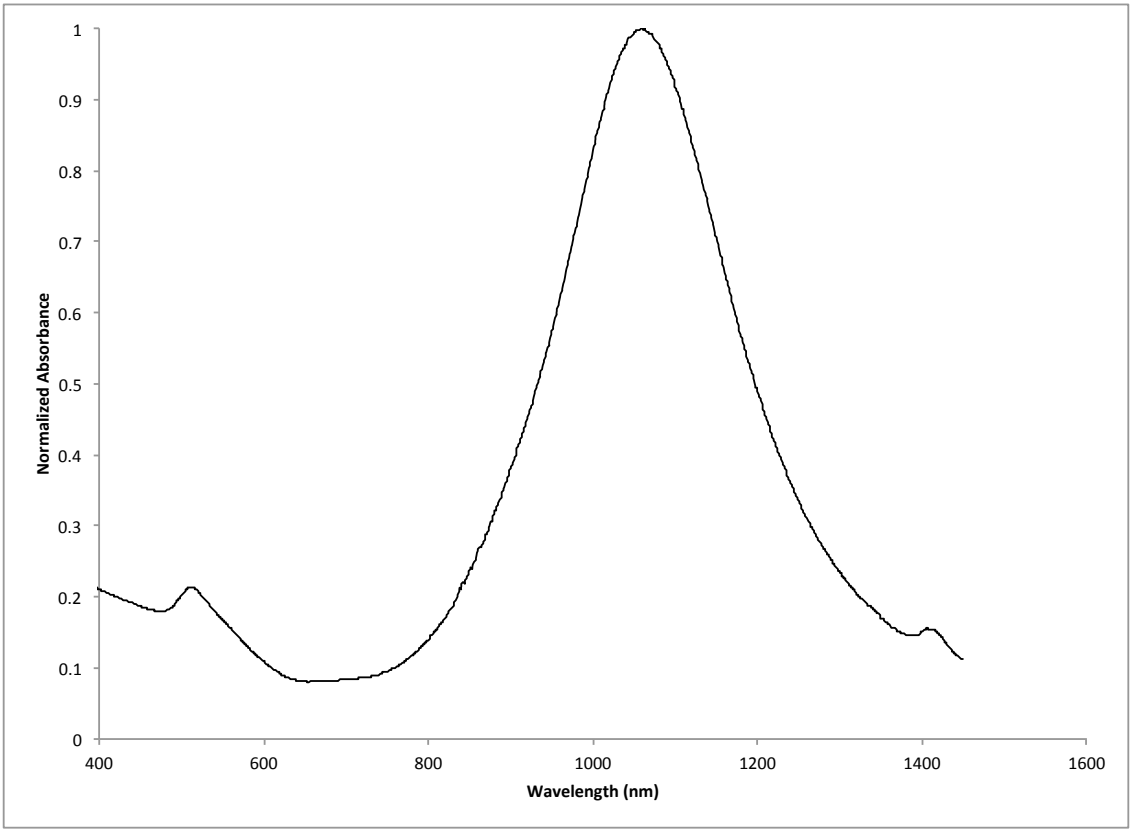


Figure 4.11. Absorption spectrum of GNRs in acetone coated in RL 49 polymer. Spectrum was taken two years after synthesis. No deformities in the distinct TSPR or LSPR peaks is observed.

4.3.3. Functionalization of GNRs Using Thiol-Containing Poly (methylmethacrylate-co-anthracene methacrylate) and poly(methyl methacrylate-co-furfuryl methacrylate)

After optimizing GNR functionalization using the simple thiol-containing PMMA, we began to test whether we could just as easily functionalize GNRs with polymers that contained Diels-Alder functionality. Following the procedure outlined above, GNRs were functionalized with both thiol-containing poly(methyl methacrylate-co-anthracene methacrylate) and thiol-containing poly(methyl methacrylate-co-furfuryl methacrylate.

Figure 4.12 shows the normalized absorption spectra of GNRs coated in

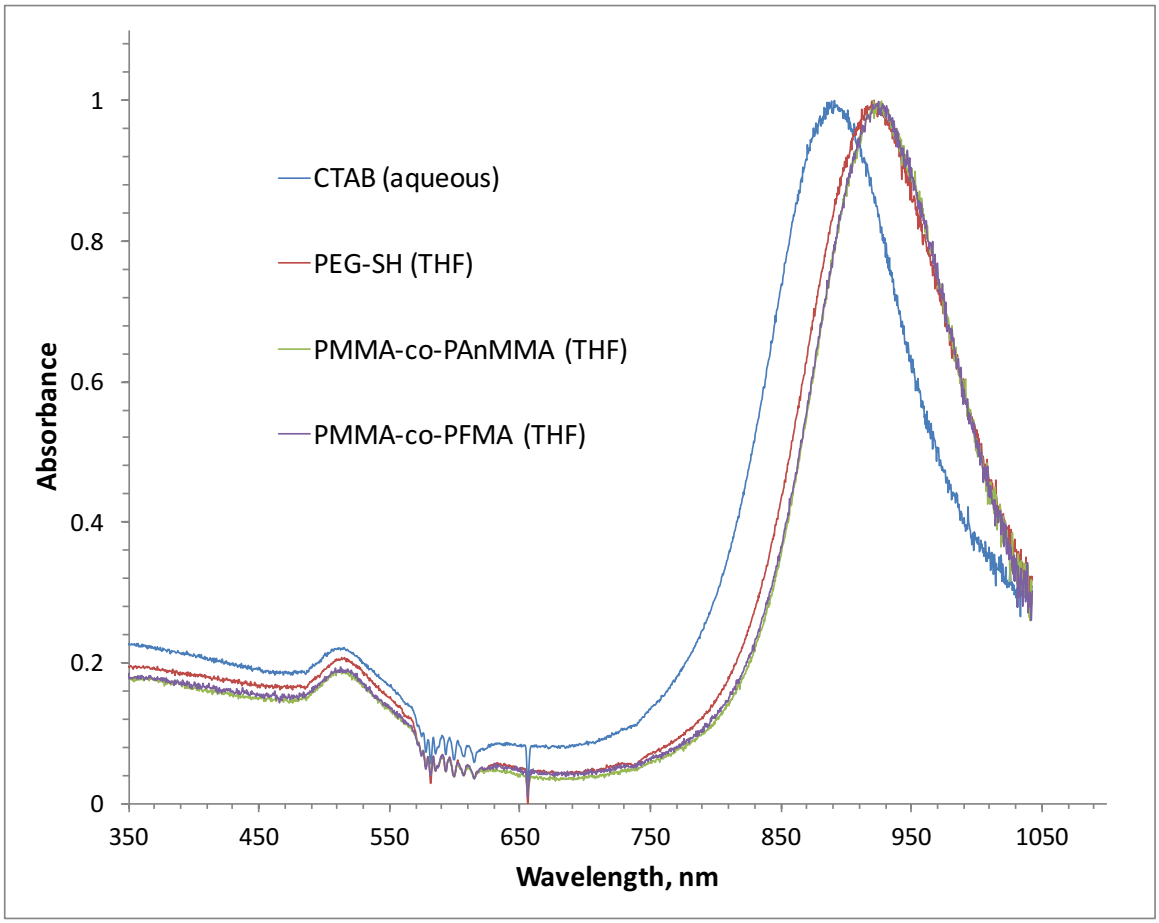


Figure 4.12. Absorption spectrum of GNRs in 4 different coatings normalized to the LSPR peak. A red shift in the absorbance of the LSPR peak is observed after replacing MPEG-SH with either PMMA-*co*-PAnMMA or PMMA-*co*-PFMA. No deformities in the spectra profile is observed, indicating that the GNRs are stable after functionalization.

CTAB, MPEG-SH in THF, and both custom polymers in THF. The distinct TSPR and LSPR absorption peaks are well defined for each coating indicating stable GNRs after functionalization.

Thermogravimetric analysis (TGA) was also used to confirm that our custom polymers were replacing the PEG-SH coating. As GNRs are heated, the compounds adhered to their surface decompose leaving bare gold in the

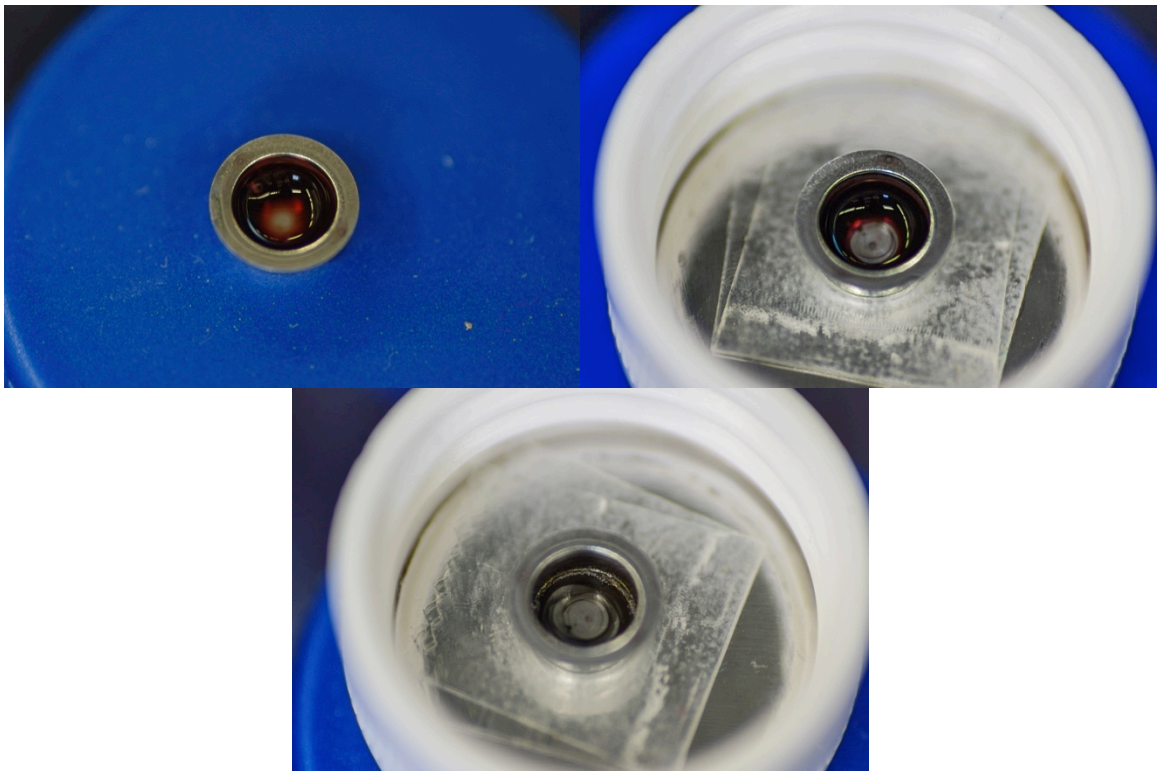


Figure 4.13. GNR sample preparation for TGA experiments. GNRs were slowly added in portions to aluminum pans. Solvent was evaporated with nitrogen before further evaporation under vacuum.

sample pan. The resulting curve shows weight loss percentage versus temperature. This profile is unique to the different GNR surface compositions. To prepare samples for TGA experiments, 1 mL of highly concentrated GNRs were centrifuged. The resulting pellet was redispersed in 50 microliters of solvent before being added slowly in 5-10 microliter portions to an aluminum pan. The solvent (either aqueous or organic) was evaporated by using a flow of nitrogen gas before another portion was added. After the desired portions were added, the pan was placed under vacuum for 1 hour.

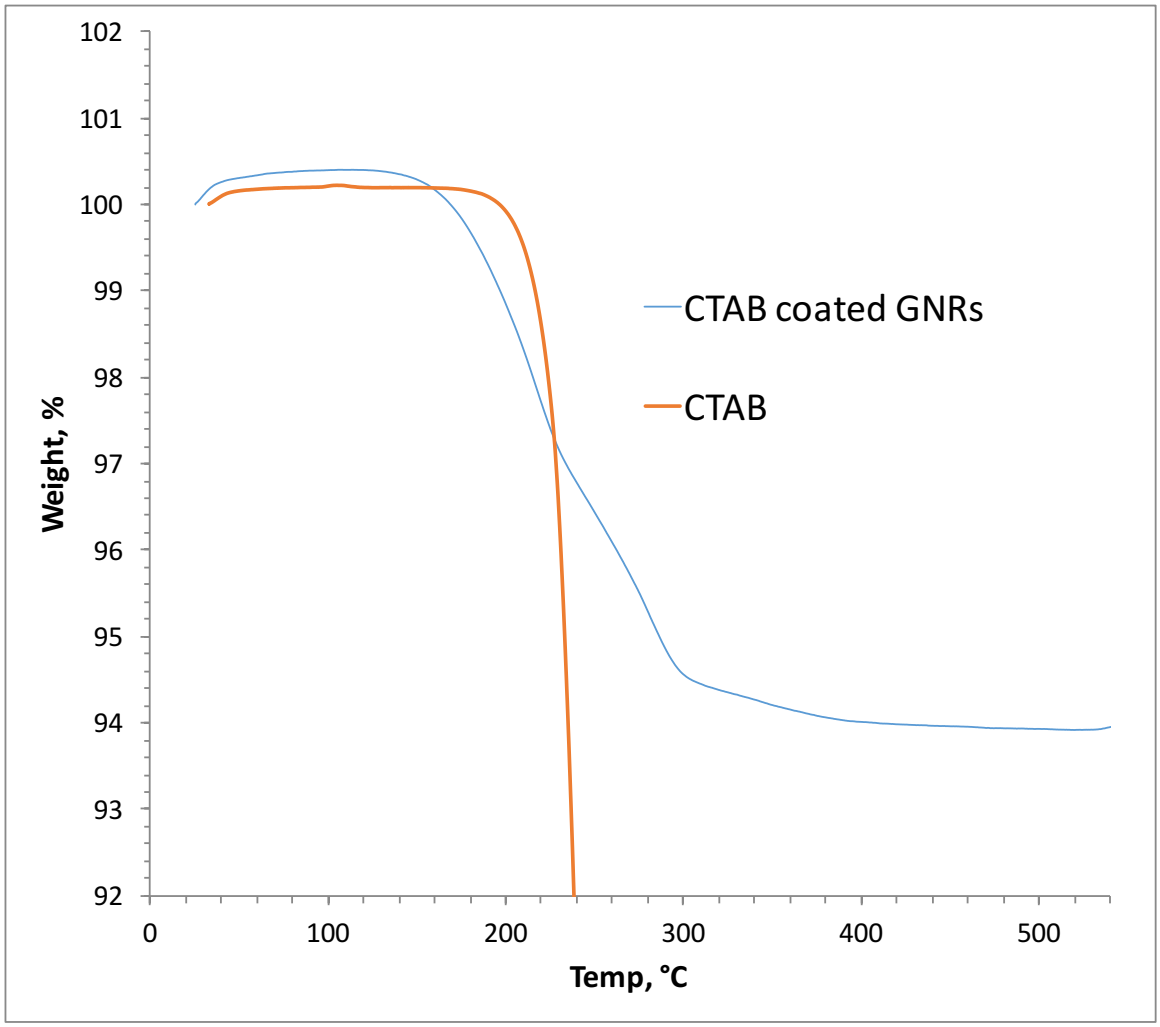


Figure 4.14. TGA traces of CTAB coated GNRs and a sample of pure CTAB. The GNR sample begins to lose weight at nearly the same temperature of pure CTAB, indicating a surface coating of CTAB on the GNRs.

In this way, enough GNR weight was added to ensure a successful TGA measurement.

GNRs are stabilized in solution by CTAB, during and after synthesis. We expect so see weight loss near a similar temperature to that of a sample of pure CTAB. Figure 4.14 shows the TGA trace of pure CTAB and GNRs

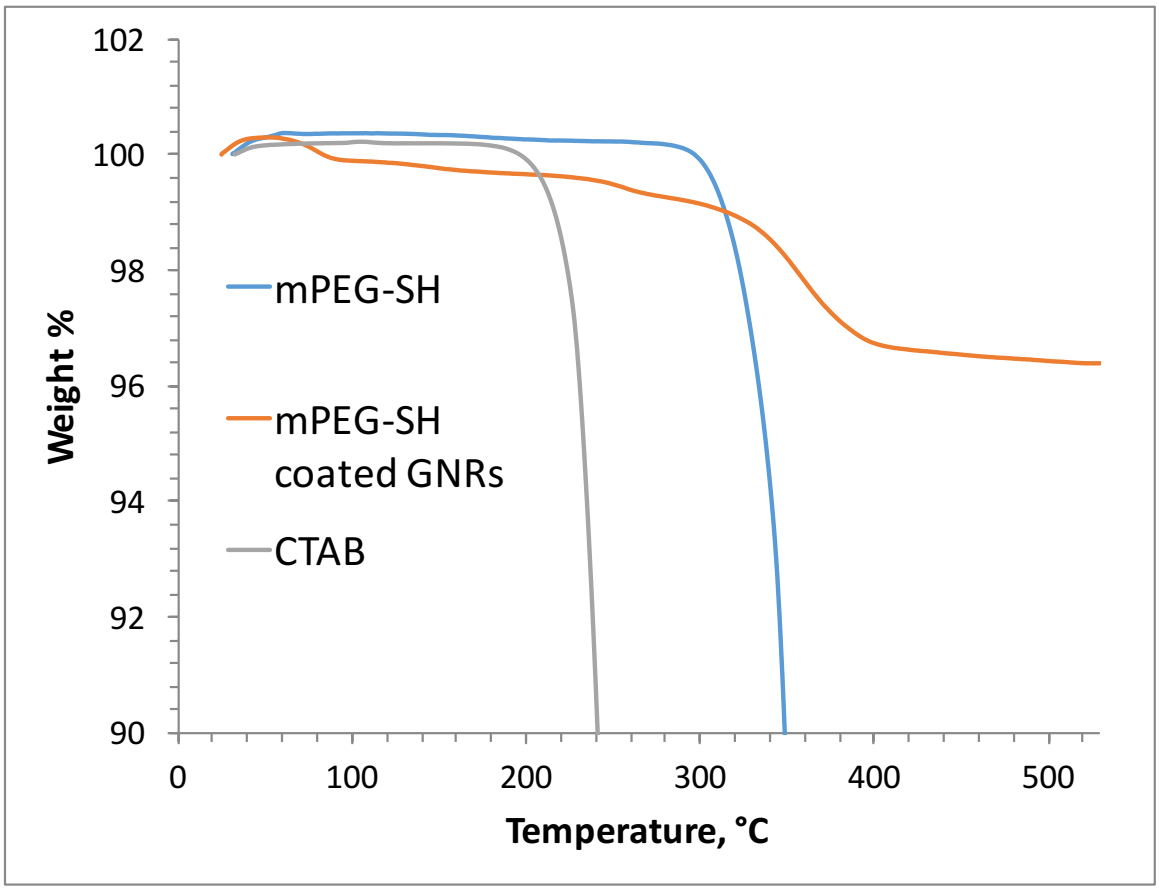


Figure 4.15. TGA traces of pure CTAB, pure mPEG-SH and GNRs after reacting with mPEG-SH. Both pure mPEG-SH and GNRs coated in mPEG-SH start losing weight near 350 °C.

after they have been synthesized. Weight percentage begins to decrease near 200 °C for both CTAB and the GNRs. These results confirm the presence of CTAB on the surface of the GNRs. After reacting with mPEG-SH, TGA was performed again. We expect to now see weight loss similar to that of a sample of pure mPEG-SH. Figure 4.15 shows a typical TGA trace of GNRs after reacting with mPEG-SH along with traces from pure CTAB and pure mPEG-SH. If any significant amount of CTAB remained on the surface of the

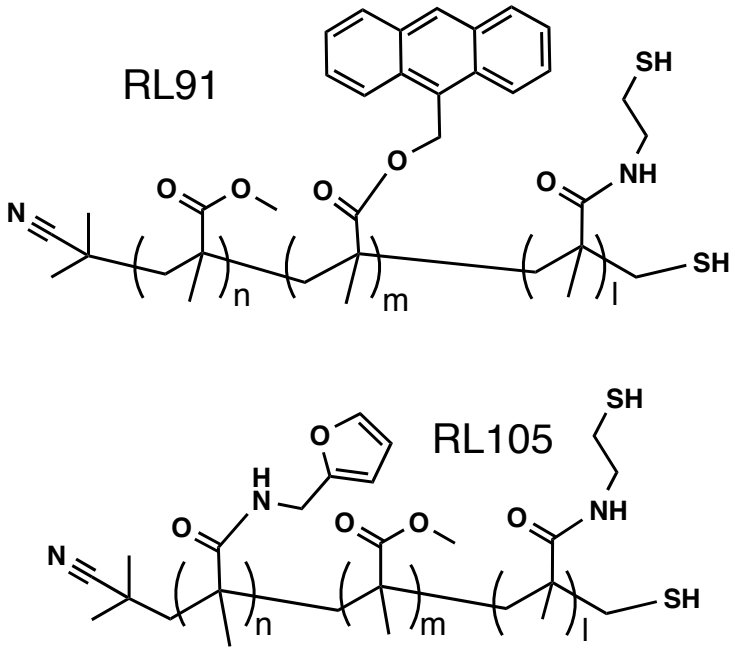


Figure 4.16. Structures of polymers used in TGA studies. Both are multi-dentate with respect to gold reactivity and contain Diels-Alder functionality.

GNRs, an obvious weight loss near 200 °C would be observed. One obvious weight loss is observed near 350 °C indicating the GNRs have been functionalized with mPEG-SH.

After GNRs were functionalized with mPEG-SH, they were reacted with the polymers found in Figure 4.16. TGA was used to determine whether the weight loss profile changed after the reaction took place. Figure 4.17 shows the TGA traces of GNRs coated in mPEG-SH and coated in RL91 polymer. A gradual weight loss profile is seen for the sample of GNRs coated in RL91 polymer. The distinctive drop in weight near 350 °C characteristic of mPEG-SH coated GNRs is no longer observed after a reaction with the multi-dentate, furan-containing RL91 polymer.

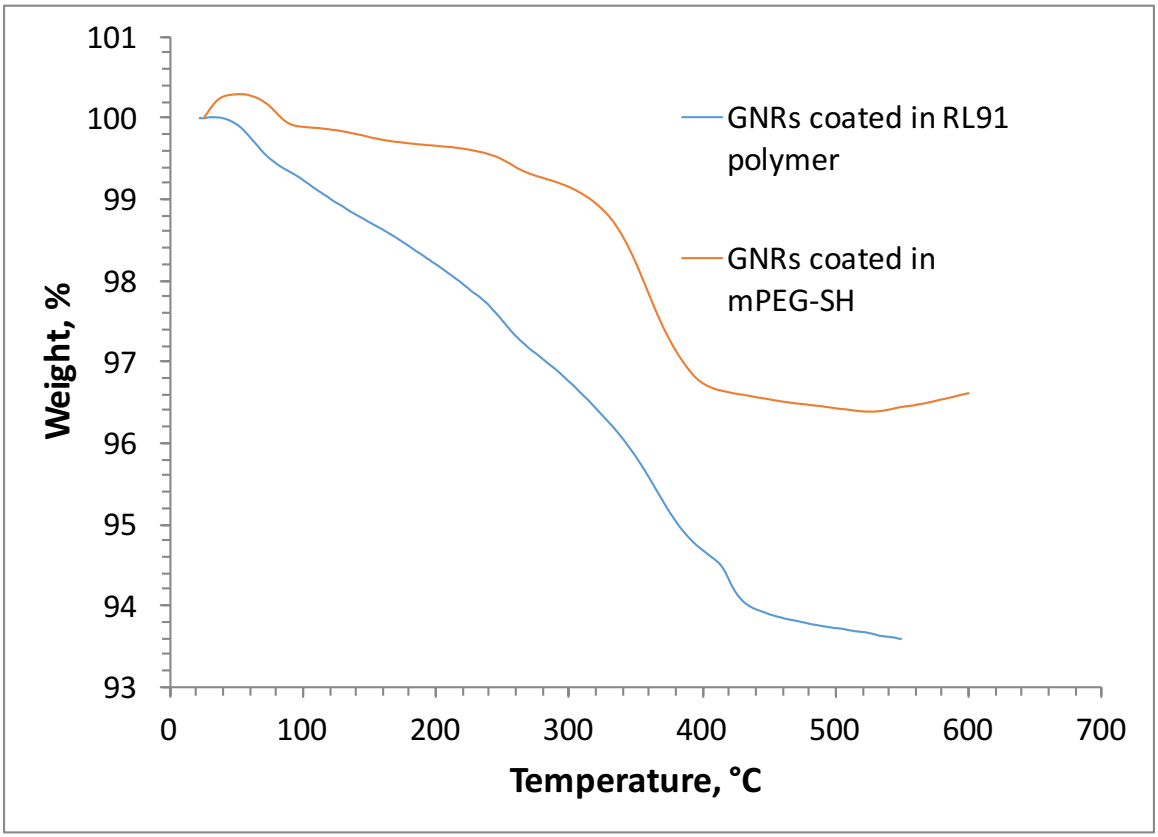


Figure 4.17. TGA traces of GNRs coated in mPEG-SH and GNRs coated in RL91 polymer. A distinctive drop in weight near 350 °C is observed for GNRs coated in mPEG-SH but not for GNRs coated in RL91. This indicates that the mPEG-SH has been replaced by RL91.

TGA was also used to study GNRs after they reacted with RL105 polymer. When this TGA experiment was performed, the aluminum pan was not tared. Therefore, the weight percent is not corrected for the pan weight. However, the shape of the weight loss curve is still accurate and shows at which temperatures the GNR sample starts to lose weight. Figure 4.18 shows the TGA trace for GNRs after they the reaction with RL105 polymer. The shape is clearly different to that of GNRs coated with mPEG-SH with a gradual loss of weight, more similar to that of GNRs coated in RL91 polymer.

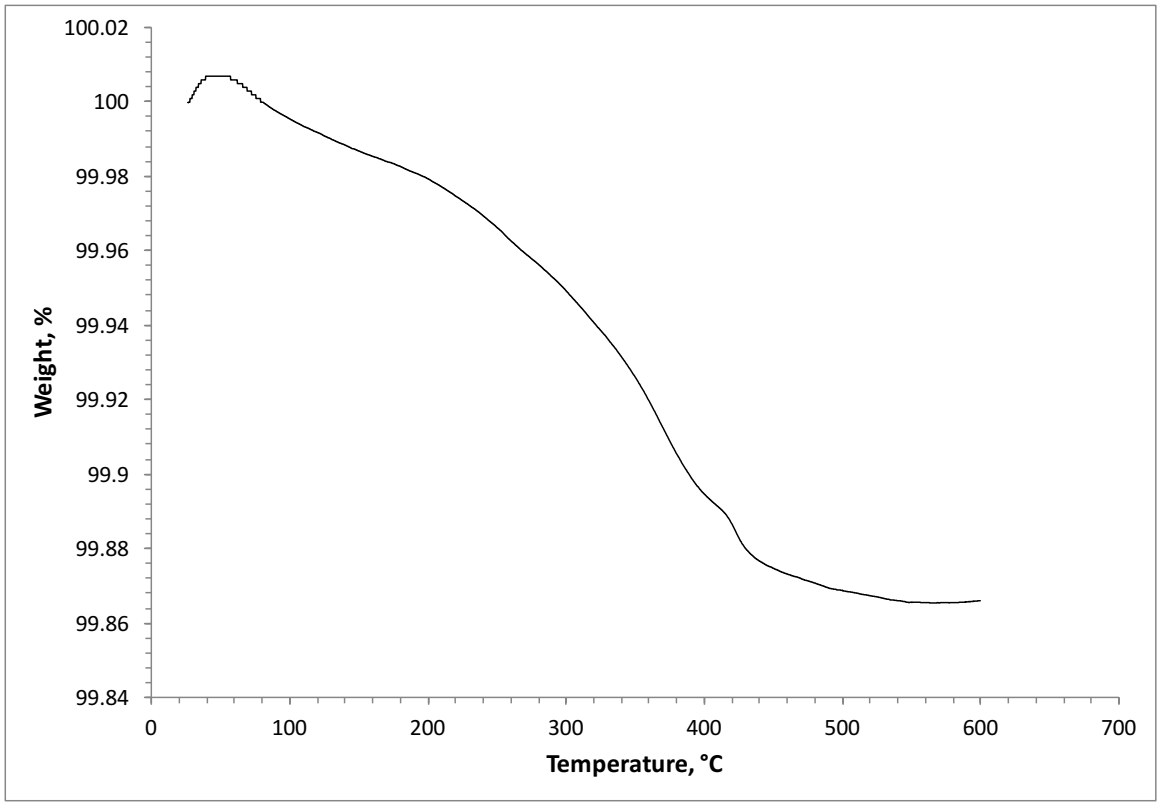


Figure 4.18. TGA trace of GNRs coated in RL105 polymer. The weight percent has not been corrected for the tare weight of the pan and sample. However, the shape of the curve still indicates that mPEG-SH has been replaced with RL105 polymer.

Finally, TGA was used to measure the weight loss curve of GNRs that had been coated in RL137 polymer. RL137 was the final polymer to be tested that has both thiol and Diels-Alder functionality. Unlike previous polymers, the thiol groups in RL137 are built into the monomer in the form of a disulfide species and can be polymerized under RAFT conditions. Figure 4.19 shows the TGA data gathered for GNRs coated in RL137 and mPEG-SH. Again, the significantly different traces of each sample show that mPEG-SH is being replaced by RL137 on the surface of the GNRs.

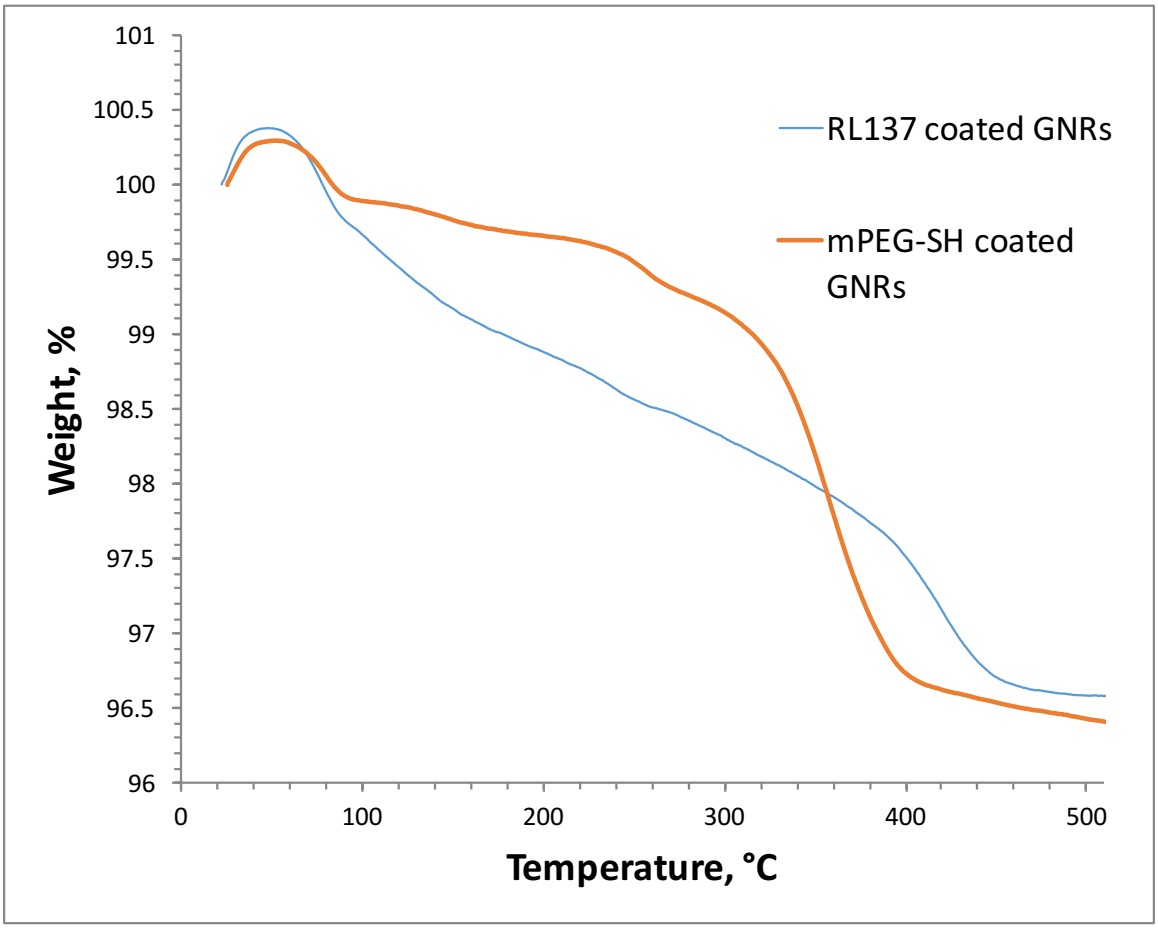


Figure 4.19. TGA traces of GNRs coated in RL137 and mPEG-SH. A gradual weight loss is observed for GNRs coated in RL137, with an additional sharp drop off near 400 °C. The trace for GNRs coated in RL137 is significantly different to that of GNRs coated in mPEG-SH.

4.3.4 Preparation of GNR-Doped Polymer Films

After optimizing the procedure for producing organic-soluble GNRs, efforts were turned towards developing a reproducible method for doping polymer films with GNRs. Films of GNRs may be used concurrently with poling of nonlinear organic chromophores. And, after discussions with a local technology company, we discovered that the unique absorption profile of GNRs can be useful in the design of laser components. The goal of this new

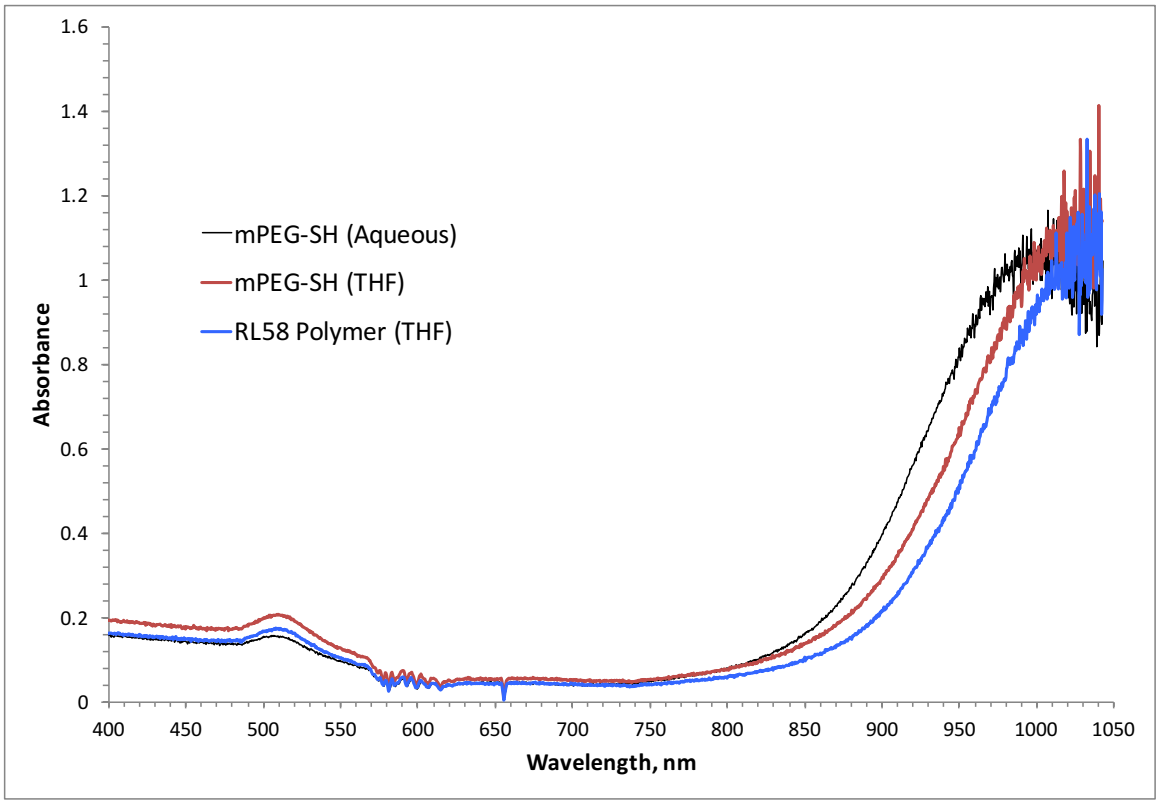


Figure 4.20. Absorption spectra of GNRs before doping into polymer films. Labels indicate coating and solvent environment. Although the LSPR peak is cut off, enough is present to suggest GNRs are stable throughout functionalization.

project was to produce a stable UV-curable film of GNRs with tuned absorption specifically at 1064 nm and high transmission at 808 nm. Results of from these studies and their consequences for commercial development are fully discussed in Chapter 5. In the material presented below, discussion will be limited to early efforts of producing GNR films in commercially available poly(methyl methacrylate-co-ethyl acrylate). This polymer was chosen for its low cost and suitable solubility in common solvents.

To begin the process, RL73 GNRs were functionalized with the thiol-containing polymer previously shown in Figure 3.4. Figure 4.20 shows the

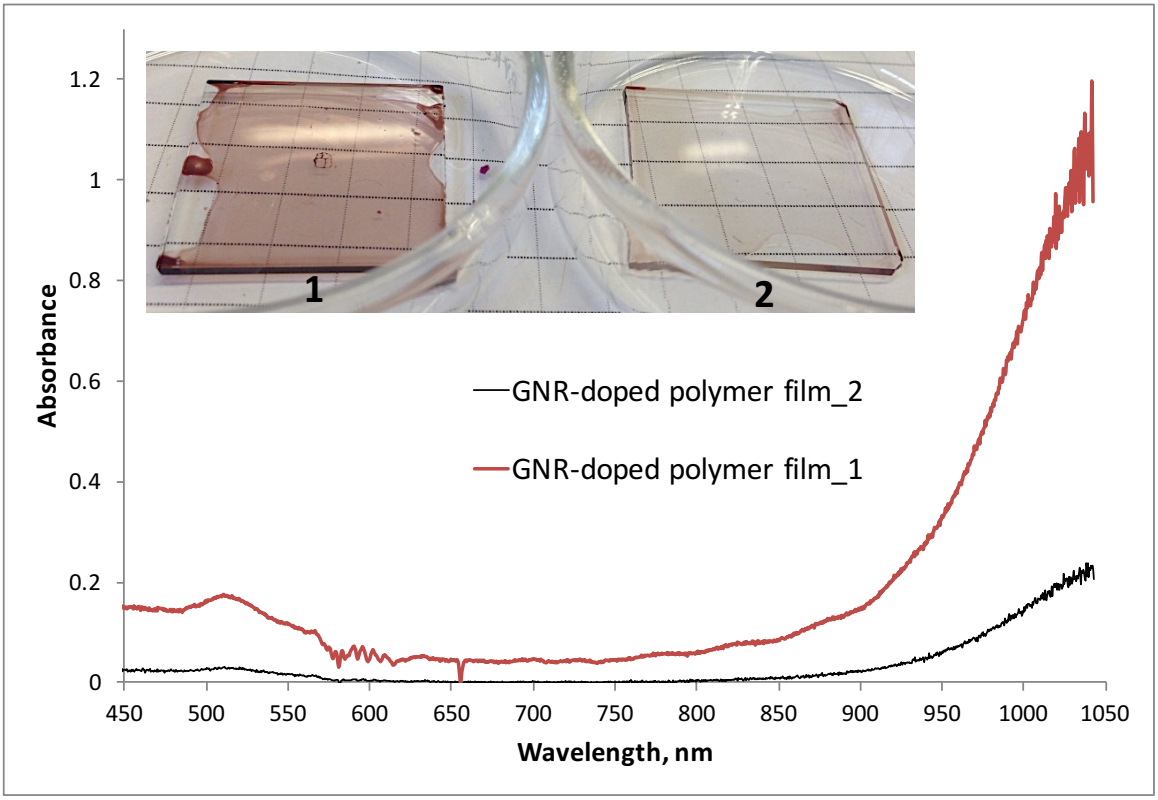


Figure 4.21. Absorption spectra of two polymer films doped with different concentration of GNRs.

absorption spectra of GNRs throughout the process. A red shift is observed as the GNRs are transferred from an aqueous environment to an organic environment. After these functionalization steps, various attempts were made to dissolve the GNRs into a solution of poly(methyl methacrylate-co-ethyl acrylate) in 1,1,1-trichloroethane (TCE). Because these solutions would be eventually spun on glass slides using a spin coater, the weight percent of polymer in TCE needed to be sufficiently viscous to produce films with a GNR density detectable by UV/Vis spectroscopy. With this requirement in mind, 1.5 mL of GNRs were centrifuged into a concentrated pellet to remove excess

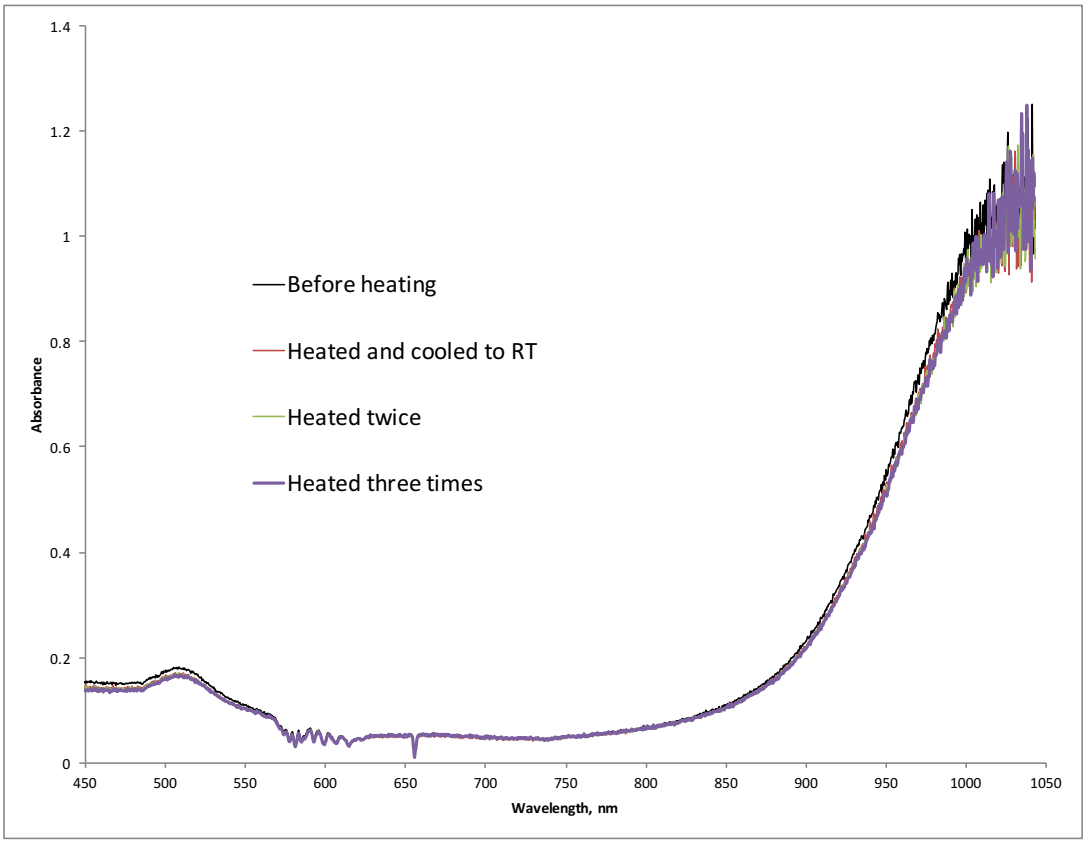


Figure 4.22. Absorption spectra of GNR-doped 'film 2' before and after heating to 100°C multiple times. Very little change in the absorption spectra is seen after heating and cooling, indicating stable films of GNRs. and after three rounds of heating and cooling to 100°C.

solvent. Typically, approximately 300 mg of an 8% weight solution of poly(methyl methacrylate-co-ethyl acrylate) in TCE was added to a GNR pellet. After sufficient mixing, the resulting viscous solution placed on a glass slide and spun using a spin coater. The resulting film was heated at 95°C under vacuum overnight to evaporate solvent. Figure 4.21 shows the absorption spectra and photos of two samples of GNRs in a polymer film. The full spectrum is not visible past 1050 nm due to the limitations of the spectrometer. However, no clouding or precipitation is observed after doping

GNRs into polymers and curing overnight. A second, similarly prepared film was heated two more times in order to observe the effects of multiple heating and cooling cycles. Figure 4.22 shows the absorption spectra of Film 2 before A slight red shift is observed after the first round, but no significant change can be seen in the spectra or the appearance of the films themselves.

In order to observe more of the LSPR peak in the absorption spectra, GNRs of a smaller aspect ratio were synthesized and studied. 4.23 shows the normalized absorption spectra comparing the smaller GNRs in water, THF, and a film of poly(methyl methacrylate-co-ethyl acrylate). Importantly, the

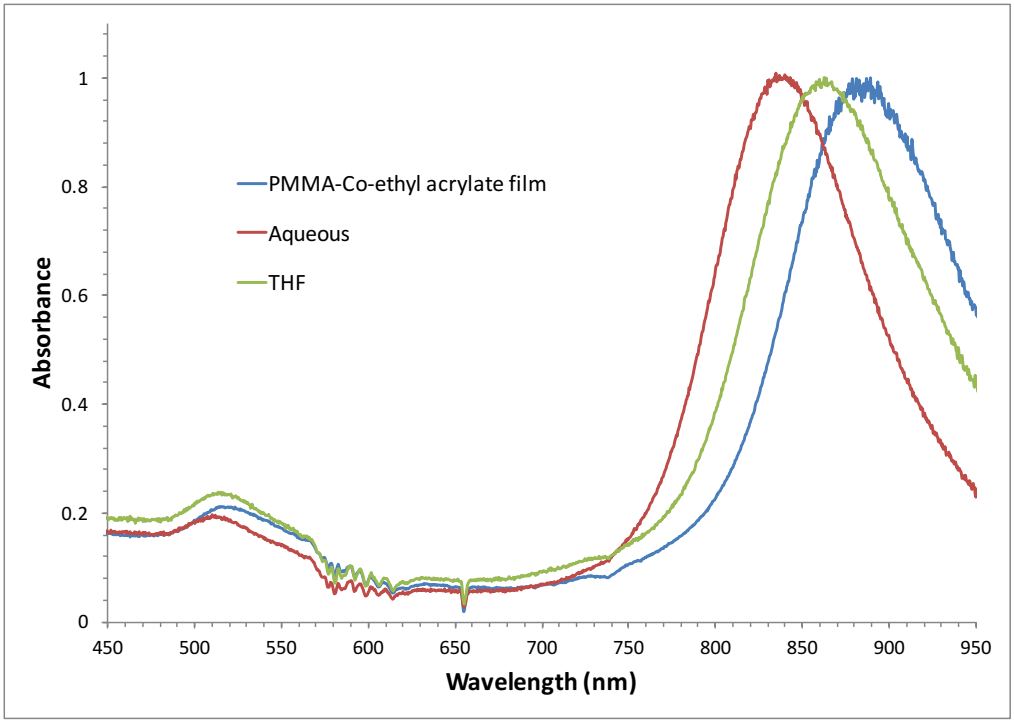


Figure 4.23. Absorption spectra of GNRs in water, THF and a thin film of poly(methyl methacrylate-co-ethyl acrylate). Absorption intensity is normalized to the LSPR peak.

distinct shape of the LSPR and TSPR peaks are not distorted as the GNRs are moved from their initial aqueous environment. However, a distinct shift in the maximum longitudinal absorption peak can be better observed for the smaller GNRs. The thermal stability of this new GNR film was tested and the polymer coated glass slide was allowed to heat at 95°C for an additional day. Figure 4.24 shows the absorption spectra of the GNR film after the first day in the vacuum oven and after one additional day of heating in ambient conditions. Both the distinctive TSPR and LSPR peaks showed no signs of

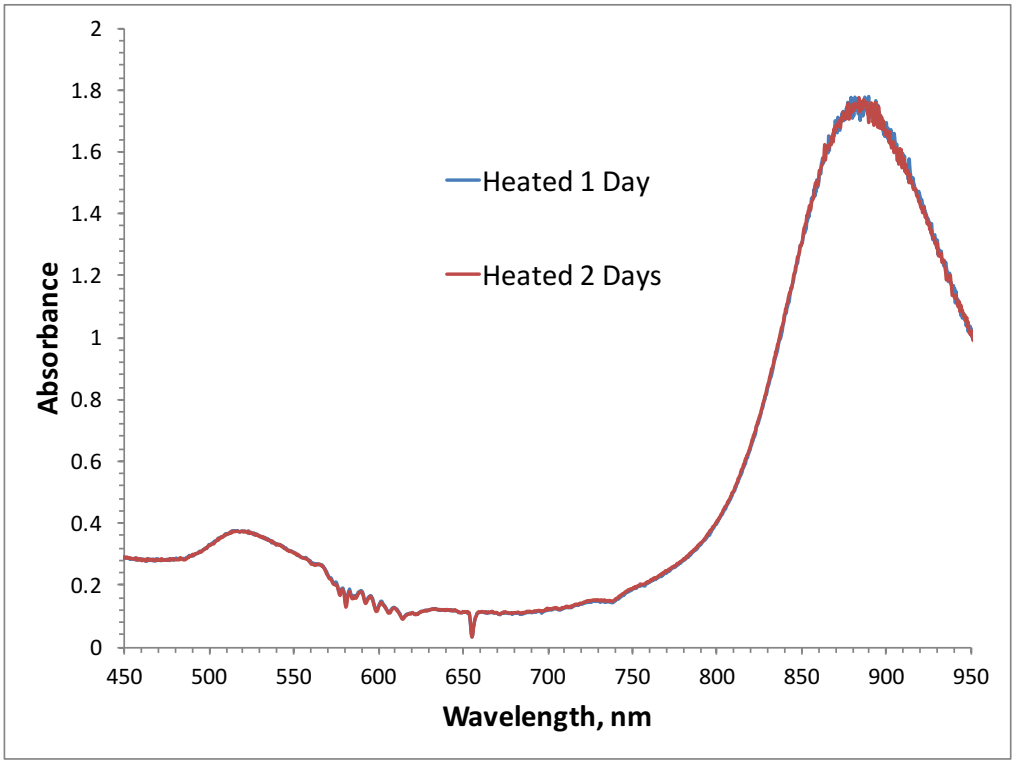


Figure 4.24. Absorption spectra of GNRs in a thin film of poly(methyl methacrylate-co-ethyl acrylate) after curing at 95°C for 1 and 2 days. Almost the entire LSPR peak is observed for this sample of smaller GNRs. No shape deformities or shifts in the LSPR peak can be detected.

degradation after heating. This result again shows that GNRs are stable in polymer films, even after heating them to relatively high temperatures. The use of GNRs in polymer and epoxy films will be discussed more thoroughly in chapter 5.

4.4 Conclusion

Data presented in this chapter demonstrate that GNRs can be synthesized at high purity and concentration. Because the surface plasmon resonance of the GNRs is due to physical size, the absorption profile of the GNRs could be tuned by synthesizing GNRs with differing aspect ratios and monitoring each sample's optical properties. These GNRs were initially synthesized in aqueous environments, stabilized by CTAB. In order to improve solubility in organic solvents, CTAB stabilizing GNRs could be functionalized with mPEG-SH at high concentrations. The mPEG-SH coating allowed for solubility in both aqueous and organic solvent environments and served as a temporary coating that was then replaced by custom made polymers that contained Diels-Alder functionality. The stability of GNRs at each functionalization step was observed using UV/Vis spectroscopy, scanning electron microscopy, transmission electron microscopy, and thermogravimetric analysis. Small differences were observed in maximum absorption of the LSPR peak after replacing mPEG-SH with custom polymers. TGA traces were dramatically different when mPEG-

SH was replaced with custom polymers, indicating successful functionalization of the GNRs. These new materials are very stable in organic solvents and thin polymer films and have the capability for attachment of nonlinear organic dyes via Diels-Alder, with the goal of producing the metamaterials outlined Chapter 2.

4.5 Experimental Section

4.5.1 Materials and Instrumentation

Cetyltriethylammonium bromide (CTAB) (Amresco, 99%), silver nitrate (Aldrich, 99%), Ascorbic Acid (Sigma, >99%), $HAuCl_4 \cdot 3H_2O$ (Aldrich, 99.9%), sodium borohydride (Fluka, >99%), poly(methyl methacrylate-*co*-ethyl ecrylate) (Aldrich), sodium oleate (Pfaltz & Bauer, 97%), and MPEG-SH_{5000} (Methoxy-Poly(Ethylene-glycol)-Thiol, (Laysan Bio Inc.) were all used without further purification.

Thermogravimetric analysis was performed using a TA Instruments Discovery TGA. Typical experiments were run at 20°C per minute. Uv/Vis spectra were obtained using either an Ocean Optics USB2000+ or a Shimadzu UV2400.

4.5.2 General Procedure
for Gold Nanorod Synthesis

Gold nanorods were synthesized using a modified seed synthesis developed by Ye et al.[14] The seed solution was prepared by mixing 5 mL of 0.5 mM $HAuCl_4 \cdot 3H_2O$ with 5 mL of 0.2M cetyltriethylammonium bromide (CTAB). 0.6 mL of freshly prepared 0.01M $NaBH_4$ was diluted to 1 mL and injected into the $HAuCl_4$-CTAB solution while vigorously for 2 minutes. The

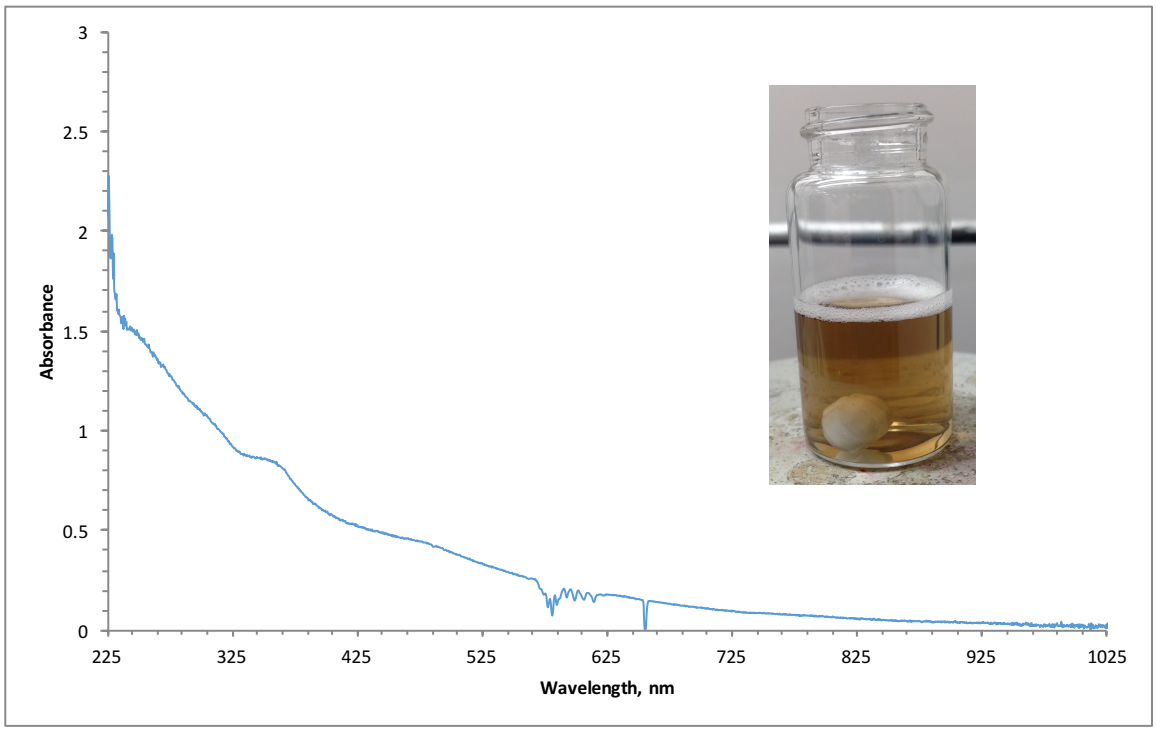


Figure 4.25. Absorption spectrum and photograph of typical seed solution.

solution turned from yellow to brown. Before use, it was allowed to age for 30 minutes at slightly above room temperature. If temperature was not elevated, crystallization of CTAB was observed. Figure 4.25 shows the absorption spectrum and photograph of a typical seed solution.

A growth solution was prepared by fully dissolving 7.0 g of CTAB and 1.234 g Sodium Oleate in 250 mL of ultrapure water while stirring at a temperature of ~50 °C. After cooling to 30 °C, 24 mL of 4 mM $AgNO_3$ was added and kept undisturbed at 30 °C for 15 minutes. 250 mL of 1 mM $HAuCl_4 \cdot 3H_2O$ was then added and stirred for ~45 minutes until the solution's color changed from yellow to clear. The pH was then adjusted by the addition of 3.6 mL concentrated HCl. After 15 minutes of slow stirring, 1.25 mL of 0.064M Ascorbic Acid was introduced and stirred vigorously for 30 seconds. 400 μL of seed solution was then injected into the growth solution and stirred for 30 seconds. The solution was left undisturbed at 30 °C for 12 hours. The color of the resulting nanorods solution was light brown, indicative of very few spherical impurities.

4.5.3 General Procedure for Gold Nanorod Functionalization

Functionalization procedure was adapted from Thierry et al.[22] 168 mL of freshly prepared GNRs were centrifuged at 6000 rpm in 14 mL falcon tubes for 1 hour. The clear supernatant was discarded and the GNR pellets were resuspended in 1.5 mL of water and centrifuged for 10 mins at 13,000 rpm. Each of the resulting pellets were resuspended in 0.5 mL of water and combined in a 14 mL falcon tube. An equivolume aqueous solution of 1 mg/mL MPEG-SH_{5000} ((Methoxy-Poly(Ethylene-glycol)-Thiol) was added to

the GNRs while vigorously shaking followed by sonication for 5 minutes. The resulting solution was left to react at room temperature overnight. Excess MPEG-SH solution was removed by centrifugation for 10 minutes at 13,000 rpm. The pellets could then readily be resuspended in organic solvents such as THF and toluene. No color change or precipitation was observed when resuspended. THF solutions of GNRs were then mixed with 5 mg/mL equivolume solutions of thiol-functionalized polymer in THF, sonicated for 90 minutes and left to react overnight. Excess polymer solution was removed by centrifugation at 13,000 rpm for 10 minutes. GNR pellets were redispersed in 4 mL of THF. This concentrated solution was diluted or concentrated as needed for UV/Vis, TGA, SEM, or TEM characterization.

4.6 References

1. Van der Zande, B., Böhmer, M. R. & Fokkink, L. Colloidal dispersions of gold rods: synthesis and optical properties. *Langmuir* **16 (2)**,451-458 (2000).

2. Hulteen, J. & Martin, C. A general template-based method for the preparation of nanomaterials. *J. Mater. Chem.* **7,** 1075–1087 (1997).

3. Kim, F., Song, J. H. & Yang, P. Photochemical synthesis of gold nanorods. *J. Am. Chem. Soc.* **124,** 14316–7 (2002).

4. Yu, YY, Chang, SS & Lee, CL. Gold nanorods: electrochemical synthesis and optical properties. *J. Phys. Chem. B* **101** 6661-6664 (1997).

5. Reetz, M. T. & Helbig, W. Size-selective synthesis of nanostructured transition metal clusters. *J. Am. Chem. Soc.* **116 (16)** 7401-7402 (1994).

6. Esumi, K., Matsuhisa, K. & Torigoe, K. Preparation of rodlike gold particles by UV irradiation using cationic micelles as a template. *Langmuir* **11,** 3285–3287 (1995).

7. Jana, N. *et al.* Liquid crystalline assemblies of ordered gold nanorods. *J. Mater. Chem.* **12,** 2909–2912 (2002).

8. Jana*, N., Gearheart, L. & Murphy*, C. Wet Chemical Synthesis of High Aspect Ratio Cylindrical Gold Nanorods. *J. Phys. Chem. B* **105,** 4065–4067 (2001).

9. Nikoobakht, B. & El-Sayed, M. A. Preparation and Growth Mechanism of Gold Nanorods (NRs) Using Seed-Mediated Growth Method. *Chem. Mater.* **15**, 1957-1962 (2003).

10. Chen, H., Shao, L., Li, Q. & Wang, J. Gold nanorods and their plasmonic properties. *Chem. Soc. Rev.* **42,** 2679–724 (2013).

11. Vigderman, L., Khanal, B. & Zubarev, E. Functional gold nanorods: synthesis, self-assembly, and sensing applications. *Adv. Mat.* **24**, 4811–41 (2012).

12. Noguez, C. Surface plasmons on metal nanoparticles: the influence of shape and physical environment. *J. Phys. Chem. C* **111**, 3806-3819 (2007).

13. Nelayah, J, Kociak, M, Stéphan, O & de Abajo, F. Mapping surface plasmons on a single metallic nanoparticle. *Nature Physics* **3**, 348-(2007).

14. Ye, X. *et al.* Improved size-tunable synthesis of monodisperse gold nanorods through the use of aromatic additives. *ACS Nano* **6,** 2804–17 (2012).

15. Ye, X., Zheng, C., Chen, J., Gao, Y. & Murray, C. B. Using binary surfactant mixtures to simultaneously improve the dimensional tunability and monodispersity in the seeded growth of gold nanorods. *Nano Lett.* **13,** 765–71 (2013).

16. Vigderman, L., Manna, P. & Zubarev, E. R. Quantitative replacement of cetyl trimethylammonium bromide by cationic thiol ligands on the surface of gold nanorods and their extremely large uptake by cancer cells. *Angew. Chem. Int. Ed. Engl.* **51,** 636–41 (2012).

17. Bao, Y., Vigderman, L., Zubarev, E. R. & Jiang, C. Robust multilayer thin films containing cationic thiol-functionalized gold nanorods for tunable plasmonic properties. *Langmuir* **28,** 923–30 (2012).

18. Xue, C. *et al.* Organo-soluble porphyrin mixed monolayer-protected gold nanorods with intercalated fullerenes. *Langmuir* **28,** 5956–63 (2012).

19. Ma, X., Xue, Y., Dai, L., Urbas, A. & Li, Q. Hydrophilic Cucurbit[7]uril-Pseudorotaxane-Anchored-Monolayer-Protected Gold Nanorods. *Eur. J. Inorg. Chem.* **2013,** 2682–2686 (2013).

20. Xue, C. *et al.* Perylene Monolayer Protected Gold Nanorods: Unique Optical, Electronic Properties and Self-Assemblies. *J. Phys. Chem. C* **116,** 10396–10404 (2012).

21. Chen, X., Lawrence, J., Parelkar, S. & Emrick, T. Novel Zwitterionic Copolymers with Dihydrolipoic Acid: Synthesis and Preparation of Nonfouling Nanorods. *Macromolecules* **46,** (2013).

22. Thierry, B., Ng, J., Krieg, T. & Griesser, H. A robust procedure for the functionalization of gold nanorods and noble metal nanoparticles. *Chem. Commun.,* **13** 1724–6 (2009)

23. Kinnear, C. *et al.* Gold Nanorods: Controlling Their Surface Chemistry and Complete Detoxification by a Two-Step Place Exchange. *Angew. Chem. Int. Ed. Engl.* **52** 1934-1938 (2013)

CHAPTER 5

LINEAR AND NONLINEAR APPLICATIONS OF FUNCTIONALIZED GOLD NANORODS

5.1 Introduction

In the previous chapter, gold nanorods (GNRs) were synthesized and functionalized to be used for photonics applications. In Chapter 5, two projects will be discussed that use GNRs as materials to study both a linear and nonlinear photonics problem. Part 1 will discuss the use of GNRs as a stable absorber to improve the efficiency of a Q-switched diode pumped solid state laser. Part 2 will discuss a two dimensional array of gold nanorods functionalized with nonlinear chromophores. This two dimensional array resembles the metamaterial architecture that was discussed in Chapter 2 of this thesis. The dye-conjugated metamaterial was studied using sum frequency generation and its nonlinear properties were compared to a flat gold surface.

5.2 Introduction to Part 1 – Improved DPSSL Design Using Epoxy Films of Gold Nanorods

Designing a high efficiency diode-pumped solid state laser (DPSSL) requires optimization of many variables such as pumping geometry, resonator geometry, and cavity design. Higher efficiency translates into less

needed input power, a smaller footprint, and ultimately application to a broader market. When considering the design of a DPSSL, the absorption properties of the materials used can significantly affect its efficiency. Unwanted absorption at either the pumping or lasing wavelengths will limit the amount of useful energy available to the system. One of the most common DPSSLs emits at 1064 nm by pumping a neodynium-doped yttrium aluminum garnet (Nd:YAG) rod with an 808 nm diode laser. Significant emission at 1064 nm occurs laterally out of the laser rod and, when reflected back into the rod by the pump cavity, a parasitic phenomenon known as amplified spontaneous emission (ASE) occurs.[1,2]

ASE is incoherent and depletes the excited state population available for stimulated emission, reducing the efficiency of the laser. This depletion can be inhibited by coating the laser rod in a material that is transparent at the pumping wavelength of 808 nm and highly absorptive at the lasing wavelength of 1064 nm. Coatings consisting of near-IR absorbing dyes are not practical because of their low solubility and high potential for photo-degradation. Experiments described in this chapter show how a Nd:YAG laser rod can be coated with a gold nanorod-doped epoxy. The coating allows for absorption and emission at the desired wavelengths with laser efficiency increasing by nearly two fold while circumventing the need for costly and complex fabrication alternatives.

5.3 Epoxy-Soluble Gold Nanorods As Linear Absorbers

DPSSLs are employed in many industrial applications, but are not always designed with maximum portability and efficiency in mind. Increased efficiency translates into lower input power and reduces the need for a large power source. A smaller footprint allows DPSSLs to be used in situations and environments that otherwise would have been impractical. While not the only way to improve laser efficiency, reducing ASE is one strategy that directly improves performance without requiring large scale changes in instrument design or power electronics. Strategies to reduce ASE hinge on finding effective ways to coat or enclose the laser rod with a material that is selectively absorptive at one wavelength and transparent at another. Currently, one common material used to combat loss of efficiency through ASE is samarium oxide-doped glass or ceramic.[3,4] In the both of these methods, yttrium, aluminum and samarium are incorporated into a glass or ceramic material, either on the edge of the gain medium or doped throughout the entire material. To produce a ceramic laser rod, time consuming slip casting and vacuum sintering techniques are required. Both of these materials are difficult to produce and the process of doping glass or ceramics requires specialized techniques and equipment.

An alternative material that coats a laser rod and increases laser efficiency while at the same time lowering cost and effort of production would

prove very useful. Ideally, a laser rod coating would be simple to apply and process and the coating process itself could be performed at any time during the laser fabrication process. We envisioned that a simple epoxy coating acting as a stable absorber would also have the added utility as an adhesive in the laser assembly process. The linchpin to this strategy is identifying an additive having the required optical properties. Organic molecules that absorb strongly at 1064 nm are known[5, 6], but tend to be complicated to synthesize and have low solubility in common solvents. These molecules can also exhibit significant absorption at 808 nm. Additionally, photo degradation would ultimately render them unstable for long-term laser operation. An ideal material would offer ease of synthesis, be stable for long-term use, and be compatible with commercially available epoxy resins.

Metallic nanoparticles stand out as attractive candidates due to their high stability and unique optical properties that depend on size, shape and aspect ratio. Gold nanorods (GNRs) in particular have emerged as popular constructs for optical, sensing, and biomedical applications.[7-9] As synthesis methods have improved, so too has the adoption of GNRs as unique optical absorbers.[10, 11] The high density of free electrons on the surface of GNRs allows for size and shape dependent surface plasmon resonances (SPR). These SPR resonances are discrete and generally quite narrow (~200 cm^{-1}). GNRs have two distinct SPR modes: longitudinal and transverse, resulting from their length and width, respectively. The transverse SPR (TSPR)

absorbs near 500 nm, while the longitudinal SPR (LSPR) varies depending on the length of the GNR. Synthesis of pure GNRs having tunable and narrow distributions in aspect ratios permits access to both the visible and near-IR regions of the electromagnetic spectrum. In this work, GNRs were synthesized and functionalized with custom polymers in order to produce thermally stable epoxy coatings that absorb at 1064 nm and are transparent at 808 nm with the goal of increasing efficiency, ease of production, and lowering the cost of DPSSLs.

5.4 Synthesis of GNRs and Gold-Reactive Polymer

In order to use GNRs in an epoxy coating, pure GNRs at a desired wavelength had to be synthesized and functionalized so that they could be integrated into the epoxy resin. The most common method of synthesizing

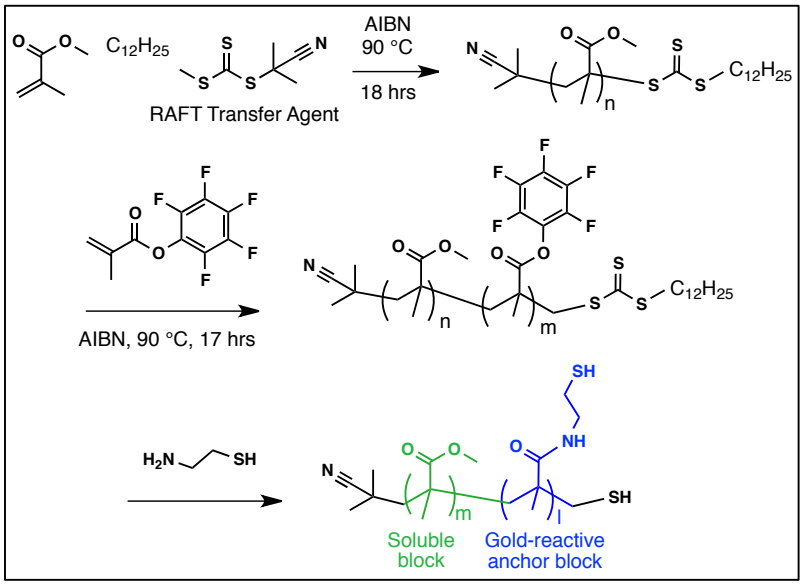


Figure 5.1. Synthesis of gold-reactive polymer using the RAFT technique.

GNRs is the surfactant based seed-mediated method.[12, 13] GNRs synthesized with this method are only stable in an aqueous environment. Useful methods have been developed to solubilize aqueous solutions of gold nanoparticles in organic solutions by replacing the typical surfactant (CTAB) that stabilizes them in water with organic-soluble alkanethiols.[14-18] Some methods are more complex than others, but one promising approach uses a relatively simple two-step process.[19] Thiol-terminated polyethylene glycol (PEG-SH) serves as an intermediate stabilization layer that makes the nanoparticles soluble in both water and in organic solvents. The PEG-SH functionalized

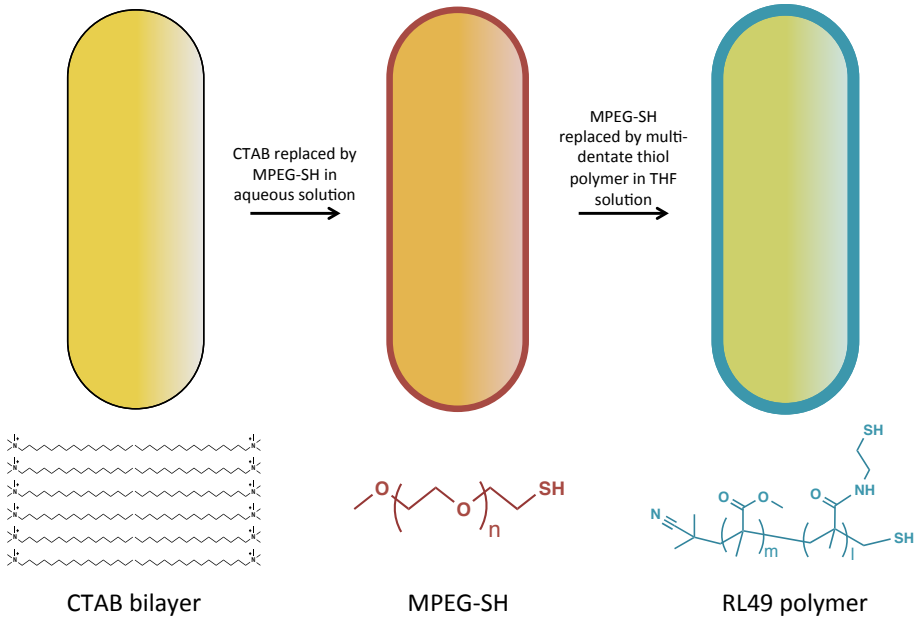


Figure 5.2. Gold nanorod functionalization. Gold nanorods are synthesized in an aqueous environment stabilized by a CTAB bilayer. The CTAB can be replaced by a solution of MPEG-SH at which point they are soluble in organic solvents like THF. The MPEG-SH is then replaced by a multi-dentate thiol polymer to produce GNRs that are very stable in organic solvents and UV-curable epoxy.

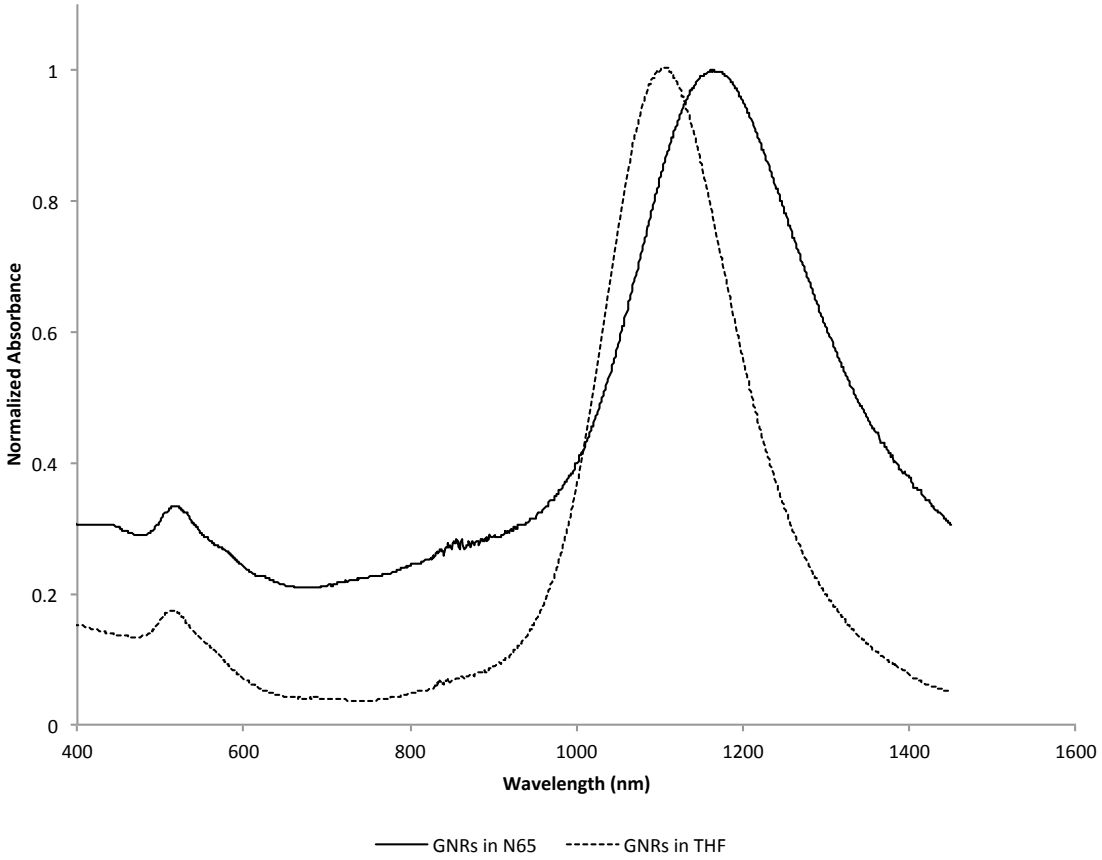


Figure 5.3. Absorption spectra of GNRs in THF solution compared to that of a GNR-doped Norland 65 epoxy film, normalized to the LSPR peak. The distinctive absorption profile of GNRs is maintained throughout the functionalization process. The LSPR peak shifts towards the right after incorporating into Norland 65 epoxy but still exhibits high absorption at 1064 nm.

nanoparticles are then dispersed in a solvent such as tetrahydrofuran and left to react with solutions of a thiol-terminated compound of choice. These steps are illustrated schematically in Figures 5.1 and 5.2. In the experiments described below, gold nanorods are made organic-soluble by using thiol-functionalized copolymers synthesized by the RAFT (Reversible Addition/Fragmentation Chain Transfer) technique.[20, 21] The RAFT polymerization technique was chosen in order to easily access a diblock

polymer that provides a highly organic-soluble block, poly(methyl methacylate), and a polydentate anchor block that binds to the GNR surface. The synthesis of the gold-reactive polymer is shown in Figure 5.1. Figure 5.2 depicts the functionalization process where the aqueous CTAB environment surrounding the GNRs is replaced with a mulitdentate thiol-polymer coating. After GNRs are coated in the polymer, they can be dissolved in organic solvents like tetrahydrofuran. Organic solutions of GNRs can then be added to solutions of commercial polymers or epoxies and applied to surfaces using

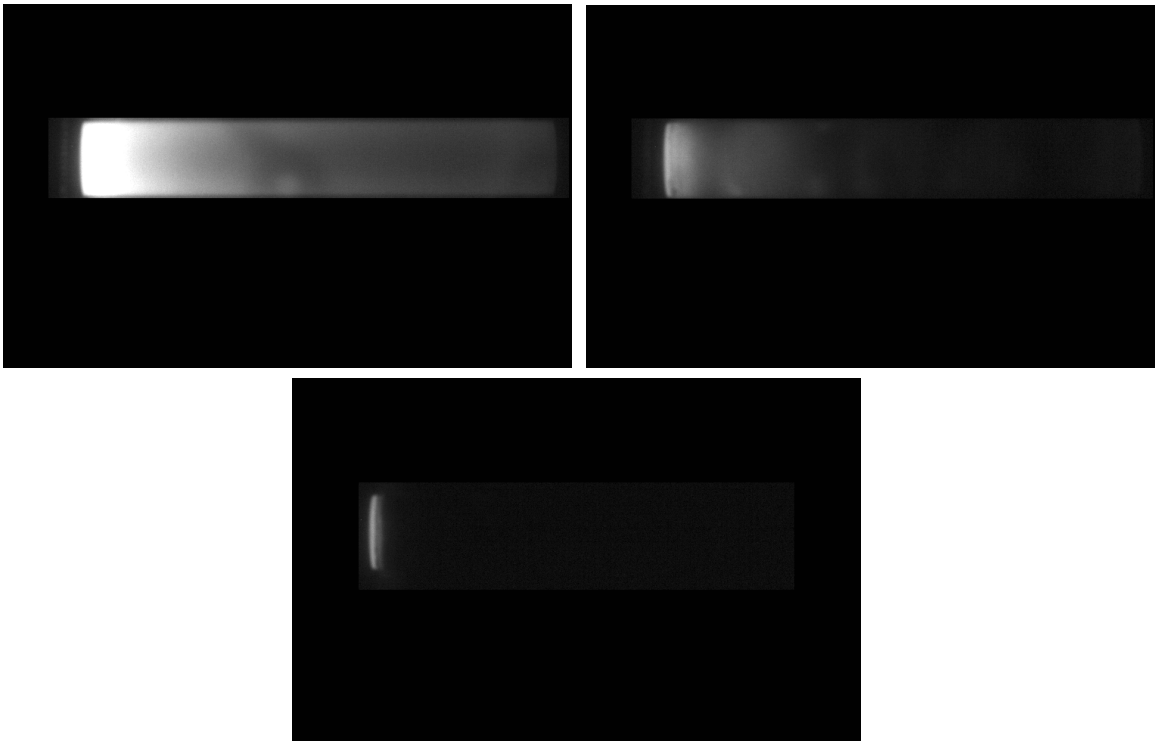


Figure 5.4. Fluorescence images at 1064 nm of a Nd:YAG laser rod pumped at 808 nm. Top left: coated in 0.0127 mm of un-doped epoxy. Top right: coated in 0.0127 mm of GNR-doped epoxy. Bottom middle: coated in 0.0254 mm of GNR-doped epoxy. Obvious suppression of 1064 nm fluorescence is observed after coating in GNR-doped epoxy.

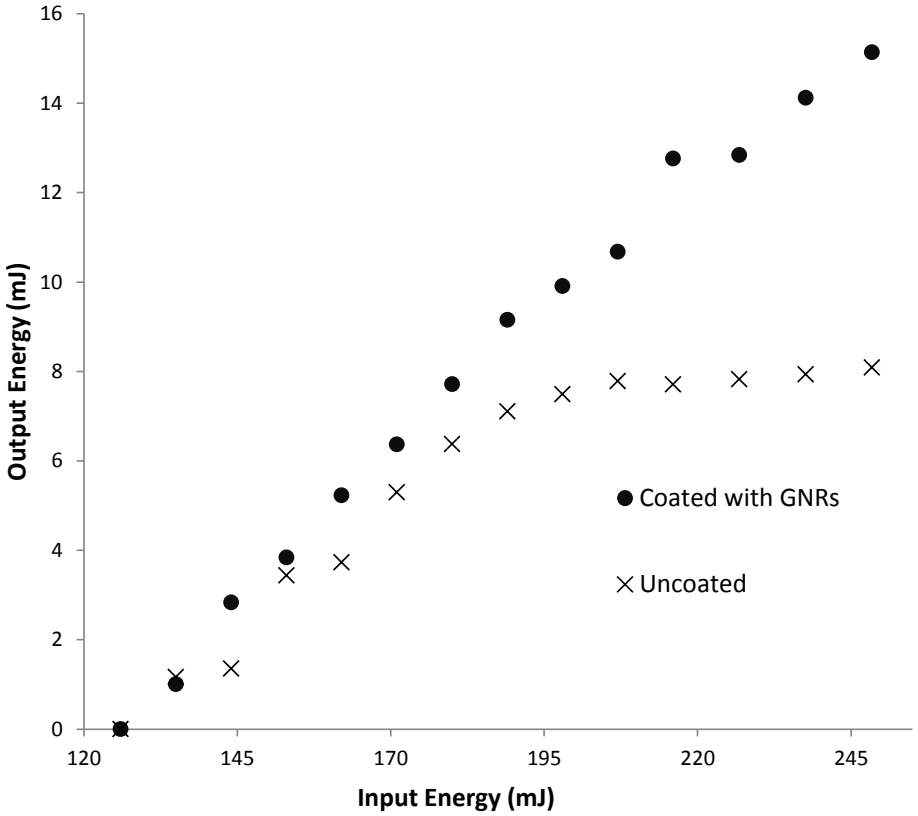


Figure 5.5: Laser Efficiency with and without GNR coating. The uncoated rod output energy rolls off in a simple Q-switch resonator due to the increase in ASE losses as the gain is increased. The rolloff in the coated rod has increased significantly allowing more stored energy and greater output energy.

casting or spin coating techniques. Figure 5.3 shows the absorption spectra of GNRs in Norland 65 epoxy when compared to GNRs in THF. After normalizing with respect to the LSPR peak, a high absorption is still observed at 1064 nm and the distinctive GNR absorption profile is still intact.

5.5 Fluorescence of GNR Coated Nd:YAG

In order to simulate the conditions of a production model laser, a Nd:YAG rod was end-pumped at 808 nm with the same laser diode and at the same distance between pump source and laser rod used in a production model. Using an Edmund Optics CMOS camera fitted with a 1064 nm filter, images of 1064 nm fluorescence were obtained perpendicular to the pump direction. Figure 5.4 shows the dramatic decrease in 1064 nm intensity after the laser rod is coated with GNR doped epoxy. Optimization of coating conditions lead to a typical coating that contained 0.015 mL of concentrated GNRs in THF and 0.110 g of epoxy. This coating consistently allowed for absorption of seventy percent of the 1064 nm fluorescence as detected by the camera. After coating the Nd:YAG rod, the laser components were fully assembled and output efficiency was tested. Figure 5.5 indicates a significant increase in output energy after the laser rod is coated in GNR doped epoxy. Without a coating, the laser output levels off near 8 mJ. With the GNR coating, the output energy reaches 15.14 mJ.

5.6 Conclusion to Part 1

The materials we have produced offer a simple and versatile solution to the problems caused by amplified spontaneous emission. At the time of this writing, Quantum Composers has sold and shipped lasers to customers

that utilize the GNR-doped epoxy material described in this chapter. Because Nd:YAG lasers are used in a wide variety of industrial and research atmospheres, the implications of this effective GNR coating are therefore highly impactful and far-reaching.

5.7 Introduction to Part 2 – SFG of Dye-Conjugated Gold Nanopillars

Metamaterials can be described as arrays of sub-wavelength polarizable elements that exhibit properties not found in natural materials.[22-24] Recently, negative refractive index metamaterials have gained great attention for their ability to demonstrate exotic phenomena like cloaking.[25-29] However, metamaterials also have the potential to enhance the optical properties of nonlinear materials and produce more efficient and unique ways to improve phase matching in wave mixing phenomena.[30,31] A metamaterial that could simultaneously enhance nonlinearity and exhibit birefringence-phase-matching behavior would possess the qualities required to act as a mirror-less optical parametric oscillator. [32-34] Such a device has the potential to reduce optical loss and introduce signal gain to nonlinear processes that are limited by their need for high power input.[35-37] In this work, sum-frequency generation (SFG) was used to probe the relative signal intensities of flat gold samples and arrays of ordered vertical gold nanorods, both hybridized with a thiol-functionalized nonlinear organic chromophores. The

dye-functionalized flat gold sample exhibited an increase in SFG signal two orders of magnitude larger than that of bare gold, although only in the PPP polarization configuration. Interestingly, the dye-functionalized nanorod metamaterial displayed significant SFG signal in both PPP and SSP polarizations. Recent modeling results[30] of similar structures predict access to a non-natural nonlinear tensor element and the results obtained here are a promising indication that such a metamaterial supports enhanced phase matching of optical fields with orthogonal polarizations.

As useful as lasers are, they are restricted by their monochromatic nature. To add utility to an already expensive instrument, intricate devices (optical parametric amplifiers or oscillators, OPA/OPO) have been designed to contort one wavelength into many through the use of nonlinear frequency mixing phenomena. In order to efficiently tune the wavelength of laser light through a nonlinear medium, two important properties must be optimized. First, a nonlinear material should have the largest possible nonlinear coefficient, and second, the process should be designed to produce efficient phase matching. Much research has been devoted to the design and synthesis of nonlinear organic materials with large second and third order nonlinear coefficients.[38-42] However, using nonlinear organic materials in a metamaterial architecture has not yet been explored experimentally. Traditional OPA and OPO designs enable tunable laser light generation, albeit while requiring high input power and a great financial cost. In this

work, we discuss hybridization of organic nonlinear materials within a metamaterial as a potential means of developing simpler, more efficient approaches for enhancing nonlinear optical processes.

5.8 Modeling to Predict Ideal Metamaterial Structure

The metamaterial of interest had an architecture that used gold nanorods as the sub-wavelength substituents in a nematic-like, alternating structure.[30] The model included an organic nonlinear optical dielectric (ONLO) coating around the gold nanorods. The resulting structure was shown to exhibit enhanced nonlinear activity compared to the ONLO alone with the ability to tune the nonlinear tensor configurations by changing the spacing and gap size of the gold nanorods. Not only does this structure display enhanced ONLO activity via field enhancement, it does so regardless of exciting the gold nanorods in the longitudinal or transverse direction. Modeling results show large enhancement of Pockels effect coefficients r_{33} and r_{31}. However, the coefficients r_{51} and r_{53} were also enhanced indicating coupling of orthogonal polarizations by an applied DC field. This type of orthogonal coupling is rare and the use of nonlinear materials with very large off-diagonal tensor elements is usually needed to produce it. The proposed metamaterial has the potential to both enhance nonlinearity and produce birefringence phase matching making it a candidate for a birefringence-phase-matched mirror-less optical parametric oscillator.

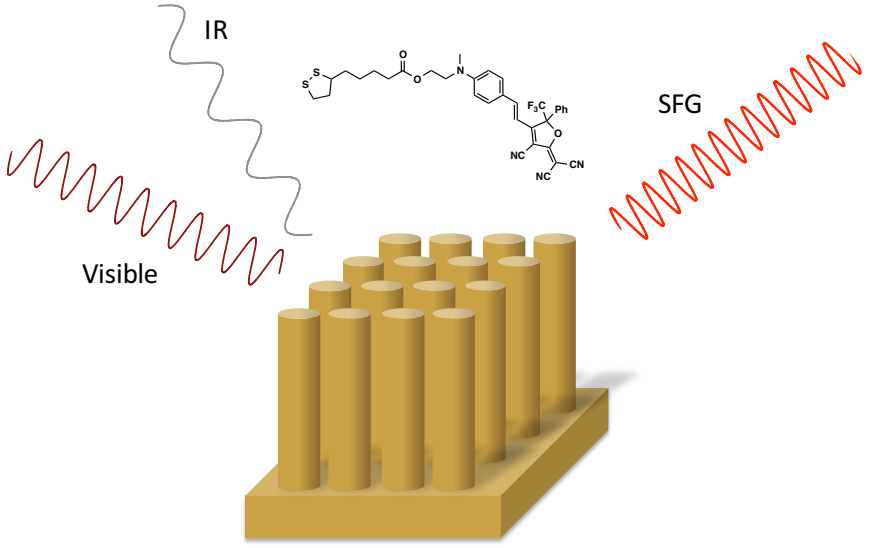


Figure 5.6. A depiction of a gold nanopillar sample studied using sum frequency generation. The metamaterial was functionalized with the nonlinear organic chromophore shown at the top and middle of the picture.

5.9 SFG of Flat and Nanopillar Gold Surfaces

In order to explore the modeling results experimentally, a structure similar to that used in the modeling results was fabricated. Recently, techniques for constructing vertical arrays of gold nanopillars have been developed through the use of porous aluminum oxide templates.[43,44] To study the nonlinear activity of these gold structures, the sum frequency generation (SFG) technique was employed. Based on modeling predictions, the nonlinear response of flat gold and nanopillar samples was expected to differ in relation to the input polarization of laser frequencies used. The SFG intensity should indicate if an enhancement has occurred and whether SFG can be obtained using orthogonal input polarizations. A depiction of the

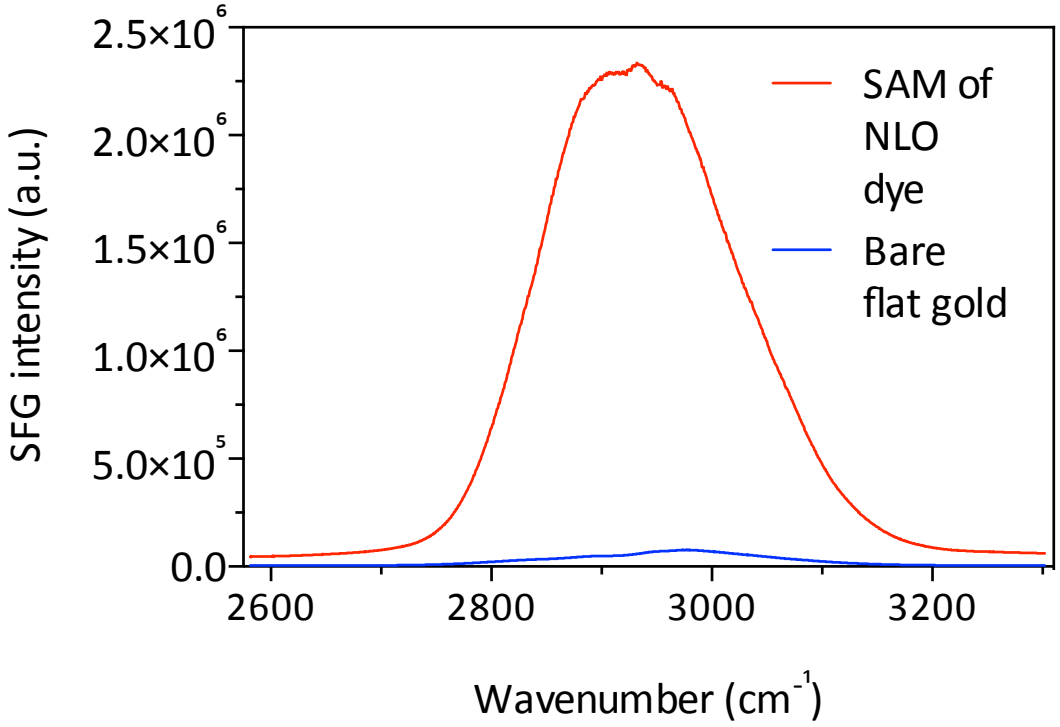


Figure 5.7. A two order of magnitude increase in SFG signal (PPP) was observed from a self-assembled monolayer of nonlinear organic dye on flat gold compared to the SFG signal of bare flat gold. Negligible SFG signal was observed in the SSP configuration.

nonlinear organic-hybridized metamaterial used in this study is shown in Figure 5.6.

The SFG responses from both the planar gold surface and from the gold nanopillar sample were obtained by subjecting samples to input wavelengths of 801 nm (visible) and 3250 nm (IR) while the output wavelength of ~650 nm (SFG) was monitored. The conventional polarization notation is used here (e.g. PPP is SFG, IR, visible). Because SFG is a second order nonlinear phenomenon, SFG is only observed if the nonlinear sample being studied exhibits an overall non-centrosymmetric structure. The

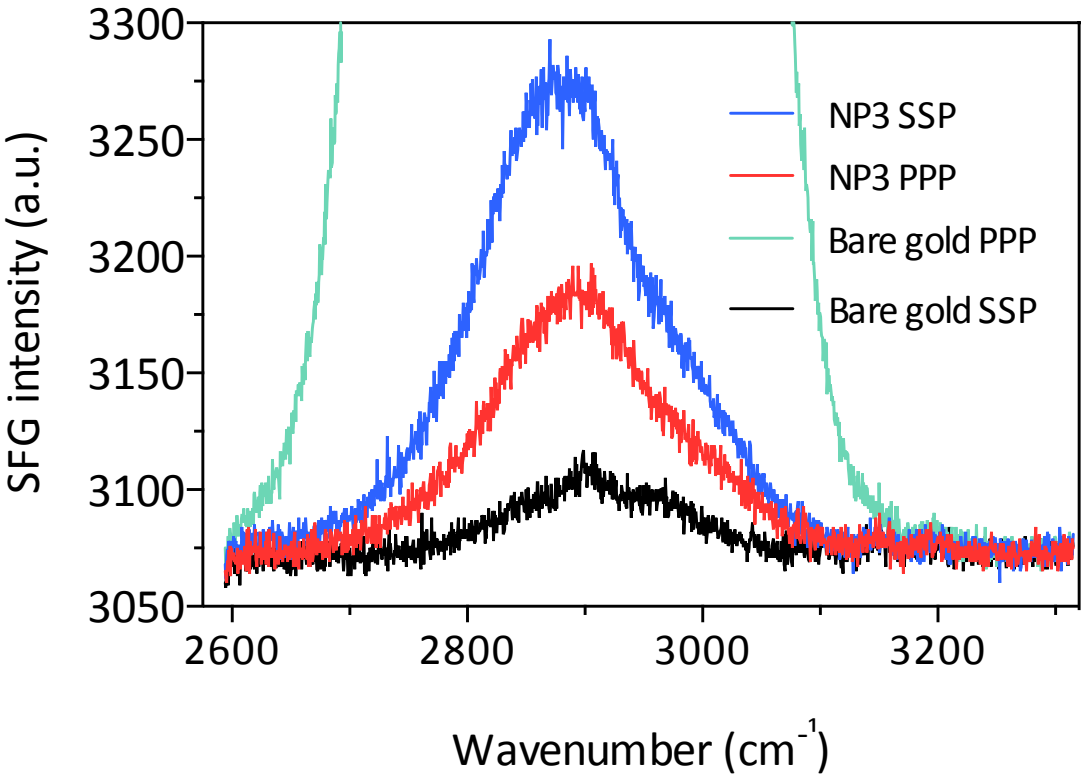


Figure 5.8. SFG of bare gold nanopillar (labeled NP3) and bare gold samples in both the PPP and SSP input configurations. The SFG signal of the nanopillar sample is less than bare gold in the PPP configuration but larger than that of bare gold in the SSP configuration.

nonlinear organic chromophores synthesized for this work were functionalized at one end with a disulfide group. These chromophores were expected to self assemble on a flat gold surface and exhibit a non-zero second order nonlinear response. Flat gold samples were prepared by submersion in 1 mM solutions of thiol-functionalized dye and left to react overnight at room temperature. Shown in Figure 5.7, a two order of magnitude signal increase was observed from the self-assembled monolayer of dye on flat gold compared

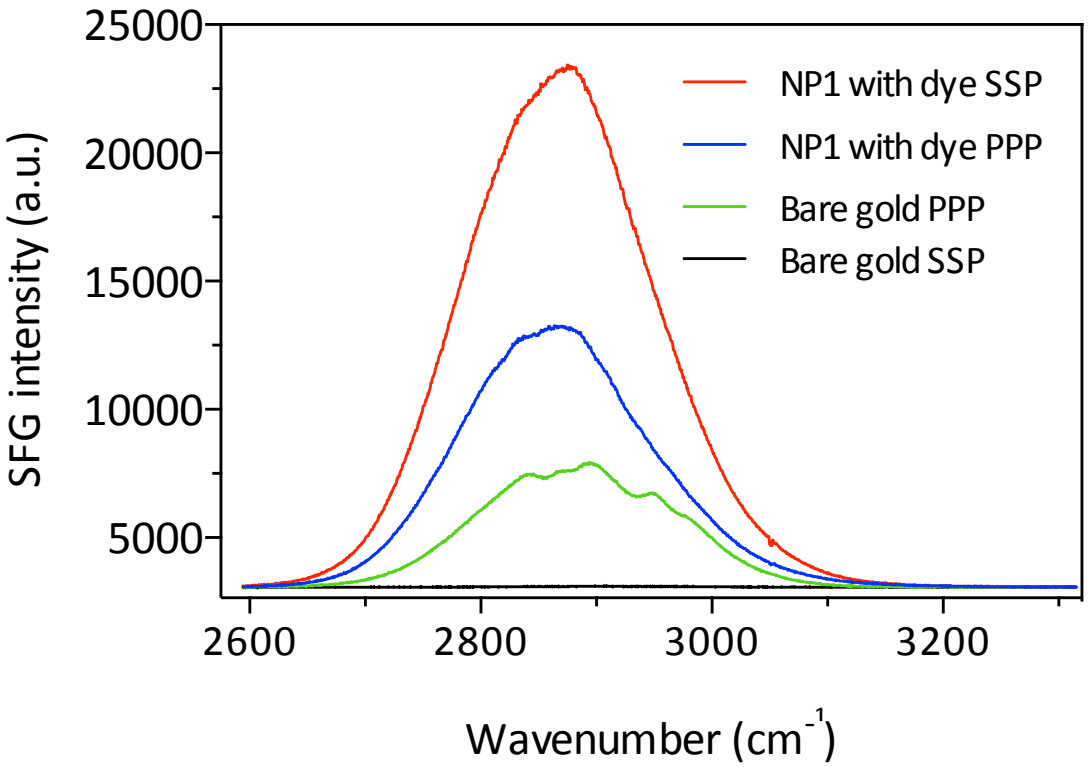


Figure 5.9. SFG signal of bare gold samples and of gold nanopillar (labeled NP1) samples functionalized with a nonlinear organic chromophore. Bare gold exhibited significant SFG signal in PPP polarization with very little in SSP. The nanopillar's SFG signal was larger than bare gold in both PPP and SSP polarization configurations.

to that of sample of bare flat gold. This large SFG signal may be due to a concentration of field at the surface plasmon resonance of the gold surface resulting in a large enhancement of the SAM of nonlinear organic chromophores. Changing polarization configurations from PPP to SSP resulted in negligible SFG response, which can be attributed to the low interaction between orthogonal input polarizations due to a weak off-diagonal χ^2 tensor element.

After studying SAMs of dye on flat gold, focused was turned towards samples of gold nanopillar metamaterials. Figure 5.8 shows the SFG intensity of a gold nanopillar sample compared to that of flat gold, in both the PPP and SSP polarization configurations. The output intensity of the nanopillar sample in the PPP configuration is much less than that of flat gold. However, the signal observed in the SSP configuration is significantly higher than the SSP signal from flat bare gold.

Analogous to the flat gold samples, nonlinear dyes were introduced on the surface of a nanopillar sample by submerging in a solution of dye in dichloromethane. Figure 5.9 shows the SFG intensity of the nanopillar samples after being coated in the nonlinear organic dye. SFG intensity of the nanopillar sample for both PPP and SSP configurations is significantly larger than the signal observed on a bare flat gold sample.

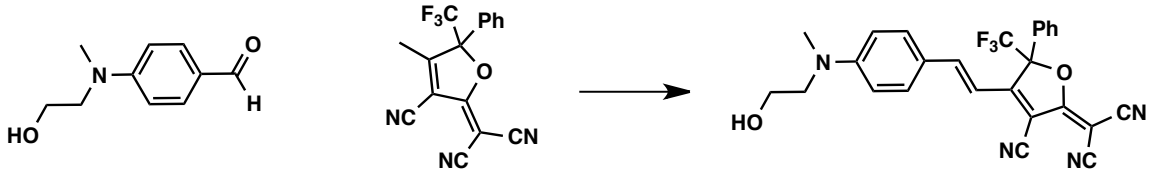
5.10 Conclusion to Part 2

These results demonstrate that the nanopillar samples produce significant SFG signal from both parallel and orthogonal input configurations. Samples of flat gold covered in dye only produced SFG signal when using the PPP configuration, while only negligible signal was observed in the SSP configuration. Fascinatingly, not only is SFG observed for the dye-covered nanopillar samples in the SSP configuration, it is higher than that of what is observed using the PPP configuration. At time of this writing,

there is no literature precedence on SFG studies of dye-conjugated gold nanopillar structures. Additional experiments need to be undertaken to further understand the results presented here.

5.11 Experimental Section

5.11.1 Synthesis of Chromophore 3



1 2 Chromophore 3

Synthesis of 2-Dicyanomethylene-3-cyano-4-methyl-5-phenyl-5-per-fluoromethyl-2,5-dihydrofuran (**2**) was prepared as previously reported.[45-47] A 100 mL round bottomed flask was charged with 1 eq (1.50g) of *N*-Methyl-*N*-(2-hydroxyethyl)-4-aminobenzaldehyde (**1**), 1.03 eq (2.72g) of 2-Dicyanomethylene-3-cyano-4-methyl-5-phenyl-5-per-fluoromethyl-2,5-dihydrofuran (**2**), and 50 mL of anhydrous ethanol. The reaction mixture was stirred at room temperature under nitrogen atmosphere for 4 hours. The flask was cooled over ice and the resulting solid was collected by filtration and washed with cold ethanol. The crude product was purified by silica gel chromatography (2% methanol in dichlromethane). 2.8g (70% yield) of metallic green chromophore **3** was obtained. ^{1}H-NMR (300 MHz; $CDCl_3$): δ 7.70 (d, J = 17.7 Hz, 1H), 7.51 (m, 5H), 7.43 (d, J = 7.8 Hz, 2H), 6.78-6.72 (m,

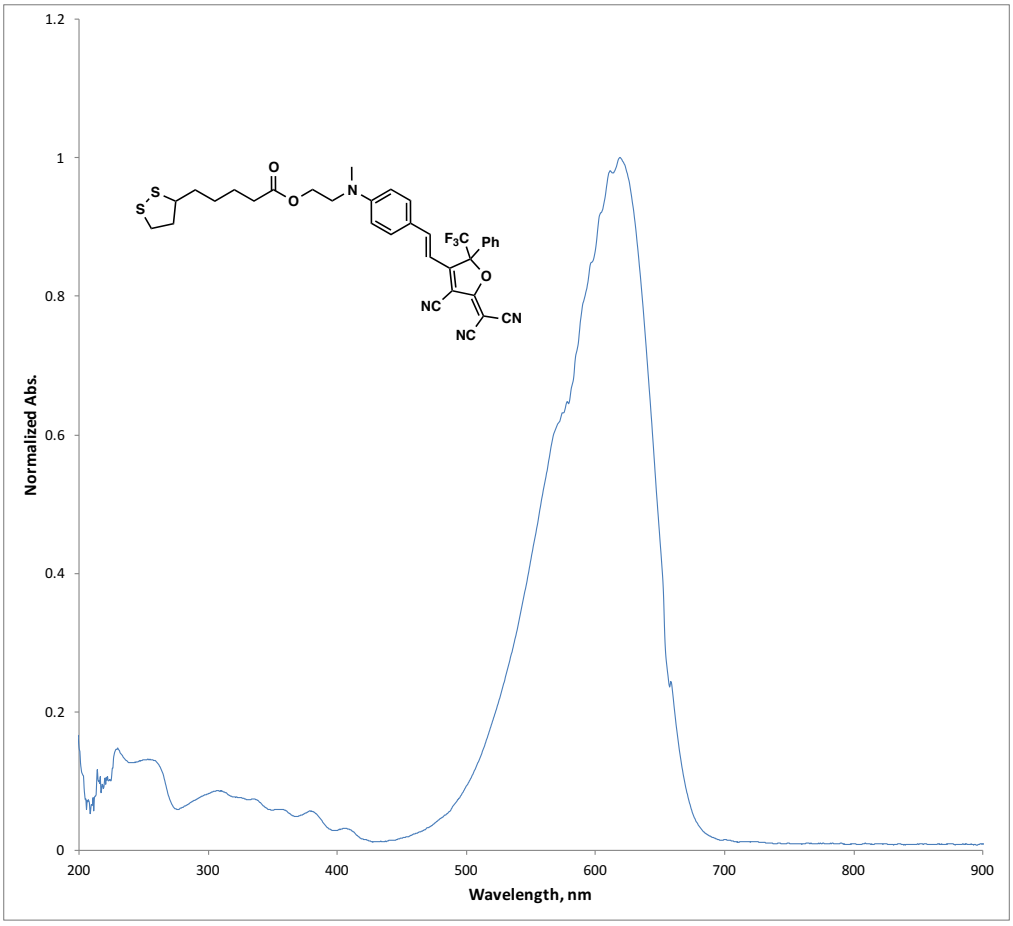
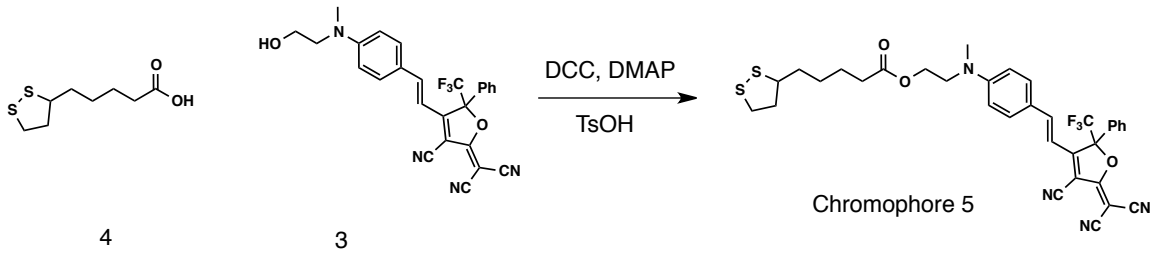


Figure 5.10. Absorption spectrum of Chromophore 5 in dichloromethane, normalized to the maxmum absorption peak near 600 nm

3H), 3.90 (bs, 2H), 3.67 (t, J = 5.8 Hz, 2H), 3.19 (s, 3H). HRMS (micrOTOF):

Calculated: 476.1460 Found: 476.1520

5.11.2 Synthesis of Gold-Reactive Chromophore 5



4 3

1 eq (1.33g) of **3** and 1.1 eq (0.844 g) of lipoic acid (**4)** were dissolved in 20 mL

of dichloromethane and cooled to 0°C. 1.36 eq (1.04 g) of *N,N'*-Dicyclohexylcarbodiimide, 0.11 eq (50 mg) of 4-Dimethylaminopyridine, and 0.105 eq (74 mg) of *p*-Toluenesulfonic acid were then added to the flask. The mixture was stirred over night under nitrogen atmosphere and allowed to warm to room temperature (~22 °C). After cooling briefly in a -20°C freezer, the mixture was filtered to remove dicyclohexylurea. The filtrate was washed with two 50 mL portions of 1 M hydrochloric acid, one 100 mL portion of saturated sodium bicarbonate solution, two 50 mL portions of brine and dried over anhydrous magnesium sulfate. The organic layer was concentrated under reduced pressure and purified by silica gel chromatography (2% acetone in dichloromethane). 0.8676 g of metallic green Chromophore **5** was obtained (47% yield) ^{1}H-NMR (300 MHz; $CDCl_3$): δ 7.70 (d, J = 15.4 Hz, 2H), 7.51 (m, 4H), 7.44 (d, J = 9.0 Hz, 2H), 6.80-6.71 (m, 3H), 4.29 (t, J = 5.8 Hz, 2H), 3.73 (t, J = 5.9 Hz, 2H), 3.51 (dt, J = 14.1, 6.9 Hz, 1H), 3.13 (m, 5H), 2.44 (td, J = 12.4, 6.5 Hz, 1H), 2.26 (t, J = 7.3 Hz, 2H), 1.87 (dq, J = 13.0, 6.6 Hz, 1H), 1.59 (m, 4H), 1.39 (m, 2H). HRMS (micrOTOF): Calculated: 664.1790 Found: 664.1876. UvVis of Chromophore 5 is shown in Figure 5.10.

5.11.3 Fabrication of Gold Nanopillar Samples

Gold nanopillar samples were fabricated by Zayats et al. using procedures found in the literature.[22, 23] Figures 5.11 and 5.12 show the absorption spectra of nanpillar Sample 1 and Sample 3. The absorption

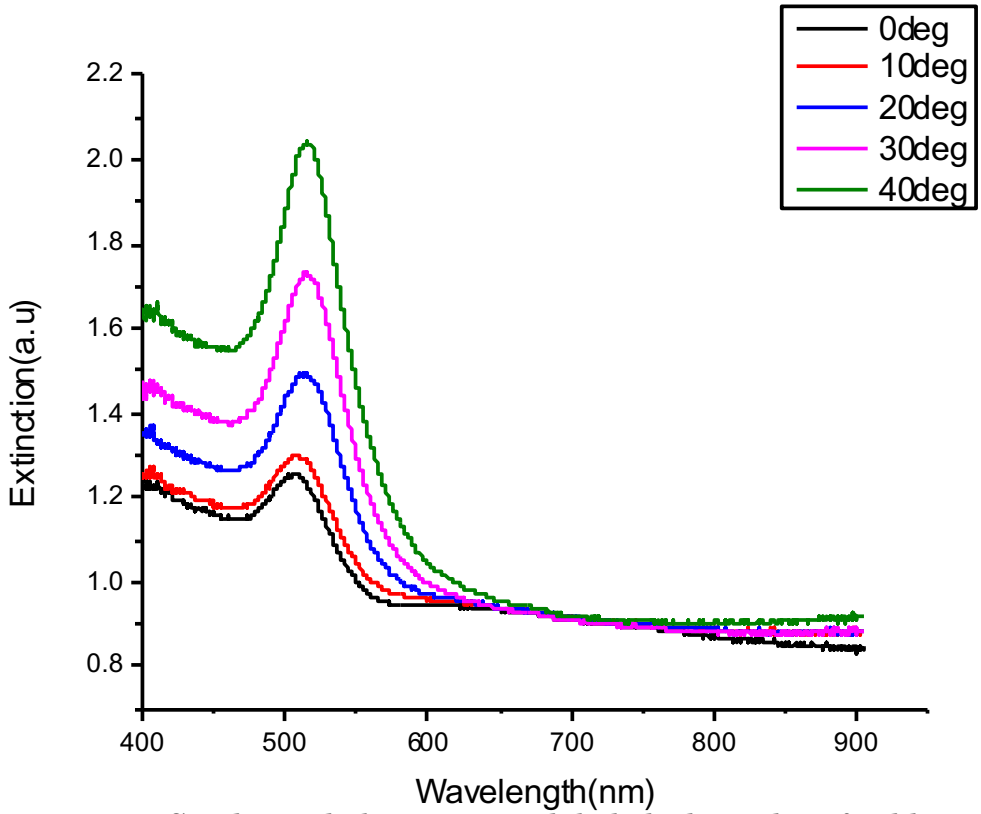


Figure 5.11. S-polarized absorption at labeled tilt angles of gold nanopillar Sample 1.

spectra was taken using an S-polarizer, where the polarization of light absorbed by the nanopillars was parallel to the lab bench surface and perpendicular to the length of the nanopillars. By rotating the samples parallel to the lab bench, a maximum absorbance is observed near 40 degrees.

5.11.4 SFG Apparatus Description

SFG measurements were made using the setup diagramed below in Figure 5.13. The setup is driven by a Libra-HE Ti:sapphire laser (Coherent, 3.5 W, 85 fs pulse duration, 1 kHz repetition rate). 80% of the Libra output is

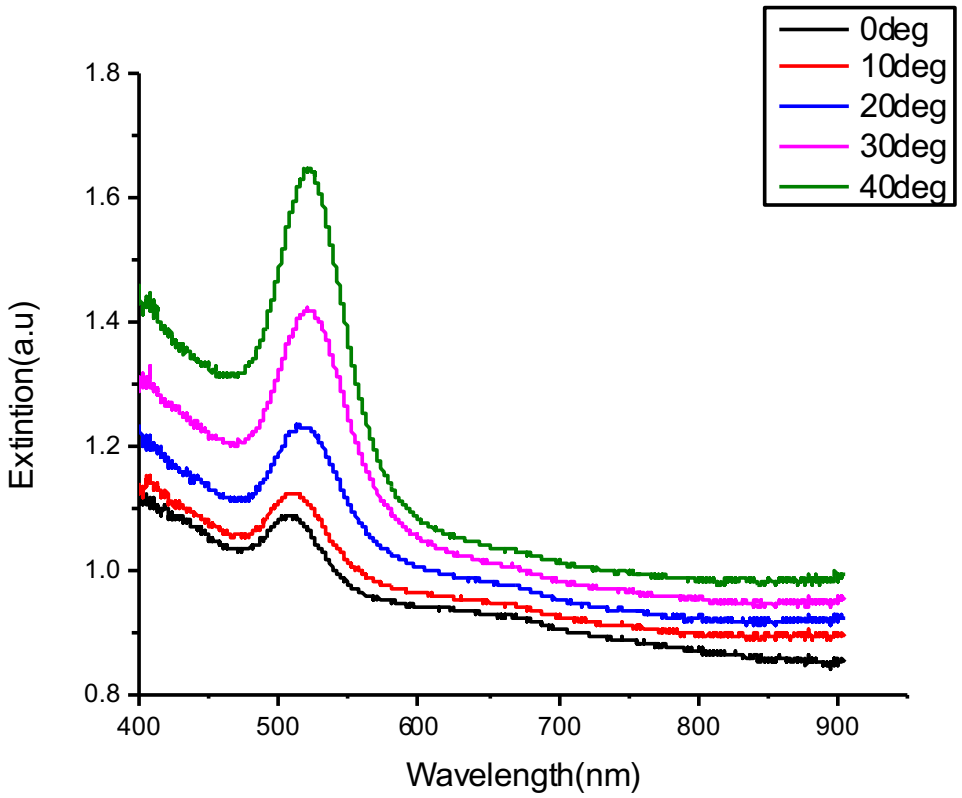


Figure 5.12. S-polarized absorption at labeled tilt angles of gold nanopillar Sample 3.

used to pump an optical parametric amplifier (Coherent OPerA Solo) that is the source of the tunable, broadband infrared frequency. The remaining 20% of the original beam is used as the upconversion source at the sample. Prior to the sample, the visible beam is spectrally narrowed by first stretching the beam using a diffraction grating (1800 g/mm), slicing out a narrow portion of the spectrum, and then recompressing the stretched beam. This narrowed beam passes through two delay stages and both incident beams pass through a waveplate and polarizer to select particular polarizations. The SFG apparatus was designed in a colinear geometry, so both beams are incident

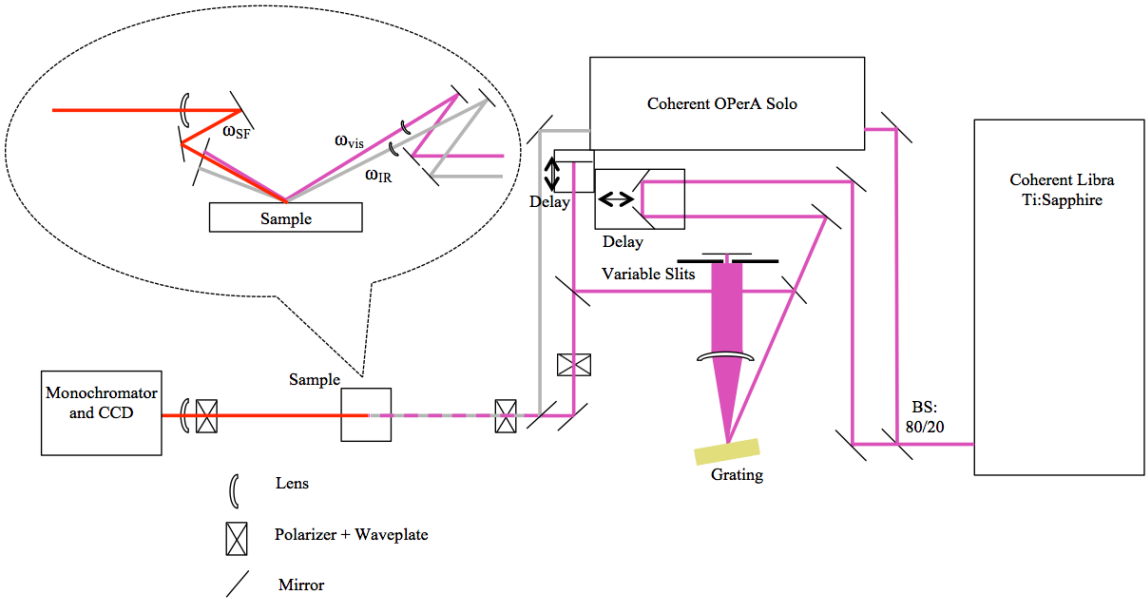


Figure 5.13. Diagram of SFG setup used in this chapter.

on the sample at the roughly the same angle (73° for the IR and 67° for the visible). When the visible and IR beams are spatially and temporally overlapped, SF signal is generated and directed into a spectrograph (SpectraPro-300i, Acton Research Corporation) where it is dispersed onto a 1340 x 100 pixel CCD (PIXIS100B, Princeton Instruments). Beam energies at the sample are generally ~5 μJ – 10 μJ for each input beam. As a broadband system, single SF spectra can be taken if the IR beam profile covers the region of interest, however, if the range of interest is too large, the "step and sum" method first reported by Esenturk *et al.*[48] can be used. In this method, SFG spectra are taken at different IR frequencies effectively scanning the region of interest in 500 nm intervals. The resulting spectra can then be summed and normalized to a gold nonresonant spectrum. In order to

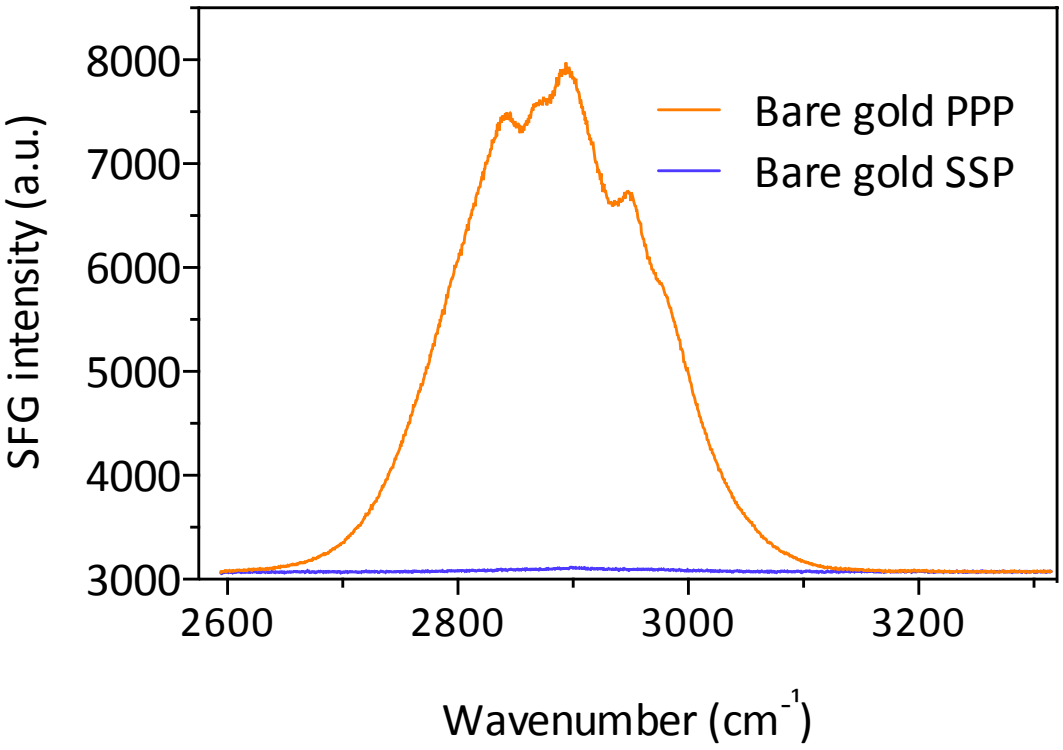


Figure 5.14. SFG of a sample of flat bare gold

combine, normalize, and calibrate spectra, homemade routines written in Igor Pro (v. 6) are used. Typical SFG of flat bare gold at both PPP and SSP polarization configurations is shown in Figure 5.14.

5.12 References

1. Lowenthal & Eggleston. ASE effects in small aspect ratio laser oscillators and amplifiers with nonsaturable absorption. *IEEE J. Quantum. Elect.* **22,** 1165–1173 (1986).

2. Barnes, N. P. & Walsh, B. M. Amplified spontaneous emission-application to Nd:YAG lasers. *IEEE J. Quantum. Elect.* **35,** 101–109 (1999).

3. Yamamoto, B. M., Bhachu, B. S., Cutter, K. P., Fochs, S. N., Letts, S. A., Parks, C. W., Rotter, M. D., Soules, T. F. The Use of Large Transparent Ceramics in a High Powered, Diode Pumped Solid-State Laser. In *Advanced Solid-State Photonics*, OSA Technical Digest Series (CD), Nara, Japan, January 27-30, 2008; WC5

4. Yagi, H., Bisson, JF, Ueda, K & Yanagitani, T. $Y_3Al_5O_{12}$ ceramic absorbers for the suppression of parasitic oscillation in high-power Nd: YAG lasers. *J. Lumin.* **121**, 88-94 (2006).

5. Fabian, J., Nakazumi, H. & Matsuoka, M. Near-infrared absorbing dyes. *Chem. Rev.* **92,** 1197-1226 (1992).

6. Langhals, H., Zgela, D. & Lüling, R. Sexterrylenetetracarboxylic Bisimides: NIR Dyes. *J. Org. Chem.* **80,** 12146–12150 (2015).

7. Chen, H., Shao, L., Li, Q. & Wang, J. Gold nanorods and their plasmonic properties. *Chem. Soc. Rev.* **42,** 2679–724 (2013).

8. Pérez-Juste, J., Pastoriza-Santos, I., Liz-Marzán, L. M. & Mulvaney, P. Gold nanorods: synthesis, characterization and applications. *Coordin. Chem. Rev.* **249**, 1870-1901, (2005)

9. Murphy, C. J. *et al.* Anisotropic metal nanoparticles: Synthesis, assembly, and optical applications. *J. Phys. Chem. B* **109**, 13857–70 (2005).

10. Lohse, S. & Murphy, C. The Quest for Shape Control: A History of Gold Nanorod Synthesis. *Chem. Mater.* **25,** (2013).

11. Dreaden, E. C., Alkilany, A. M., Huang, X., Murphy, C. J. & El-Sayed, M. A. The golden age: gold nanoparticles for biomedicine. *Chem. Soc. Rev.* **41,** 2740–79 (2012).

12. Jana, N., Gearheart, L. & Murphy, C. Wet Chemical Synthesis of High Aspect Ratio Cylindrical Gold Nanorods. *J. Phys. Chem. B* **105,** 4065–4067 (2001).

13. Nikoobakht, B. & El-Sayed, M. Preparation and Growth Mechanism of Gold Nanorods (NRs) Using Seed-Mediated Growth Method. *Chem. Mater.* **15,** 1957–1962 (2003).

14. Wei, GT, Yang, Z, Lee, CY & Yang, HY. Aqueous-organic phase transfer of gold nanoparticles and gold nanorods using an ionic liquid. *J. Am. Chem. Soc.* **126**, 5036-5037 (2004).

15. Hotchkiss, J., Lowe, A. & Boyes, S. Surface Modification of Gold Nanorods with Polymers Synthesized by Reversible Addition−Fragmentation Chain Transfer Polymerization. *Chem. Mater.* **19,** 6-13 (2007).

16. Xue, C. *et al.* Organo-soluble porphyrin mixed monolayer-protected gold nanorods with intercalated fullerenes. *Langmuir* **28,** 5956–63 (2012).

17. Mitamura, K, Imae, T & Saito, N. Fabrication and self-assembly of hydrophobic gold nanorods. *J. Phys. Chem. B* **111**, 8891-8898 (2007).

18. Alkilany, A. M., Thompson, L. B. & Murphy, C. J. Polyelectrolyte coating provides a facile route to suspend gold nanorods in polar organic solvents and hydrophobic polymers. *ACS Appl. Mater. Interfaces* **2,** 3417–21 (2010).

19. Thierry, B., Ng, J., Krieg, T. & Griesser, H. J. A robust procedure for the functionalization of gold nanorods and noble metal nanoparticles. *Chem. Commun.* **13,** 1724–6 (2009).

20. Meuer, S., Oberle, P., Theato, P., Tremel, W. & Zentel, R. Liquid Crystalline Phases from Polymer-Functionalized TiO2 Nanorods. *Adv. Mat.* **19,** 2073–2078 (2007)

21. Zorn, M. *et al.* Liquid crystalline phases from polymer functionalised semiconducting nanorods. *J. Mater. Chem.* **18,** 3050–3058 (2008).

22. Veselago, V. G. The electrodynamics of substances with simultaneously negative values of ε and μ. *Sov. Phys. Usp.* **10**, 509–514 (1968).

23. Zheludev, N. I. & Kivshar, Y. S. From metamaterials to metadevices. *Nat. Mater.* **11,** 917–24 (2012).

24. Liu, Y. & Zhang, X. Metamaterials: a new frontier of science and technology. *Chem. Soc. Rev.* **40,** 2494–507 (2011).

25. Pendry, J. B., Schurig, D. & Smith, D. R. Controlling electromagnetic fields. *Science* **312**, 1780–2 (2006).

26. Schurig, D. *et al.* Metamaterial electromagnetic cloak at microwave frequencies. *Science* **314**, 977–980 (2006).

27. Landy, N. & Smith, D. R. A full-parameter unidirectional metamaterial cloak for microwaves. *Nat. Mater.* **12**, 25–8 (2013).

28. Burgos, S. P., de Waele, R., Polman, A. & Atwater, H. A. A single-layer wide-angle negative-index metamaterial at visible frequencies. *Nat. Mater.* **9,** 407–412 (2010).

29. Cai, W. S., Chettiar, U. K., Kildishev, A. V. & Shalaev, V. M. Optical cloaking with metamaterials. *Nature Photon.* **1**, 224–227 (2007).

30. Rose, A., Latterman, R., Smith, D. & Sullivan, P. Lower poling thresholds and enhanced Pockels coefficients in nanoparticle-polymer composites. *Appl. Phys. Lett.* **103,** 031102 (2013).

31. Rose, A. & Smith, D. Overcoming phase mismatch in nonlinear metamaterials [Invited]. *Opt. Mater. Express,* **Vol. 1, No. 7**, 1231-1243 (2011).

32. Suchowski, H, O'Brien, K, Wong, ZJ, Salandrino, A & Yin, X. Phase Mismatch–Free Nonlinear Propagation in Optical Zero-Index Materials. *Science*, **6**, 1223-1226 (2013).

33. Choi, M. *et al.* A terahertz metamaterial with unnaturally high refractive index. *Nature* **470**, 369-374 (2011)

34. Shin, J., Shen, J.-T. T. & Fan, S. Three-dimensional metamaterials with an ultrahigh effective refractive index over a broad bandwidth. *Phys. Rev. Lett.* **102,** 093903 (2009).

35. Hess, O. *et al.* Active nanoplasmonic metamaterials. *Nat. Mater.* **11,** 573–584 (2012).

36. Canalias, C & Pasiskevicius, V. Mirrorless optical parametric oscillator. *Nature Photon.,* **1**, 459-462 (2007).

37. Litchinitser, NM & Shalaev, VM. Metamaterials: Loss as a route to transparency. *Nature Photon.*, **1**, 75-76, (2009)

38. Prasad, P. & Reinhardt, B. Is there a role for organic materials chemistry in nonlinear optics and photonics? *Chem. Mater.* **2**, 660-669 (1990).

39. Dalton., L.R. Rational design of organic electro-optic materials. *J. Phys. Condens. Matter.* **15,** R897-R934 (2003).

40. Marder, S. Organic nonlinear optical materials: where we have been and where we are going. *Chem. Commun.* **0**, 131-134 (2005).

41. Dalton, L., Sullivan, P. & Bale, D. Electric field poled organic electro-optic materials: state of the art and future prospects. *Chem. Rev.* **110**, 25–55 (2009)

42. Sullivan, P. A. & Dalton, L. R. Theory-inspired development of organic electro-optic materials. *Acc. Chem. Res.* **43,** 10–8 (2010).

43. Evans *et al.* Growth and properties of gold and nickel nanorods in thin film alumina. *Nanotechnology* **17,** 5746–5753 (2006).

44. Wurtz, G. A. *et al.* Designed ultrafast optical nonlinearity in a plasmonic nanorod metamaterial enhanced by nonlocality. *Nat. Nanotechnol.* **6,** 107–11 (2011).

45. Liao, Y. *et al.* Systematic Study of the Structure−Property Relationship of a Series of Ferrocenyl Nonlinear Optical Chromophores. *J. Am. Chem. Soc.* **127**, (2005).

46. Liu *et al.* Focused Microwave-Assisted Synthesis of 2,5-Dihydrofuran Derivatives as Electron Acceptors for Highly Efficient Nonlinear Optical Chromophores. *Adv. Mater.* **15**, (2003).

47. He, M., Leslie, T. & Sinicropi, J. α-Hydroxy Ketone Precursors Leading to a Novel Class of Electro-optic Acceptors. *Chem. Mater.* **14**, (2002).

48. Esenturk, O. & Walker, R. A. Surface vibrational structure at alkane liquid/vapor interfaces. *J.Chem. Phys.* **125,** 174701 (2006).

CHAPTER 6

CONCLUSION

6.1 Summary of Work

The main goal of this thesis was to explore the possibility of a metamaterial that would enhance the inherently weak properties of nonlinear processes. With this goal in mind, gold nanorods were synthesized and functionalized with gold-reactive polymers and nonlinear chromophores and used as versatile optical absorbers in both the linear and nonlinear optical regimes.

One method for enhancing nonlinear processes is through the concept of field enhancement. Chapter Two consisted of modeling results describing a metamaterial consisting of overlapping gold nanorods. Such an array of nanoparticle was predicted to confine and enhance electric fields. By hybridizing this metallic array with a nonlinear medium, it was shown that Pockels coefficients could be enhanced by more than order of magnitude. The modeling results in Chapter Two signify the potential of combining metamaterials with nonlinear materials into "nonlinear metamaterials." Nonlinear metamaterials have the potential to not only improve current technologies, but to generate a new revolution in optoelectronics.

Chapter Three described the synthesis and characterization of polymers that could be used to introduce nonlinear organic chromophores into a metallic metamaterial architecture like the one described in Chapter Two. Gold-reactive polymers containing anthracene or furan functional groups were synthesized. Both anthracene and furan offer the potential for coupling with a maleimde-functionalized nonlinear dye through a Diels Alder reaction. Chapter 4 described how these Diels-Alder reactive polymers were used to funcionalize the surface of gold nanorods. Through the use of thermogravimetric analysis, it was confirmed that the original surface coating, cetyltriethylammonium bromide, was replaced by gold-reactive polymers.

In Chapter 5, organic-soluble gold nanorods were used in an engineering project that sought to improve the efficiency of Nd:YAG diode-pumped solid state lasers (DPSSL). High concentrations of gold nanorods were produced so that only a small amount would be needed per batch of UV-curable epoxy. The GNR doped epoxy was applied to Nd:YAG laser rods, suppressing amplified spontaneous emission and improving efficiency of the laser by almost two fold. Because Nd:YAG DPPSLs are used for a wide range of commercial and research related enterprises, improving their efficiency was a far reaching application.

In Chapter 6, two dimensional nanopillar structures, along with flat gold, were functionalized with a gold-reactive nonlinear chromophore and

studied using sum frequency generation. These two dimensional nanopillar arrays were very similar to the three dimensional nanorod structure that was modeled and studied in Chapter Two. A massive SFG signal was observed for flat gold samples functionalized with nonlinear chromophores, but only in the PPP polarization configuration. This large signal was attributed to a field concentration due to the surface plasmon resonance of the gold surface. Unlike flat gold, the dye-conjugated nanopillar samples exhibited significant SFG signal in both PPP and SSP polarization configurations. These data may indicate the material's ability to produce a non-natural tensor element. The work in described Chapter 6 is largely unknown in the literature making it both significant and worthy of further investigation.

6.2 Future Work and Directions

There are two obvious routes to explore that would push forward this thesis' goals of studying nonlinear metamaterials. First, the materials produced in Chapters Three and Four have the potential to produce a self-assembled three dimensional metamaterial with bulk field enhancing properties. Noted in Chapter Three, at high enough concentrations, liquid crystalline phases can result from gold nanorods. And, if a nonlinear dye can be introduced into this three dimensional material, a large enhancement in nonlinear activity is predicted. But, the key to these materials is that the gold nanorods are alternating, overlapping, and ordered and that second

order nonlinear chromophores are in an acentric phase. Obviously, there are many challenges to producing this ideal material. A useful step towards producing an ideal three dimensional material would be to introduce nonlinear chromophores onto the surface of gold nanorods, or onto polymers that are attached to gold nanorods. A solution of the dye-GNR hybrids could be studied using a non-coherent second harmonic generation technique, Hyper-Rayleigh Scattering. However, there are challenges to observing and and characterizing how many nonlinear chromophores are attached to each gold-nanorod. To compare a solution of dye to a solution of dye-GNR hybrids, the amount of dye per nanorod must be measured.

The most impactful and novel future work involves additional SFG studies of dye-conjugated gold nanopillar arrarys. Two specific variables can be changed that would expand the understanding of these novel materials. First, because the nanopillar samplers are synthesized using pourous aluminum templates, the height and spacing of the nanopillar arrays can be tuned. And, like gold nanorods, the absorption properties change depending on the size and shape of the nanopillar arrays. Second, the absorption properties of the nonlinear chromophore can be tuned by changing the electron donor, electron acceptor, and conjugation length in the molecule. Changing the absorption properties of both the gold nanopillars and nonlinear chromophores will help determine whether the polarization dependent SFG signal that was observed is a general observation or if it

depends on some combination of nanopillar and chromophore absorption profile. But, regardless of which variable is changed, any SFG data collected on gold nanostructures hybridized with nonlinear chromophores should produce a better understanding of how the coupling between each variable may affect nonlinear phenomena.

REFERENCES CITED

Chapter 1

1. Smith, D., Pendry, J. & Wiltshire, M. Metamaterials and negative refractive index. *Science* **305**, 788–92 (2004).

2. Zheludev, N. & Kivshar, Y. From metamaterials to metadevices. *Nat Mater.* **11**, 917–24 (2012).

3. Liu, Y. & Zhang, X. Metamaterials: a new frontier of science and technology. *Chem. Soc. Rev.* **40**, 2494–507 (2011).

4. Veselago, V.G. The electrodynamics of substances with simultaneously negative values of ε and μ. *Sov. Phys. Usp.* **10**, 509-412 (1968)

5. Pendry, J. B. Negative refraction makes a perfect lens. *Phys. Rev. Lett.* **85,** 3966–9 (2000).

6. Pendry, J. B., Schurig, D. & Smith, D. R. Controlling electromagnetic fields. *Science* **312,** 1780–2 (2006).

7. Landy, N. & Smith, D. A full-parameter unidirectional metamaterial cloak for microwaves. *Nat. Mater.* **12**, 25–8 (2012).

8. Smith, D., Pendry, J. & Wiltshire, M. Metamaterials and negative refractive index. *Science* **305**, 788–92 (2004).

9. Zheludev, N. What diffraction limit? *Nat. Mater.* **7**, 420–2 (2008).

10. Rose, A., Larouche, S., Smith, D. R. Quantitative study of the enhancement of bulk nonlinearities in metamaterials. *Phys. Rev. Lett.* **84**, 053805 (2011).

11. http://www.kymetacorp.com/

12. Sullivan, P. & Dalton, L. Theory-inspired development of organic electro-optic materials. *Acc. Chem. Res.* **43**, 10–8 (2010).

13. Dalton, L., Sullivan, P. & Bale, D. Electric field poled organic electro-optic materials: state of the art and future prospects. *Chem. Rev.* **110**, 25–55 (2009)

14. Sullivan, P. A. & Dalton, L. R. Theory-inspired development of organic electro-optic materials. *Acc. Chem. Res.* **43,** 10–8 (2010).

15. Dalton. Rational design of organic electro-optic materials. *J. Phys. Condens. Matter.* **15,** R897 (2003).

16. Marder, S. Organic nonlinear optical materials: where we have been and where we are going. *Chemical Communications* **0,** 131–134 (2005).

17. Prasad, P. & Reinhardt, B. Is there a role for organic materials chemistry in nonlinear optics and photonics? *Chem. Mater.* (1990).

18. Zheludev, N. The road ahead for metamaterials. *Science* **328**, 582–3 (2010).

19. Pendry, J. B., Holden, A. J., Robbins, D. J. & Stewart, W. J. Magnetism from conductors and enhanced nonlinear phenomena. *IEEE Transactions on Microwave Theory and Techniques* **47,** (1999)

Chapter 2

1. Burland, D., Miller, R. & Walsh, C. Second-order nonlinearity in poled-polymer systems. *Chem. Rev.* **94,** 31–75 (1994).

2. Dalton, L. Theory-inspired development of organic electro-optic materials. *Thin Solid Films* **518,** 428–431 (2009).

3. Dalton, L. *et al.* From molecules to opto-chips: organic electro-optic materials. *J. Mater. Chem.* **9,** 1905–1920 (1999).

4. Dalton, L. R., Sullivan, P. A. & Bale, D. H. Electric field poled organic electro-optic materials: state of the art and future prospects. *Chem. Rev.* **110,** 25–55 (2010).

5. Baehr-Jones *et al.* Optical modulation and detection in slotted Silicon waveguides. *Opt. Express* **13,** 5216 (2005).

6. Hochberg, M. *et al.* Terahertz all-optical modulation in a silicon-polymer hybrid system. *Nat. Mater.* **5,** 703–9 (2006)

7. Wang, X. *et al.* Effective in-device r_33 of 735 pm/V on electro-optic polymer infiltrated silicon photonic crystal slot waveguides. *Opt. Lett.* **36,** 882 (2011).

8. Huang, S. *et al.* Advanced Materials **24**, OP42 (2012), ISSN 1521-4095.

9. Sipe, J.E., & Boyd, R. W. Nonlinear susceptibility of composite optical materials in the Maxwell Garnett model. *Phys. Rev. A* **46,** 1614–1629 (1992).

10. Fischer, G. *et al.* Enhanced Nonlinear Optical Response of Composite Materials. *Phys. Rev. Lett.* **74,** 1871–1874 (1995).

11. Boyd, R., Gehr, R., Fischer, G. & Sipe. Nonlinear optical properties of nanocomposite materials. *Pure Appl. Opt. J. European Opt Soc. Part A* **5,** 505–512 (1996).

12. Pendry, J. B., Holden, A. J., Robbins, D. J. & Stewart, W. J. Magnetism from conductors and enhanced nonlinear phenomena. *IEEE T. Microw. Theory* **47,** (1999).

13. Bouhelier A., Beversluis M., Hartschuh A. & Novotny L. Near-Field Second-Harmonic Generation Induced by Local Field Enhancement. *Phys. Rev. Lett.* **90,** (2003).

14. Soljacic, M. & Joannopoulos J. D. Enhancement of nonlinear effects using photonic crystals. *Nat. Mater.* **3,**211–219 (2004).

15. Rose, A., Larouche S., & Smith, D. R. Quantitative study of the enhancement of bulk nonlinearities in metamaterials. *Phys. Rev. A* **84**, 053805 (2011).

16. Wurtz, G. A. *et al.* Designed ultrafast optical nonlinearity in a plasmonic nanorod metamaterial enhanced by nonlocality. *Nat. Nanotechnol.* **6,** 107–11 (2011).

17. Ciracì, C., Poutrina E., Scalora M., & Smith, D. R. *Phys. Rev. B* **85**, 201403 (2012).

18. Zharov, A., Shadrivov, I. & Kivshar, Y. Nonlinear Properties of Left-Handed Metamaterials. *Phys. Rev. Lett.* **91,** (2003).

19. O'Brien, S., McPeake, D., Ramakrishna, A., & Pendry, J. B. Near-infrared photonic band gaps and nonlinear effects in negative magnetic metamaterials. *Phys. Rev. B* **69,** (2004).

20. Klein, M.W., Enkrich, C., Wegener, & M.,Linden, S. Second-Harmonic Generation from Magnetic Metamaterials. *Science* **313,** 502–504 (2006).

21. Larouche, S., Rose, A., Poutrina, E., Huang, D. & Smith, D. Experimental determination of the quadratic nonlinear magnetic susceptibility of a varactor-loaded split ring resonator metamaterial. *Appl. Phys. Lett.* **97,** 011109 (2010).

22. Rose, A., Larouche, S., Poutrina, E., & Smith, D. R. Nonlinear magnetoelectric metamaterials: Analysis and homogenization via a microscopic coupled-mode theory. *Phys. Rev. A* **86**, 033816 (2012).

23. Rose, A., Huang, D. & Smith, D. R. Demonstration of nonlinear magnetoelectric coupling in metamaterials. *Appl. Phys. Lett* **101,** 051103 (2012).

24. Rose, A., Huang, D. & Smith, D. R. Nonlinear Interference and Unidirectional Wave Mixing in Metamaterials. *Phys. Rev. Lett.* **110,** (2013).

25. Liu, Q. *et al.* Self-alignment of plasmonic gold nanorods in reconfigurable anisotropic fluids for tunable bulk metamaterial applications. *Nano Lett.* **10,** 1347–53 (2010).

26. Thorkelsson, K., Mastroianni, A. J., Ercius, P. & Xu, T. Direct nanorod assembly using block copolymer-based supramolecules. *Nano Lett.***12,** 498–504 (2012).

27. Vigderman, L., Khanal, B. P. & Zubarev, E. R. Functional gold nanorods: synthesis, self-assembly, and sensing applications. *Adv. Mater.* **24,** 4811–41, 5014 (2012).

28. Smith, D. R., Vier, D., Koschny, T. & Soukoulis, C. Electromagnetic parameter retrieval from inhomogeneous metamaterials. *Phys. Rev. E* **71,** (2005).

29. Larouche, S. & Smith, D. R. A retrieval method for nonlinear metamaterials. *Opt. Commun.* **283,** 1621–1627 (2010).

30. Rose, A., Larouche, S., Huang, D., Poutrina, E. & Smith, D. Nonlinear parameter retrieval from three- and four-wave mixing in metamaterials. *Phys. Rev. E* **82,** (2010).

31. Rose, A. & Smith, D. Overcoming phase mismatch in nonlinear metamaterials [Invited]. *Opt. Mater. Express* **1,** 1232 (2011).

32. Boyd, R. W. Nonlinear Optics (Academic Press, Burlington, MA, 2008).

Chapter 3

1. Zorn, M. *et al.* Liquid crystalline phases from polymer functionalised semiconducting nanorods. *J. Mater. Chem.* **18,** 3050–3058 (2008).

2. Meuer, Oberle, Theato, Tremel & Zentel. Liquid Crystalline Phases from Polymer-Functionalized TiO2 Nanorods. *Adv. Mater.* **19,** 2073–2078 (2007).

3. Thierry, B., Ng, J., Krieg, T. & Griesser, H. J. A robust procedure for the functionalization of gold nanorods and noble metal nanoparticles. *Chem. Commun.* 1724–6 (2009).

4. Chiefari, J. *et al.* Living Free-Radical Polymerization by Reversible Addition−Fragmentation Chain Transfer: The RAFT Process. *Macromolecules* **31,** 5559–5562 (1998).

5. Moad, G., Rizzardo, E. & Thang, S. Living Radical Polymerization by the RAFT Process. *Aust. J. Chem.* **58,** 379 (2005).

6. Moad, G., Rizzardo, E. & Thang, S. Living Radical Polymerization by the RAFT Process—A First Update. *Aust. J. Chem.* **59,** 669 (2006).

7. Moad, G., Rizzardo, E. & Thang, S. Living Radical Polymerization by the RAFT Process – A Second Update. *Aust. J. Chem.* **62,** 1402 (2009).

8. Moad, G., Rizzardo, E. & Thang, S. Material Matters **5.1**, 2 (2010).

9. Kang, Y. & Taton, T. Controlling shell thickness in core-shell gold nanoparticles via surface-templated adsorption of block copolymer surfactants. *Macromolecules* **38,** 146115-6121 (2005)

10. Eberhardt, M. & Théato, P. RAFT Polymerization of Pentafluorophenyl Methacrylate: Preparation of Reactive Linear Diblock Copolymers. *Macromol. Rapid. Comm.* **26,** 1488–1493 (2005).

11. Eberhardt, M., Mruk, R., Zentel, R. & Théato, P. Synthesis of pentafluorophenyl(meth)acrylate polymers: New precursor polymers for the synthesis of multifunctional materials. *Eur. Polym. J.* **41,** 1569–1575 (2005).

12. Gibson, M., Fröhlich, E. & Klok, H. Postpolymerization modification of poly(pentafluorophenyl methacrylate): Synthesis of a diverse water-soluble polymer library. *J. Polym. Sci. Part Polym. Chem.* **47,** 4332–4345 (2009).

13. Laita, Boufi & Gandini. The application of the Diels-Alder reaction to polymers bearing furan moieties. 1. Reactions with maleimides. *Eur. Polym. J.* **33,** 1203–1211 (1997).

14. Mansfeld, U., Pietsch, C., Hoogenboom, R., Becer, C. & Schubert, U. Clickable initiators, monomers and polymers in controlled radical polymerizations – a prospective combination in polymer science. *Polymer Chemistry* **1,** (2010).

15. Gacal *et al.* Anthracene−Maleimide-Based Diels−Alder 'Click Chemistry' as a Novel Route to Graft Copolymers. *Macromolecules* **39,** 5330–5336 (2006).

16. Kim, T.-D. *et al.* Ultralarge and Thermally Stable Electro-optic Activities from Diels–Alder Crosslinkable Polymers Containing Binary Chromophore Systems. *Advanced Materials* **18,** (2006).

17. Sullivan, P. *et al.* Tri-component Diels–Alder polymerized dendrimer glass exhibiting large, thermally stable, electro-optic activity. *J. Mater. Chem.* **17,** 2899–2903 (2007).

18. Kavitha, A. & Singha, N. Atom-Transfer Radical Copolymerization of Furfuryl Methacrylate (FMA) and Methyl Methacrylate (MMA): A Thermally-Amendable Copolymer. *Macromol. Chem. Physic.* **208,** 2569–2577 (2007).

19. Pramanik, N., Bag, D., Alam, S., Nando, G. & Singha, N. Thermally amendable tailor-made functional polymer by RAFT polymerization

and 'click reaction'. *J. Polym. Sci. Part Polym. Chem.* **51,** 3365–3374 (2013).

20. Demetriou, M. & Krasia-Christoforou, T. Well-defined diblock copolymers possessing fluorescent and metal chelating functionalities as novel macromolecular sensors for amines and metal ions. *J. Polym. Sci. Part Polym. Chem.* **50,** 52–60 (2012).

21. Moon, B., Hoye, T. & Macosko, C. Synthesis and application of fluorescently labeled phthalic anhydride (PA) functionalized polymers by ATRP. *Polymer* **43,** 5501–5509 (2002).

22. Liu, X. *et al.* Kinetic study of Diels–Alder reaction involving in maleimide–furan compounds and linear polyurethane. *Polym. Bull.* **70,** 23192335 (2013).

23. Dispinar, T., Sanyal, R. & Sanyal, A. A Diels-Alder/retro Diels-Alder strategy to synthesize polymers bearing maleimide side chains. *J. Polym. Sci. A Polym. Chem.* **45,** 4545–4551 (2007).

24. Chen, X., Lawrence, J., Parelkar, S. & Emrick, T. Novel Zwitterionic Copolymers with Dihydrolipoic Acid: Synthesis and Preparation of Nonfouling Nanorods. *Macromolecules* **46,** (2013).

25. Gandini, A. The furan/maleimide Diels–Alder reaction: A versatile click–unclick tool in macromolecular synthesis. *Prog. Polym. Sci.* **38,** (2013).

26. Fan, M., Liu, J., Li, X., Zhang, J. & Cheng, J. Recyclable Diels–Alder Furan/Maleimide Polymer Networks with Shape Memory Effect. *Ind. Eng. Chem. Res.* **53,** (2014).

Chapter 4

1. Van der Zande, B., Böhmer, M. R. & Fokkink, L. Colloidal dispersions of gold rods: synthesis and optical properties. *Langmuir* **16 (2)**,451-458 (2000).

2. Hulteen, J. & Martin, C. A general template-based method for the preparation of nanomaterials. *J. Mater. Chem.* **7,** 1075–1087 (1997).

3. Kim, F., Song, J. H. & Yang, P. Photochemical synthesis of gold nanorods. *J. Am. Chem. Soc.* **124,** 14316–7 (2002).

4. Yu, YY, Chang, SS & Lee, CL. Gold nanorods: electrochemical synthesis and optical properties. *J. Phys. Chem. B* **101** 6661-6664 (1997).

5. Reetz, M. T. & Helbig, W. Size-selective synthesis of nanostructured transition metal clusters. *J. Am. Chem. Soc.* **116 (16)** 7401-7402 (1994).

6. Esumi, K., Matsuhisa, K. & Torigoe, K. Preparation of rodlike gold particles by UV irradiation using cationic micelles as a template. *Langmuir* **11,** 3285–3287 (1995).

7. Jana, N. *et al.* Liquid crystalline assemblies of ordered gold nanorods. *J. Mater. Chem.* **12,** 2909–2912 (2002).

8. Jana*, N., Gearheart, L. & Murphy*, C. Wet Chemical Synthesis of High Aspect Ratio Cylindrical Gold Nanorods. *J. Phys. Chem. B* **105,** 4065–4067 (2001).

9. Nikoobakht, B. & El-Sayed, M. A. Preparation and Growth Mechanism of Gold Nanorods (NRs) Using Seed-Mediated Growth Method. *Chem. Mater.* **15**, 1957-1962 (2003).

10. Chen, H., Shao, L., Li, Q. & Wang, J. Gold nanorods and their plasmonic properties. *Chem. Soc. Rev.* **42,** 2679–724 (2013).

11. Vigderman, L., Khanal, B. & Zubarev, E. Functional gold nanorods: synthesis, self-assembly, and sensing applications. *Adv. Mat.* **24**, 4811–41 (2012).

12. Noguez, C. Surface plasmons on metal nanoparticles: the influence of shape and physical environment. *J. Phys. Chem. C* **111**, 3806-3819 (2007).

13. Nelayah, J, Kociak, M, Stéphan, O & de Abajo, F. Mapping surface plasmons on a single metallic nanoparticle. *Nature Physics* **3**, 348-(2007).

14. Ye, X. *et al.* Improved size-tunable synthesis of monodisperse gold nanorods through the use of aromatic additives. *ACS Nano* **6,** 2804–17 (2012).

15. Ye, X., Zheng, C., Chen, J., Gao, Y. & Murray, C. B. Using binary surfactant mixtures to simultaneously improve the dimensional tunability and monodispersity in the seeded growth of gold nanorods. *Nano Lett.* **13,** 765–71 (2013).

16. Vigderman, L., Manna, P. & Zubarev, E. R. Quantitative replacement of cetyl trimethylammonium bromide by cationic thiol ligands on the surface of gold nanorods and their extremely large uptake by cancer cells. *Angew. Chem. Int. Ed. Engl.* **51,** 636–41 (2012).

17. Bao, Y., Vigderman, L., Zubarev, E. R. & Jiang, C. Robust multilayer thin films containing cationic thiol-functionalized gold nanorods for tunable plasmonic properties. *Langmuir* **28,** 923–30 (2012).

18. Xue, C. *et al.* Organo-soluble porphyrin mixed monolayer-protected gold nanorods with intercalated fullerenes. *Langmuir* **28,** 5956–63 (2012).

19. Ma, X., Xue, Y., Dai, L., Urbas, A. & Li, Q. Hydrophilic Cucurbit[7]uril-Pseudorotaxane-Anchored-Monolayer-Protected Gold Nanorods. *Eur. J. Inorg. Chem.* **2013,** 2682–2686 (2013).

20. Xue, C. *et al.* Perylene Monolayer Protected Gold Nanorods: Unique Optical, Electronic Properties and Self-Assemblies. *J. Phys. Chem. C* **116,** 10396–10404 (2012).

21. Chen, X., Lawrence, J., Parelkar, S. & Emrick, T. Novel Zwitterionic Copolymers with Dihydrolipoic Acid: Synthesis and Preparation of Nonfouling Nanorods. *Macromolecules* **46,** (2013).

22. Thierry, B., Ng, J., Krieg, T. & Griesser, H. A robust procedure for the functionalization of gold nanorods and noble metal nanoparticles. *Chem. Commun.,* **13** 1724–6 (2009)

23. Kinnear, C. *et al.* Gold Nanorods: Controlling Their Surface Chemistry and Complete Detoxification by a Two-Step Place Exchange. *Angew. Chem. Int. Ed. Engl.* **52** 1934-1938 (2013)

Chapter 5

1. Lowenthal & Eggleston. ASE effects in small aspect ratio laser oscillators and amplifiers with nonsaturable absorption. *IEEE J. Quantum. Elect.* **22,** 1165–1173 (1986).

2. Barnes, N. P. & Walsh, B. M. Amplified spontaneous emission-application to Nd:YAG lasers. *IEEE J. Quantum. Elect.* **35,** 101–109 (1999).

3. Yamamoto, B. M., Bhachu, B. S., Cutter, K. P., Fochs, S. N., Letts, S. A., Parks, C. W., Rotter, M. D., Soules, T. F. The Use of Large Transparent Ceramics in a High Powered, Diode Pumped Solid-State Laser. In *Advanced Solid-State Photonics*, OSA Technical Digest Series (CD), Nara, Japan, January 27-30, 2008; WC5

4. Yagi, H., Bisson, JF, Ueda, K & Yanagitani, T. $Y_3Al_5O_{12}$ ceramic absorbers for the suppression of parasitic oscillation in high-power Nd: YAG lasers. *J. Lumin.* **121**, 88-94 (2006).

5. Fabian, J., Nakazumi, H. & Matsuoka, M. Near-infrared absorbing dyes. *Chem. Rev.* **92,** 1197-1226 (1992).

6. Langhals, H., Zgela, D. & Lüling, R. Sexterrylenetetracarboxylic Bisimides: NIR Dyes. *J. Org. Chem.* **80,** 12146–12150 (2015).

7. Chen, H., Shao, L., Li, Q. & Wang, J. Gold nanorods and their plasmonic properties. *Chem. Soc. Rev.* **42,** 2679–724 (2013).

8. Pérez-Juste, J., Pastoriza-Santos, I., Liz-Marzán, L. M. & Mulvaney, P. Gold nanorods: synthesis, characterization and applications. *Coordin. Chem. Rev.* **249**, 1870-1901, (2005)

9. Murphy, C. J. *et al.* Anisotropic metal nanoparticles: Synthesis, assembly, and optical applications. *J. Phys. Chem. B* **109**, 13857–70 (2005).

10. Lohse, S. & Murphy, C. The Quest for Shape Control: A History of Gold Nanorod Synthesis. *Chem. Mater.* **25,** (2013).

11. Dreaden, E. C., Alkilany, A. M., Huang, X., Murphy, C. J. & El-Sayed, M. A. The golden age: gold nanoparticles for biomedicine. *Chem. Soc. Rev.* **41,** 2740–79 (2012).

12. Jana, N., Gearheart, L. & Murphy, C. Wet Chemical Synthesis of High Aspect Ratio Cylindrical Gold Nanorods. *J. Phys. Chem. B* **105,** 4065–4067 (2001).

13. Nikoobakht, B. & El-Sayed, M. Preparation and Growth Mechanism of Gold Nanorods (NRs) Using Seed-Mediated Growth Method. *Chem. Mater.* **15,** 1957–1962 (2003).

14. Wei, GT, Yang, Z, Lee, CY & Yang, HY. Aqueous-organic phase transfer of gold nanoparticles and gold nanorods using an ionic liquid. *J. Am. Chem. Soc.* **126**, 5036-5037 (2004).

15. Hotchkiss, J., Lowe, A. & Boyes, S. Surface Modification of Gold Nanorods with Polymers Synthesized by Reversible Addition−Fragmentation Chain Transfer Polymerization. *Chem. Mater.* **19,** 6-13 (2007).

16. Xue, C. *et al.* Organo-soluble porphyrin mixed monolayer-protected gold nanorods with intercalated fullerenes. *Langmuir* **28,** 5956–63 (2012).

17. Mitamura, K, Imae, T & Saito, N. Fabrication and self-assembly of hydrophobic gold nanorods. *J. Phys. Chem. B* **111**, 8891-8898 (2007).

18. Alkilany, A. M., Thompson, L. B. & Murphy, C. J. Polyelectrolyte coating provides a facile route to suspend gold nanorods in polar organic solvents and hydrophobic polymers. *ACS Appl. Mater. Interfaces* **2,** 3417–21 (2010).

19. Thierry, B., Ng, J., Krieg, T. & Griesser, H. J. A robust procedure for the functionalization of gold nanorods and noble metal nanoparticles. *Chem. Commun.* **13,** 1724–6 (2009).

20. Meuer, S., Oberle, P., Theato, P., Tremel, W. & Zentel, R. Liquid Crystalline Phases from Polymer-Functionalized TiO2 Nanorods. *Adv. Mat.* **19,** 2073–2078 (2007)

21. Zorn, M. *et al.* Liquid crystalline phases from polymer functionalised semiconducting nanorods. *J. Mater. Chem.* **18,** 3050–3058 (2008).

22. Veselago, V. G. The electrodynamics of substances with simultaneously negative values of ε and μ. *Sov. Phys. Usp.* **10**, 509–514 (1968).

23. Zheludev, N. I. & Kivshar, Y. S. From metamaterials to metadevices. *Nat. Mater.* **11,** 917–24 (2012).

24. Liu, Y. & Zhang, X. Metamaterials: a new frontier of science and technology. *Chem. Soc. Rev.* **40,** 2494–507 (2011).

25. Pendry, J. B., Schurig, D. & Smith, D. R. Controlling electromagnetic fields. *Science* **312**, 1780–2 (2006).

26. Schurig, D. *et al.* Metamaterial electromagnetic cloak at microwave frequencies. *Science* **314**, 977–980 (2006).

27. Landy, N. & Smith, D. R. A full-parameter unidirectional metamaterial cloak for microwaves. *Nat. Mater.* **12**, 25–8 (2013).

28. Burgos, S. P., de Waele, R., Polman, A. & Atwater, H. A. A single-layer wide-angle negative-index metamaterial at visible frequencies. *Nat. Mater.* **9,** 407–412 (2010).

29. Cai, W. S., Chettiar, U. K., Kildishev, A. V. & Shalaev, V. M. Optical cloaking with metamaterials. *Nature Photon.* **1**, 224–227 (2007).

30. Rose, A., Latterman, R., Smith, D. & Sullivan, P. Lower poling thresholds and enhanced Pockels coefficients in nanoparticle-polymer composites. *Appl. Phys. Lett.* **103,** 031102 (2013).

31. Rose, A. & Smith, D. Overcoming phase mismatch in nonlinear metamaterials [Invited]. *Opt. Mater. Express,* **Vol. 1, No. 7**, 1231-1243 (2011).

32. Suchowski, H, O'Brien, K, Wong, ZJ, Salandrino, A & Yin, X. Phase Mismatch–Free Nonlinear Propagation in Optical Zero-Index Materials. *Science*, **6**, 1223-1226 (2013).

33. Choi, M. *et al.* A terahertz metamaterial with unnaturally high refractive index. *Nature* **470**, 369-374 (2011)

34. Shin, J., Shen, J.-T. T. & Fan, S. Three-dimensional metamaterials with an ultrahigh effective refractive index over a broad bandwidth. *Phys. Rev. Lett.* **102,** 093903 (2009).

35. Hess, O. *et al.* Active nanoplasmonic metamaterials. *Nat. Mater.* **11,** 573–584 (2012).

36. Canalias, C & Pasiskevicius, V. Mirrorless optical parametric oscillator. *Nature Photon.,* **1**, 459-462 (2007).

37. Litchinitser, NM & Shalaev, VM. Metamaterials: Loss as a route to transparency. *Nature Photon.*, **1**, 75-76, (2009)

38. Prasad, P. & Reinhardt, B. Is there a role for organic materials chemistry in nonlinear optics and photonics? *Chem. Mater.* **2**, 660-669 (1990).

39. Dalton., L.R. Rational design of organic electro-optic materials. *J. Phys. Condens. Matter.* **15,** R897-R934 (2003).

40. Marder, S. Organic nonlinear optical materials: where we have been and where we are going. *Chem. Commun.* **0**, 131-134 (2005).

41. Dalton, L., Sullivan, P. & Bale, D. Electric field poled organic electro-optic materials: state of the art and future prospects. *Chem. Rev.* **110**, 25–55 (2009)

42. Sullivan, P. A. & Dalton, L. R. Theory-inspired development of organic electro-optic materials. *Acc. Chem. Res.* **43,** 10–8 (2010).

43. Evans *et al.* Growth and properties of gold and nickel nanorods in thin film alumina. *Nanotechnology* **17,** 5746–5753 (2006).

44. Wurtz, G. A. *et al.* Designed ultrafast optical nonlinearity in a plasmonic nanorod metamaterial enhanced by nonlocality. *Nat. Nanotechnol.* **6,** 107–11 (2011).

45. Liao, Y. *et al.* Systematic Study of the Structure−Property Relationship of a Series of Ferrocenyl Nonlinear Optical Chromophores. *J. Am. Chem. Soc.* **127**, (2005).

46. Liu *et al.* Focused Microwave-Assisted Synthesis of 2,5-Dihydrofuran Derivatives as Electron Acceptors for Highly Efficient Nonlinear Optical Chromophores. *Adv. Mater.* **15**, (2003).

47. He, M., Leslie, T. & Sinicropi, J. α-Hydroxy Ketone Precursors Leading to a Novel Class of Electro-optic Acceptors. *Chem. Mater.* **14**, (2002).

48. Esenturk, O. & Walker, R. A. Surface vibrational structure at alkane liquid/vapor interfaces. *J.Chem. Phys.* **125,** 174701 (2006).